SPATIAL DISTRIBUTION OF CHLORIDE AND ^{36}Cl DEPOSITION IN THE CONTERMINOUS UNITED STATES

by

Joseph M. Sterling

INDEPENDENT STUDY

Submitted to the Faculty of the

Department of Earth and Environmental Science

NEW MEXICO INSTITUTE OF MINING AND TECHNOLOGY

In Partial Fulfillment of the Requirements
For the Degree of

MASTER OF SCIENCE

New Mexico Institute of Mining and Technology, Socorro, NM

June 2000

ACKNOWLEDGEMENTS

I thank my advisor, Dr. Fred M. Phillips, for the opportunity to work on this project, and for his continuous guidance, suggestions, and rapid response to questions throughout my course of study. In addition, I thank my other committee members, Dr. Jan Hendrickx and Dr. Robert Bowman, for their comments and contributions. Scotty Dossett with the Program Office of the National Atmospheric Deposition Program was very helpful in providing detailed information about the collectors and methods used within the program's network of stations. Doug Moore provided data on dry deposition within the Sevilleta National Wildlife Refuge. Mitch Plummer and Roseanna Neupauer provided insight and helpful suggestions on numerous occasions throughout the project. I thank the Oregon Climate Service and the USDA-NRCS National Water and Climate Center for allowing free access to the PRISM precipitation model, which forms the backbone of the model developed in this study. Funding for this project was provided by NSF grant no. EAR-9614509. I thank my family for their continual support, and all my friends and fellow classmates for my sanity. Finally, I could not have completed this degree without the companionship and encouragement of the best friend anyone could ask for, my wife Jenny.

Table of Contents

List of Figures

List of Tables

ABSTRACT

Chlorine-36 is a valuable tool to study numerous processes in hydrologic systems, and ^{36}Cl applications expanded rapidly following measurement of this radioactive isotope by accelerator mass spectrometry. Most ^{36}Cl applications require knowledge of the initial input function in both time and space, but relatively little research has focused on establishing the form of this input function. A new model of atmospheric stable chloride deposition, combined with a theoretical model of atmospheric ^{36}Cl deposition, was constructed to evaluate the spatial variability of $^{36}Cl/Cl$ ratios across the United States. This new model incorporated dry deposition measurements from 89 stations across the country, and is the first of its kind employing measurements of the dry deposition flux rather than cursory approximations.

The wet component of atmospheric chloride deposition was linearly related to precipitation, although deposition reached a ceiling value at extreme precipitation amounts. The slope of this linear relationship was a function of the distance of the measurement point from the coast, and the slope decreased as a power-law with increasing inland distance. The chloride deposition / precipitation regression slopes were combined with a precipitation model to calculate the wet chloride deposition. The wet deposition and dry deposition were summed to calculate the total atmospheric stable chloride flux. Total chloride deposition ranged from less than 100 mg m^{-2} yr^{-1} throughout the Midwest, to several hundred mg m^{-2} yr^{-1} in the eastern U.S., to over 1000 mg m^{-2} yr^{-1} in the Pacific Northwest, Florida, and near the Great Salt Lake, Utah. Dry deposition accounted for 10 to 30 percent of the total deposition throughout the Midwest and eastern U.S., and for over 50 percent of the total throughout Texas and the Southwest.

Atmospheric ^{36}Cl deposition was calculated using a recently proposed model, where the ^{36}Cl flux was a function of latitude and the fraction of mean latitudinal precipitation falling locally. The model predicted deposition values of 40 to 65 atoms m^{-2} s^{-1} throughout the eastern United States, 5 to 20 atoms m^{-2} s^{-1} throughout the Midwest and Southwest, and values of several hundred atoms m^{-2} s^{-1} in the Pacific Northwest. The model-predicted $^{36}Cl/Cl$ ratios ranged from less than 100×10^{-15} at several coastal locations to greater than 1000×10^{-15} in portions of the northern Midwest, and shared a similar distribution pattern with previous models.

The average absolute error of the wet deposition model was 10 percent, providing a good match to the measured values over most of the country, with a slight bias toward underprediction. The ^{36}Cl model fit the measured data moderately well, with an average absolute error of 27 percent. The model-predicted $^{36}Cl/Cl$ ratios were within ±25 percent of the measured values throughout much of the Midwest, but were significantly overestimated in the eastern United States, and underestimated in the Pacific Northwest. The $^{36}Cl/Cl$ ratio model can be improved by implementing minor modifications to the linear chloride / precipitation regressions, and by incorporating functional relationships between model parameters and the distance from the coast.

CHAPTER 1 - INTRODUCTION

Chloride has been used extensively in environmental studies, particularly as a hydrologic tracer. Chlorine has an exceptional electron affinity (second only to fluorine) and thus exists as the chloride anion (Cl) in virtually all natural aqueous systems. Having a negative charge, chloride is rarely adsorbed onto mineral surfaces and acts conservatively in most groundwater systems, moving at the same rate as water. This, in combination with chloride's highly hydrophilic nature, makes chloride an ideal groundwater tracer. The utility of chloride in the environmental sciences has been greatly expanded by the recognition of its single long-lived radioactive isotope, ^{36}Cl. Chlorine-36 has a half-life of $(3.01\pm0.04) \times 10^5$ years, making it suitable for groundwater dating to a maximum of approximately one million years (Bentley et al., 1986a).

1.1 Chlorine-36 as an Environmental Tracer

Measurements of ^{36}Cl began in the 1950's using screen-wall counters (Davis and Schaeffer, 1955) which required very large sample sizes and were too insensitive for application to most natural samples (Bentley et al., 1986a). The use of liquid scintillation through the 1960's improved the sensitivity but the required sample size was still very large. In spite of this, Schaeffer et al. (1960) were able to measure the ^{36}Cl bomb pulse in rainwater, with a monumental sampling effort to collect 4000 to 8000 liters of rainwater for analysis. The development and application of accelerator mass spectrometry (AMS) to ^{36}Cl measurement (Elmore et al., 1979) provided a radical improvement to the sensitivity and decrease of the required sample size. The sensitivity was increased by a factor of approximately 50 while the required sample size was decreased by a factor of 10^4, from

~20 g of Cl to ~2 mg (Phillips, 1999). The use of AMS allowed the measurement of ^{36}Cl in nearly all natural systems and led to numerous new environmental applications. Initial investigations included the measurement of the ^{36}Cl bomb pulse to identify recent groundwater recharge (Bentley et al., 1982). An extensive study of ^{36}Cl in groundwater by Bentley et al. (1986b) focused on groundwater dating in the Great Artesian Basin, Australia. A comprehensive list of potential ^{36}Cl applications was given by Fabryka-Martin et al. (1987), and an extensive review of ^{36}Cl was recently provided by Phillips (1999).

Chlorine-36 is commonly used as a dating tool, particularly for groundwater. Precipitation recharging to the subsurface contains both dissolved stable chloride and ^{36}Cl. The concentration of chloride and ^{36}Cl in recharge water can change drastically as a result of evapotranspiration. However, the ratio of the amount of radioactive ^{36}Cl to the amount of stable chloride (the $^{36}Cl/Cl$ ratio) remains the same, as neither is preferentially removed or concentrated by evapotranspiration. Thus, the $^{36}Cl/Cl$ ratio is typically used as the measure of ^{36}Cl in hydrologic systems, rather than its absolute concentration. As water percolates into and through a groundwater aquifer, the ^{36}Cl undergoes radioactive decay, causing a change in the $^{36}Cl/Cl$ ratio. The relative age difference of groundwater between two points along a groundwater flowpath can be found by measuring the amount of decay between the upgradient and downgradient points. However, in order to measure the absolute age of groundwater at a point within an aquifer the initial amount of ^{36}Cl in water at the time of recharge must be known (Bentley et al., 1986a; Fabryka-Martin et al., 1987; Davis et al., 1998).

The decay of ^{36}Cl can be described by a typical exponential equation (Bentley et al., 1986a), which in the simplest case is of the form (Davis et al., 1998)

$$N_t = N_o e^{-\lambda_{36} t} \qquad \text{Eqn 1.1}$$

where λ_{36} is the decay constant for ^{36}Cl, t is the elapsed time, N_o is the initial amount of ^{36}Cl in a sample, and N_t is the amount of ^{36}Cl remaining at time t. This assumes that there are no additional sources of ^{36}Cl and that radioactive decay is the only process acting to change the ^{36}Cl values. This assumption does not generally apply in groundwater systems because there is a subsurface source of ^{36}Cl. Chlorine-36 can be produced in the subsurface by neutron activation of ^{35}Cl and spallation of K and Ca (Phillips, 1999). Neutrons in the subsurface can arise from the nuclear decay of uranium and thorium and from cosmic rays which penetrate the atmosphere. Chlorine-36 decays and is simultaneously produced in the subsurface. Over very long time periods, the production and decay of ^{36}Cl (in the subsurface) arrive at equilibrium, such that a constant abundance of ^{36}Cl exists in the subsurface. This is termed 'secular equilibrium'. The change in ^{36}Cl with time in a closed system where ^{36}Cl is both produced and decays is described by (Bentley et al., 1986a; Davis et al., 1998)

$$N_t = N_o e^{-\lambda_{36} t} + N_{se}\left(1 - e^{-\lambda_{36} t}\right) \qquad \text{Eqn 1.2}$$

where N_{se} is the amount of ^{36}Cl in the sample at secular equilibrium (as t approaches infinity). In the case where ^{36}Cl is measured as the $^{36}Cl/Cl$ ratio, the values of N in

Equation 1.2 can be replaced by the equivalent values of the ratio (R). Groundwater age can be calculated by rewriting Equation 1.2 as (Bentley et al., 1986a)

$$t = \frac{1}{\lambda_{36}} \ln\left(\frac{R - R_{se}}{R_o - R_{se}}\right) \qquad \text{Eqn 1.3}$$

where R is the measured $^{36}Cl/Cl$ ratio, R_o is the initial ratio, and R_{se} is the ratio at secular equilibrium. A calculation of R_{se} in the subsurface is provided by Bentley et al. (1986a).

1.2 Objectives of This Study

The initial $^{36}Cl/Cl$ ratio is required for most of the applications of ^{36}Cl listed by Fabryka-Martin et al. (1987) but, to date, there have been relatively few studies to determine the temporal and spatial atmospheric input function for ^{36}Cl. Initial studies to determine this input function have concentrated on the spatial component of initial $^{36}Cl/Cl$ ratios by either combining theoretical calculations of atmospheric ^{36}Cl production with measured concentrations of total chloride in precipitation (Bentley et al., 1986a; Hainsworth, 1994) or by assuming that $^{36}Cl/Cl$ ratios measured in shallow groundwater represent the initial recharge value (Bentley et al., 1986b; Moysey, 1999). The temporal component of the ^{36}Cl input function has been associated with Earth's historical geomagnetic field intensity using comparisons of $^{36}Cl/Cl$ ratios and ^{14}C from fossil rat urine recovered from packrat middens in the western United States (Plummer et al., 1997), and by measurements of ^{36}Cl variation in a Greenland ice-core (Baumgartner et al., 1998).

The main goal of this study was to construct a new model to estimate the $^{36}Cl/Cl$ ratios in precipitation across the conterminous United States in order to determine the

spatial component of the atmospheric input function. An important aspect of this model was that it would be parameter based. The model was intended to incorporate the climatic and geographic controls on both the stable chloride and ^{36}Cl atmospheric flux, such that the effect of changes of these parameters on the $^{36}Cl/Cl$ flux could be assessed. For instance, the amount of stable chloride deposited to the land surface was found to depend on the amount of precipitation. Knowing the modern distribution of rainfall across the country, the modern stable-chloride flux could be calculated. The advantage of the parameter-based model is that it can also be applied for past (or future) conditions. If a reasonable estimate of ancient precipitation distribution can be made, then the chloride flux during that time period can be easily calculated with the parameter-based model. If the model were based on modern atmospheric flux measurements alone (as with previous models), then it would be unclear how to modify the modern distribution to account for past conditions. In addition, the ancient distribution would not necessarily share the pattern of the modern distribution, creating further difficulties in using a model based on modern measurements alone to assess $^{36}Cl/Cl$ ratios in the past. Given that ^{36}Cl is useful for dating very old groundwater, the $^{36}Cl/Cl$ ratio of water which recharged long ago can be expected to differ from the measured modern value at the same location. Thus, the parameter-based model is a powerful tool to estimate the initial $^{36}Cl/Cl$ ratio, whether in the past, present, or future.

The parameter-based $^{36}Cl/Cl$ ratio distribution model described in this paper was constructed by combining a new model of the stable atmospheric chloride flux with a recent model of ^{36}Cl deposition by Phillips (1999). Chapters 2 and 3 provide background on the sources and deposition processes for stable chloride and ^{36}Cl, respectively. Chapter 4 describes the construction of each component of the model and presents the model

output. Chapter 5 presents a model error assessment, comparing the model results with measured values and highlighting weaknesses in the current model. Chapter 6 discusses the potential refinements and improvements that can be made to the model, and Chapter 7 provides the conclusions of this study.

CHAPTER 2 - ATMOSPHERIC DISTRIBUTION OF CHLORIDE

After hydrogen and oxygen, chlorine is the most abundant element in the hydrosphere, owing to its dominance in the oceans (Feth, 1981), and is the 15th most abundant element in the outer lithosphere. The chloride anion is the primary form of chlorine in the hydrosphere. Having a negative charge, the chloride anion is generally not adsorbed to silicate surfaces (which are also negatively charged) and dissolved chloride is advected at essentially the same rate as the water (Phillips, 1999). This property of the chloride anion has led to its extensive use as a hydrogeologic tracer. A major goal of this study was to assess and model the spatial distribution of the atmospheric deposition of chloride and its long-lived radioactive isotope, ^{36}Cl. This requires an understanding of the source of atmospheric chloride, and the mechanisms by which it is deposited to the land surface. This chapter discusses the sources and deposition of stable (non-radioactive) chloride, while the following chapter describes the same for ^{36}Cl.

2.1 Sources of Atmospheric Stable Chloride

The primary source of chloride deposited on the continents is ocean-derived salt (Boyce, 1951; Eriksson, 1960; Feth, 1981). The bursting of bubbles at the sea surface ejects salt particles, or aerosols, into the atmosphere. Breaking waves are the most significant source of bubbles (Blanchard and Woodcock, 1957) but eject relatively few salt particles by the direct mechanical disintegration of water (Boyce, 1951). High-speed film has shown that as a bubble bursts a small jet of water is ejected into the air. The air-entrained droplets may evaporate under low relative humidity, leaving a solid-gas aerosol, or remain liquid as a liquid-gas aerosol (Feth, 1981). Aerosols produced at the ocean

surface are predominantly in the size range $1.0 < r < 10$ microns (μ) (Junge, 1972; Cicerone, 1981). Particles smaller than approximately 20μ remain suspended in the atmosphere almost indefinitely, as their settling velocity is low enough that normal atmospheric eddy currents are sufficient to keep them aloft (Junge, 1972). Once aerosols are entrained in the atmosphere they can be transported around the globe by regional winds. Typically, 90 percent of ocean-derived aerosols are redeposited over the oceans, with only 10 percent falling on the continents (Eriksson, 1960). Aerosols transported over the continents are subject to both wet and dry deposition mechanisms, discussed in greater detail in following sections.

The oceanic source of atmospheric chloride is readily apparent in the distribution of chloride across the continents. Chloride concentration in precipitation decreases at a nearly exponential rate with increasing inland distance, up to a few hundred kilometers, until becoming approximately constant in the continental interior (Simpson and Herczeg, 1994; Feth, 1981). Observations of precipitation chemistry by the National Atmospheric Deposition Program / National Trends Network (NADP/NTN) illustrate this distribution, as shown in Figure 2.1. The decrease in chloride concentration can be attributed both to the cumulative loss of marine aerosols by precipitation (as air masses progress inland) and to more intense vertical mixing of the lower atmosphere by convective eddy diffusion within continental interiors (Simpson and Herczeg, 1994; Feth, 1981).

Other potential sources for atmospheric chloride are wind entrainment of fine continental material (Simpson and Herczeg, 1994) and anthropogenic sources. Re-suspension of evaporite dusts is the likely cause of the increased chloride concentration in precipitation near the Great Salt Lake, Utah, as seen in Figure 2.1. The main

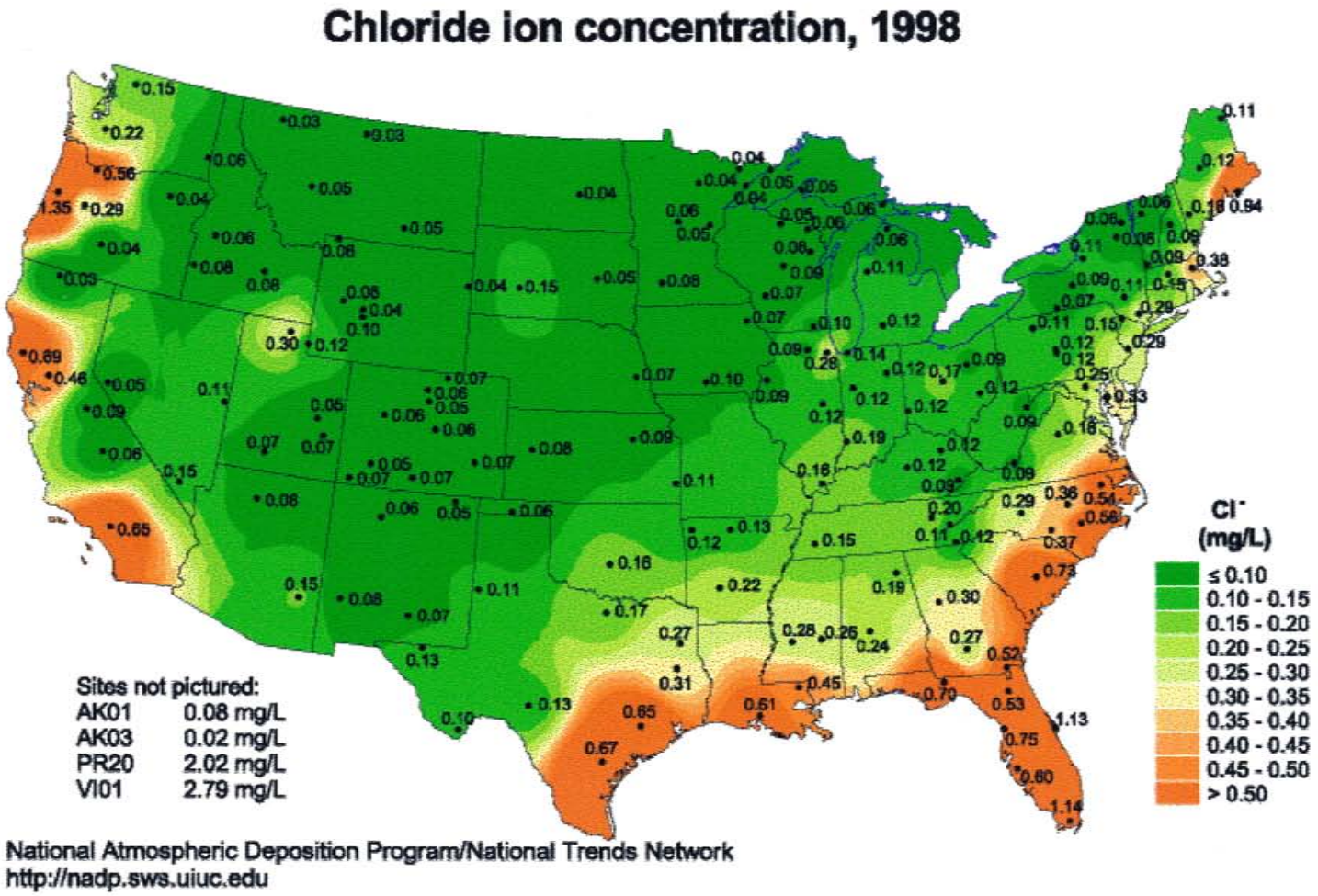

Figure 2.1: Concentration of chloride in precipitation. NADP/NTN (1998)

anthropogenic source of chloride to the atmosphere is the burning of fossil fuels which releases HCl (Simpson and Herczeg, 1994; Li, 1992; Eriksson, 1960).

2.2 Stable Chloride Deposition

Aerosols produced at the ocean surface, or derived from continental or anthropogenic sources, are incorporated into the lower atmosphere and distributed by global and regional wind patterns. As the aerosols are advected over the continents, both wet and dry deposition mechanisms act to transport chloride to the land surface. Wet deposition occurs during active precipitation (i.e. rain or snow) while dry deposition occurs during the intervening periods.

2.2.1 Wet deposition mechanisms

Two mechanisms are recognized for the transport of atmospheric aerosols to the land surface by precipitation; rainout (or snowout) and washout (Fuquay, 1970). Rainout refers to processes within a cloud whereby aerosols are incorporated into raindrops, which fall to the ground. Washout refers to the interception of aerosols beneath the cloud by falling raindrops.

Aerosols drawn into a cloud act as condensation nuclei, leading to the formation of very small water droplets. Initially, these droplets are small enough to remain in suspension and have been termed cloud drops (Sumner, 1988). Turbulent conditions within the cloud cause these cloud drops to collide and coalesce into drops large enough to fall from the cloud. This process is illustrated in Figure 2.2. In the case of snow, the co-existence of ice particles and super-cooled water allows the growth of ice crystals at the

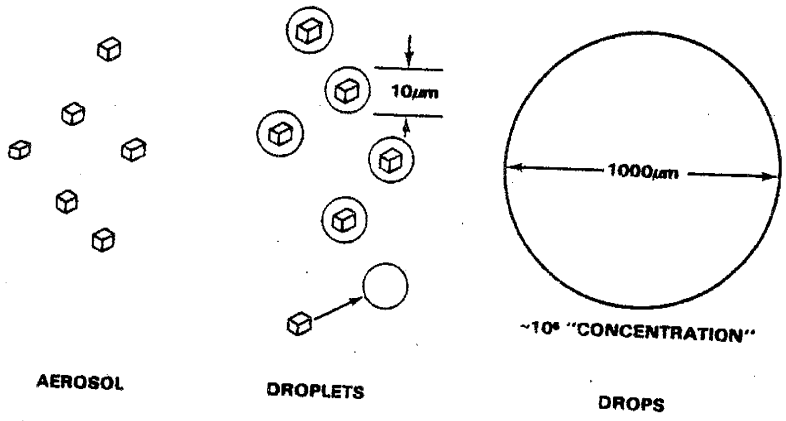

Figure 2.2: Schematic illustrating the progression of aerosols to rain drops by condensation and coalescence. (Scott, 1981)

expense of adjacent super-cooled water drops, known as the Bergeron-Findeisen process (Sumner, 1988). Two other mechanisms for raindrop coalescence have been proposed, the wake effect and electrostatic attraction (Sumner, 1988). The wake effect results from the induced reduction of pressure between two droplets falling closely together at similar speeds, drawing the droplets together. Cloud drops can have opposing charges that may encourage coalescence when drops are close together. The coalescence of rain drops by collisions within the cloud and the Bergeron-Findeisen process are the dominant mechanisms leading to rainout; the contribution by the wake effect and electrostatic attraction is considered small (Sumner, 1988).

The processes of rainout and washout acting to remove aerosols from the atmosphere are collectively known as scavenging. Scavenging is an efficient process, as the number of aerosol particles contained within a single raindrop (or snowflake) is approximately 10^6 (Davidson, 1989; Scott, 1981). Simple models of wet deposition incorporate a scavenging coefficient (ψ) to describe the decrease in atmospheric aerosol concentration during precipitation. The scavenging coefficient is given by Scott (1981) as

$$\psi = \frac{L_{ac} + L_{ap}}{C_a} \qquad \text{Eqn 2.1}$$

where L_{ac} is related to the rate of aerosol accumulation into cloud water, L_{ap} is related to the rate of aerosol accumulation into precipitation water, and C_a is the particle concentration in the atmosphere. A simple model of wet deposition by Davidson (1989) uses a first-order decay of atmospheric aerosol concentration dependant on the scavenging rate

$$\frac{dC_a}{dt} = -\psi C_a \qquad \text{Eqn 2.2(a)}$$

The wet deposition flux then depends on the vertically integrated scavenging coefficient and on the vertical distribution of atmospheric aerosols, given by (Scott, 1981; Davidson, 1989)

$$D_w = -\int_0^\infty \psi C_a dz = C_p P \qquad \text{Eqn 2.2(b)}$$

where D_w is the wet deposition flux, C_p is the concentration in precipitation, and P is the net precipitation rate. Wet deposition can thus be determined by measurement of rainfall chemistry and volume.

2.2.2 Dry deposition mechanisms

Dry deposition occurs as a result of particle transport by eddy diffusion, gravitational settling, thermophoresis, and diffusiophoresis (Seinfeld and Pandis, 1998; Prodi, 1980). Eddy diffusion is caused by turbulent air movement leading to particles impacting the land surface. Thermophoresis and diffusiophoresis result from particulate drift in response to non uniformities in atmospheric temperature and concentration, respectively (Slinn and Hales, 1970). Dry deposition can be linked to atmospheric concentration by a deposition velocity (Hicks et al., 1987; Erisman et al., 1999; Prodi, 1980)

$$v_d(z) = -\frac{F_d}{C_a(z)} \qquad \text{Eqn 2.3}$$

where $v_d(z)$ is the deposition velocity, $C_a(z)$ is the particulate concentration in the atmosphere, F_d is the net deposition flux, and z is altitude. The deposition velocity incorporates the complexities of the transfer of atmospheric particles to the land surface and is typically expressed using a resistance analog (Hicks et al., 1987)

$$v_d(z) = \frac{1}{R_a + R_b + R_c} \qquad \text{Eqn 2.4}$$

R_a is an aerodynamic resistance determined by atmospheric processes (predominately turbulent exchange), R_b is a quasi-laminar boundary layer resistance accounting for molecular diffusivity acting near the receptor surface, and R_c is a surface or canopy resistance. I do not discuss the detailed functional forms of R_a, R_b, and R_c here, but the terms can be calculated using standard atmospheric and surface field parameters. The interested reader is referred to Hicks et al. (1987) for a detailed description, and to Erisman et al. (1999) for an application to field study.

2.3 Modern Distribution of Stable Chloride across the United States

The NADP/NTN measures precipitation chemistry at stations throughout the United States. The amount of chloride deposited to the land surface can be calculated using the volume of precipitation captured by the collector (liters), the concentration of chloride in the rainwater (mg/L), and the surface area of the collector funnel (m^2). Only

chemistry from wet deposition is reported by the NADP/NTN, although the dry data is available upon request. The atmospheric flux of chloride (wet deposition only) is shown in Figure 2.3.

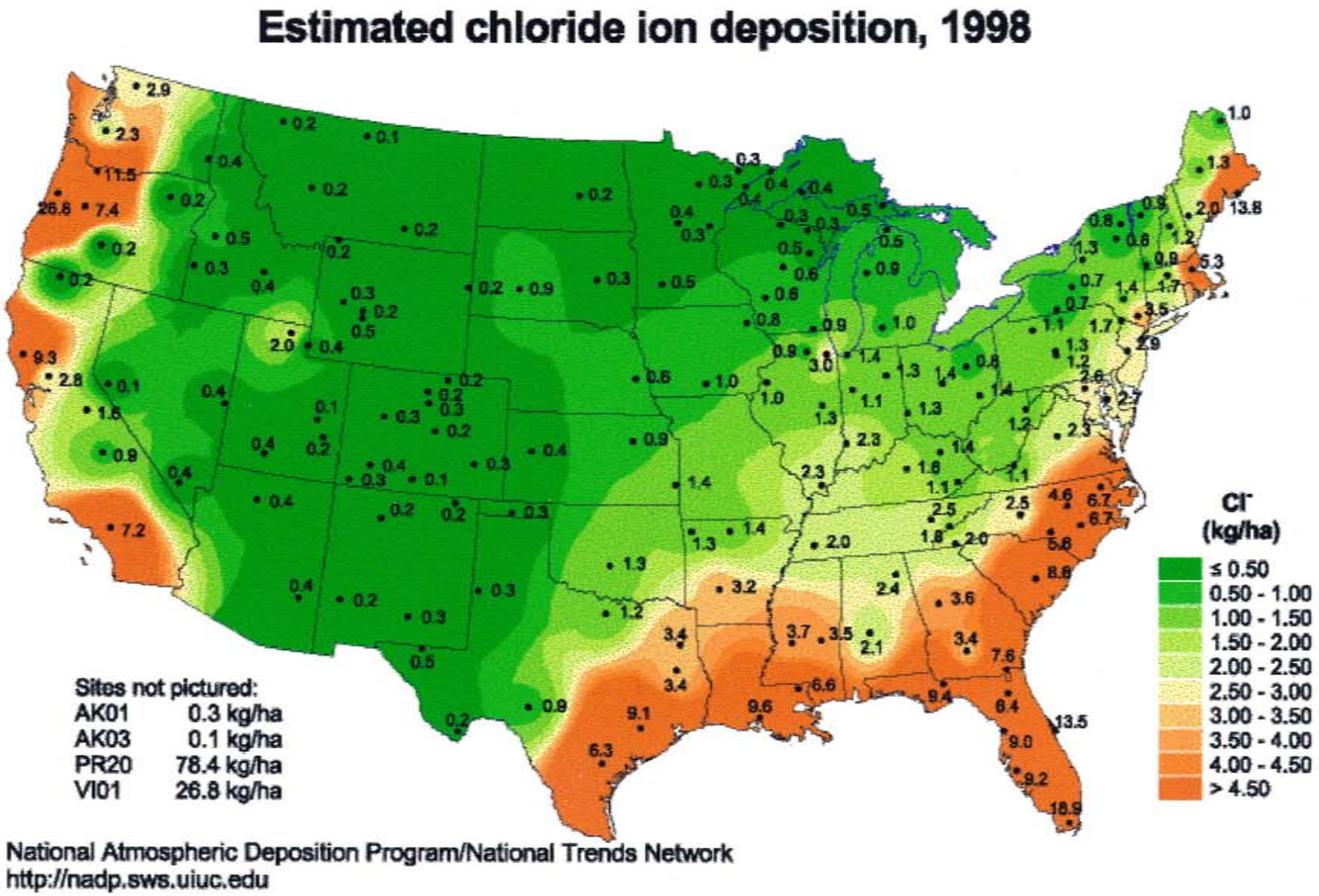

Figure 2.3: Continental stable chloride deposition in the U.S. NADP/NTN (1998)

CHAPTER 3 - METEORIC ^{36}Cl

Chlorine-36 is a long-lived radioactive isotope produced on Earth by interactions with incoming high-energy particles. The research reported here concerns ^{36}Cl produced in the atmosphere (meteoric ^{36}Cl), although ^{36}Cl is also produced in the lithosphere. The half-life of ^{36}Cl is 3.01 x 10^5 years. Chlorine-36 decays by beta emission to produce ^{36}Ar (Bentley et al., 1986a; Hainsworth, 1994).

3.1 Atmospheric Production of ^{36}Cl

The Earth is under continuous bombardment by high-energy cosmic-ray particles produced by intense galactic events, such as supernovae. The majority of these incident particles are protons, but the Earth is also the target of beta and alpha particles, and heavier atomic nuclei. Upon entering the Earth's atmosphere, these highly energetic particles collide with the nuclei of atmospheric gas atoms, resulting in nuclear disintegration of the target nucleus and the release of energetic neutrons and protons. The mass of the target nucleus may be reduced by the ejection (spalling) of some nucleons, leading to the term 'spallation' reaction. The secondary particles produced by the initial spallation can in turn (if energetic enough themselves) produce further nuclear disintegrations and a cascading shower of particles. The residual nuclear mass of the target atom releases additional particles to lower its energy state, becoming a new stable nuclide or radionuclide (Phillips, 1999).

Chlorine-36 is produced primarily by the cosmic-ray spallation of ^{40}Ar (Bentley et al., 1986a) in the atmosphere. It is also produced in the upper lithosphere by neutron activation of ^{35}Cl and spallation of K and Ca (Phillips, 1999). Lal and Peters (1967)

estimated the spallation reaction cross-section of Ar to arrive at a calculated mean global ^{36}Cl production rate of ~11 atoms m^{-2} s^{-1} in the atmosphere. More recently, Parrat et al. (1996) calculated a mean global production rate of 20 atoms m^{-2} s^{-1}, using new measurements of the reaction cross-section. Both of these production rates are below historically measured deposition rates (Parrat et al., 1996), but the cause of this underestimation is presently unclear. Phillips (1999) normalised the measured ^{36}Cl deposition rates and found that a linear scaling of the Parrat et al. (1996) deposition by 1.47 produced a good fit to measured data. The mean global ^{36}Cl production rate estimated using this method was ~30 atoms m^{-2} s^{-1} (Phillips, 1999).

3.2 Spatial Distribution of ^{36}Cl Fallout

The Earth's atmosphere can be divided into a number of layers extending to approximately 2400 kilometers (1500 miles) above the surface. The most important atmospheric layers with regard to ^{36}Cl production are the troposphere and the stratosphere. The troposphere encompasses approximately the lower 10 to 12 kilometers (km) of the atmosphere. The stratosphere extends from the top of the troposphere to a height of 45 to 50 km. Figure 3.1 illustrates the major layers of Earth's atmosphere and, in particular, the change in temperature with increasing height. The boundary between the stratosphere and the troposphere is known as the tropopause and is located at the lower point of reversal in the temperature gradient. Holton et al. (1995) defined the tropopause more specifically as the lowest height in the atmosphere where the negative temperature gradient does not exceed 2 K km^{-1} and remains so for at least two additional kilometers. Approximately 70 percent of meteoric ^{36}Cl is produced in the stratosphere, and 30 percent in the troposphere

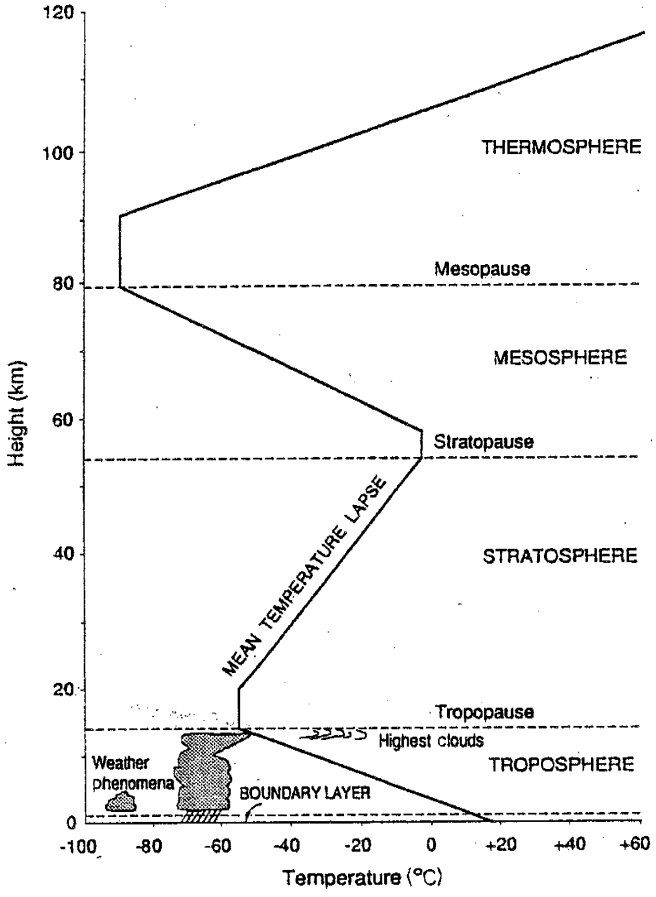

Figure 3.1: Vertical layering of Earth's atmosphere. (Sumner, 1988)

(Lal and Peters, 1967; Bentley et al., 1986a). The processes by which stratospheric and tropospheric air are mixed have been found to exert great influence on the spatial distribution of ^{36}Cl.

3.2.1 Latitude dependence of ^{36}Cl deposition

The Earth's geomagnetic field modulates the atmospheric production of cosmogenic nuclides (Elsasser et al., 1956; Lal and Peters, 1967) as charged particles are deflected by the interaction with the dipole magnetic field. This effect is strongest over the equator and diminishes toward the poles as a consequence of the changing field strength with latitude. Cosmogenic nuclide production is thus greatest at the geomagnetic poles and at a minimum at the equator (Lal and Peters, 1967), as shown in Figure 3.2. The latitude dependence of cosmogenic nuclide production is strong in the stratosphere and much weaker in the troposphere. The latitude dependency of cosmogenic production differs from the latitude dependence of fallout for long-lived cosmogenic nuclides, shown in Figure 3.3. Deposition of cosmogenic nuclides is greatest in the mid-latitudes (30^{o} to 60^{o}) while production is greatest at the poles. Inasmuch as tropospheric production shows little latitude dependence, the difference between these two curves must be due to a redistribution of nuclides produced in the stratosphere.

Two major processes are responsible for the redistribution of stratospheric air and the concentration of fallout at mid-latitudes. Global-scale atmospheric circulation patterns influence the distribution of ^{36}Cl fallout. Warm air originating at the equator rises and moves toward the poles while cold polar air descends and moves toward the equator. Each hemisphere has developed three major thermal-convection cells, illustrated in Figure 3.4.

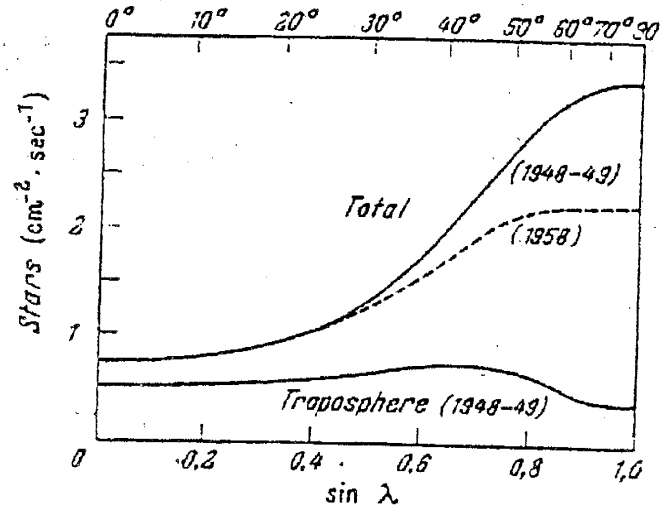

Figure 3.2: Global cosmogenic isotope production (which can be scaled from star production) as a function of latitude. (Lal and Peters, 1967)

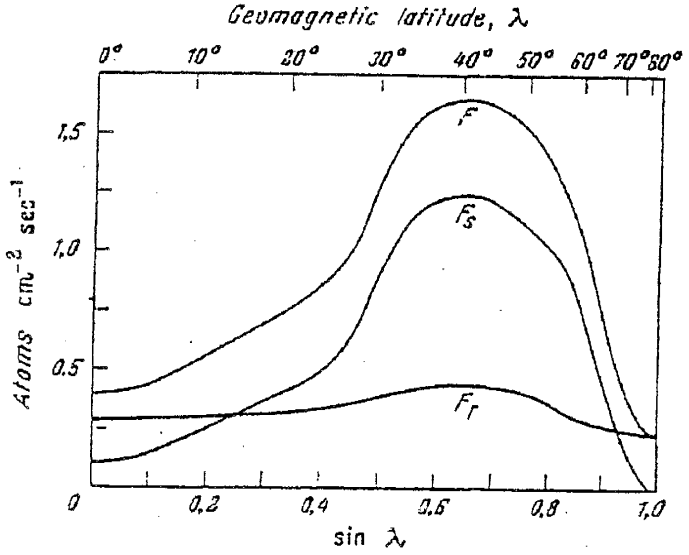

Figure 3.3: Global cosmogenic isotope fallout as a function of latitude. The three curves represent total fallout (F), stratosphere-derived fallout (F_S) and troposphere-derived fallout (F_T). (Lal and Peters, 1967)

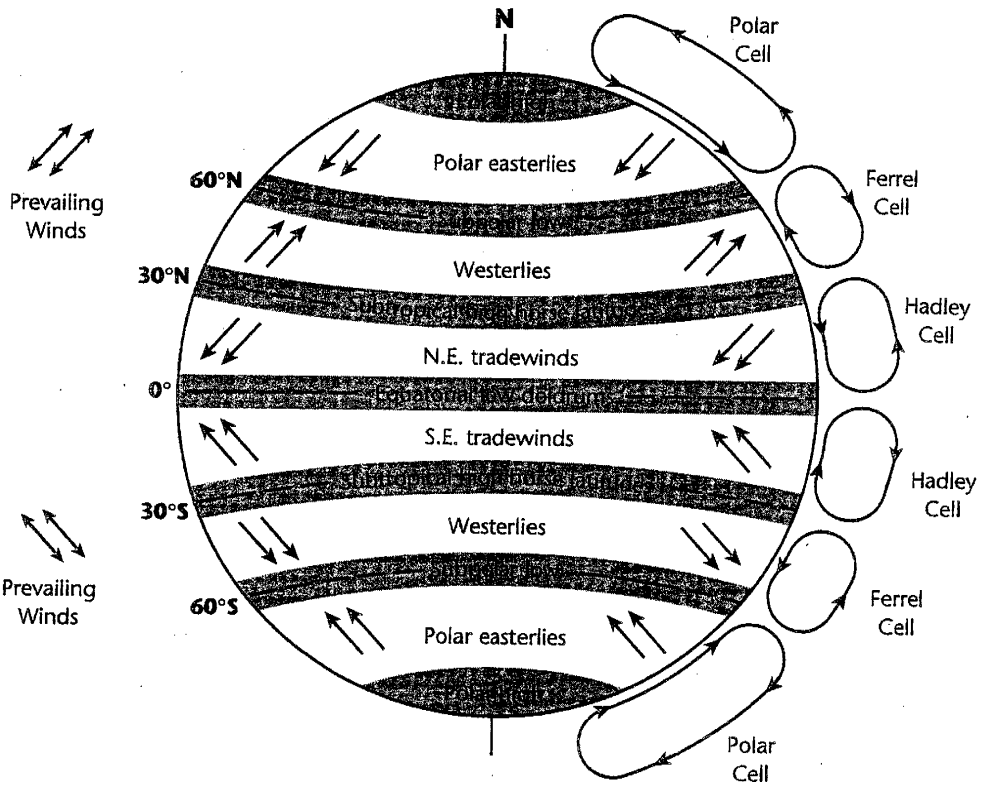

Figure 3.4: Global-scale atmospheric circulation cells. Nuclides produced in the stratosphere are transported to the troposphere within the Horse latitudes where the Ferrel and Hadley cells converge. (Barnes-Svarney, 1995)

The Polar and Hadley cells operate in the same direction at the poles and the equator, respectively, while the Ferrel cell circulates in an opposite direction in the mid-latitudes. The Ferrel and Hadley cells can extend well into the stratosphere (Reiter, 1975) and act to concentrate stratospheric fallout in the Horse latitudes (around 30^{o}) where air descends. Seasonal variability in the size and location of these cells causes the fallout to be focused over the range of latitudes from approximately 20^{o} to 45^{o} (Reiter, 1975). The second major influence on the redistribution of stratospheric nuclides is a process known as tropopause folding, in association with the jet stream. The jet stream separates the flow of warm air from that of cold air and can contain significant vertical vortices which act to bend the tropopause. The tropopause is depressed where air is descending and raised where air is ascending. Exchange of air from the stratosphere to the troposphere can then occur along equithermal surfaces, as illustrated in Figure 3.5. The location of the jet stream varies seasonally but is typically between 30^{o} and 60^{o}N in the northern-hemisphere. Barry and Chorley (1992) discuss the seasonal variability of the jet stream location and provide a map of the mean location of the summer-time jet stream in the northern hemisphere,as shown in Figure 3.6.

The latitude dependence of fallout presented in Figure 3.3 was derived by Lal and Peters (1967) for a hypothetical stable isotope with a global average production rate of 1 atom cm^{-2}. This curve can be modified to represent the expected latitude dependency of an individual isotope, such as ^{36}Cl, by multiplying the curve by the actual average global production rate and a factor correcting for decay in the atmosphere. Lal and Peters (1967) provide the following equations to scale the tropospheric (F_T) and stratospheric (F_S) components of the curve for a particular isotope of interest:

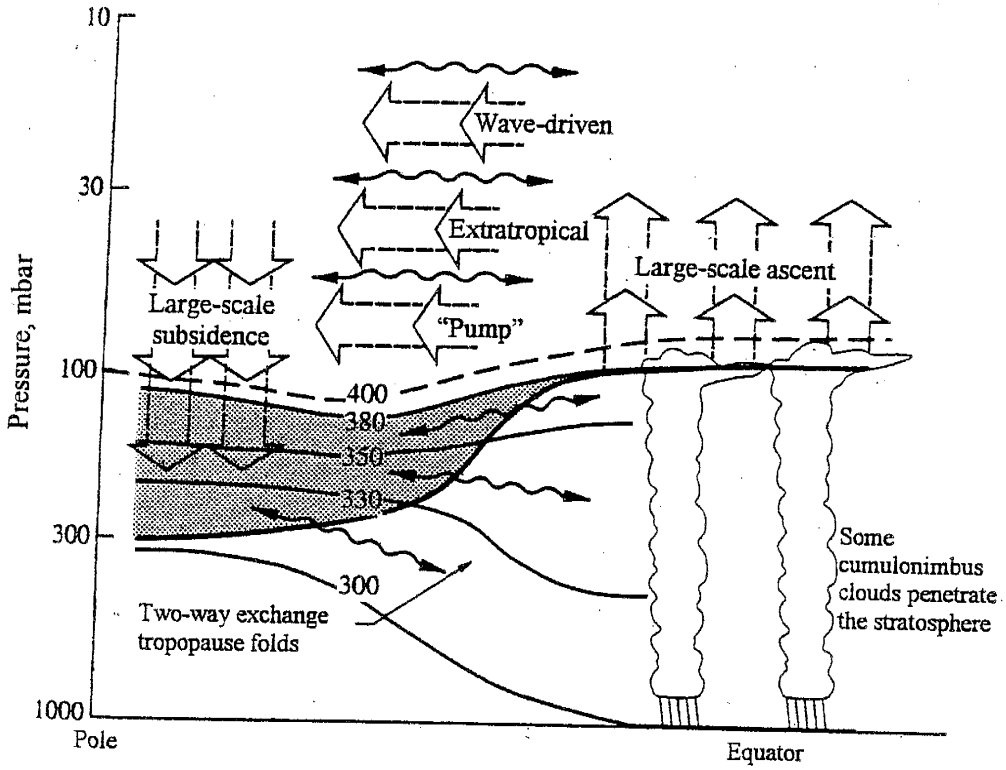

Figure 3.5: Conceptual model of tropopause folding as a mechanism for stratosphere-troposphere exchange. The tropopause is represented by the thick black line and equithermal surfaces by thin black lines. Exchange can occur within the shaded region. (Seinfeld and Pandis, 1998)

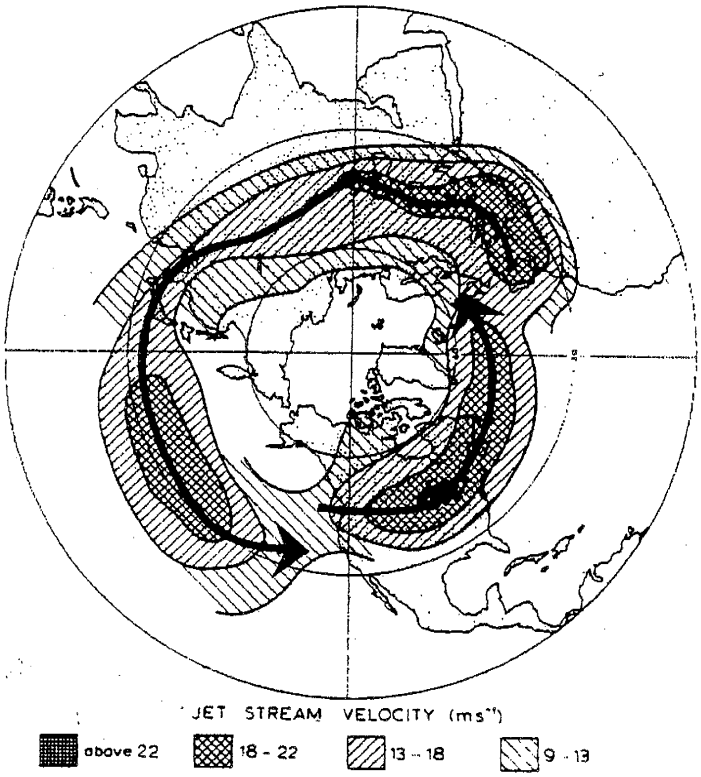

Figure 3.6: The mean location of the summertime jet stream in the northern hemisphere. (Barry and Chorley, 1992)

$$F_T = \frac{Q_T}{1 + \lambda \tau_F} \qquad \text{Eqn 3.1}$$

$$F_S = \frac{y Q'_S K_{ST}}{(\lambda + K_{ST})(1 + \lambda \tau_F)} \qquad \text{Eqn 3.2}$$

where: F_T = global fallout of troposphere-produced nuclide

Q_T = global production of nuclide in the troposphere

λ = decay constant for nuclide

τ_F = average tropospheric residence time

F_S = global fallout of stratosphere-produced nuclide

Q's = global average spallations in stratosphere

y = nuclide yield per spallation

K_{ST} = inverse of troposphere/stratosphere exchange time

Bentley et al. (1986a) incorporated these scaling factors to calculate the latitude dependence of ^{36}Cl fallout shown in Figure 3.7.

3.2.2 Model of the spatial ^{36}Cl distribution

Phillips (1999) provides a comprehensive review of ^{36}Cl in the environment and its applications in hydrogeologic systems. This review combines the most current understanding of ^{36}Cl production and deposition mechanisms and proposes a new model describing the geographical distribution of meteoric ^{36}Cl fallout. The Phillips (1999) model was incorporated into this research, and is described here.

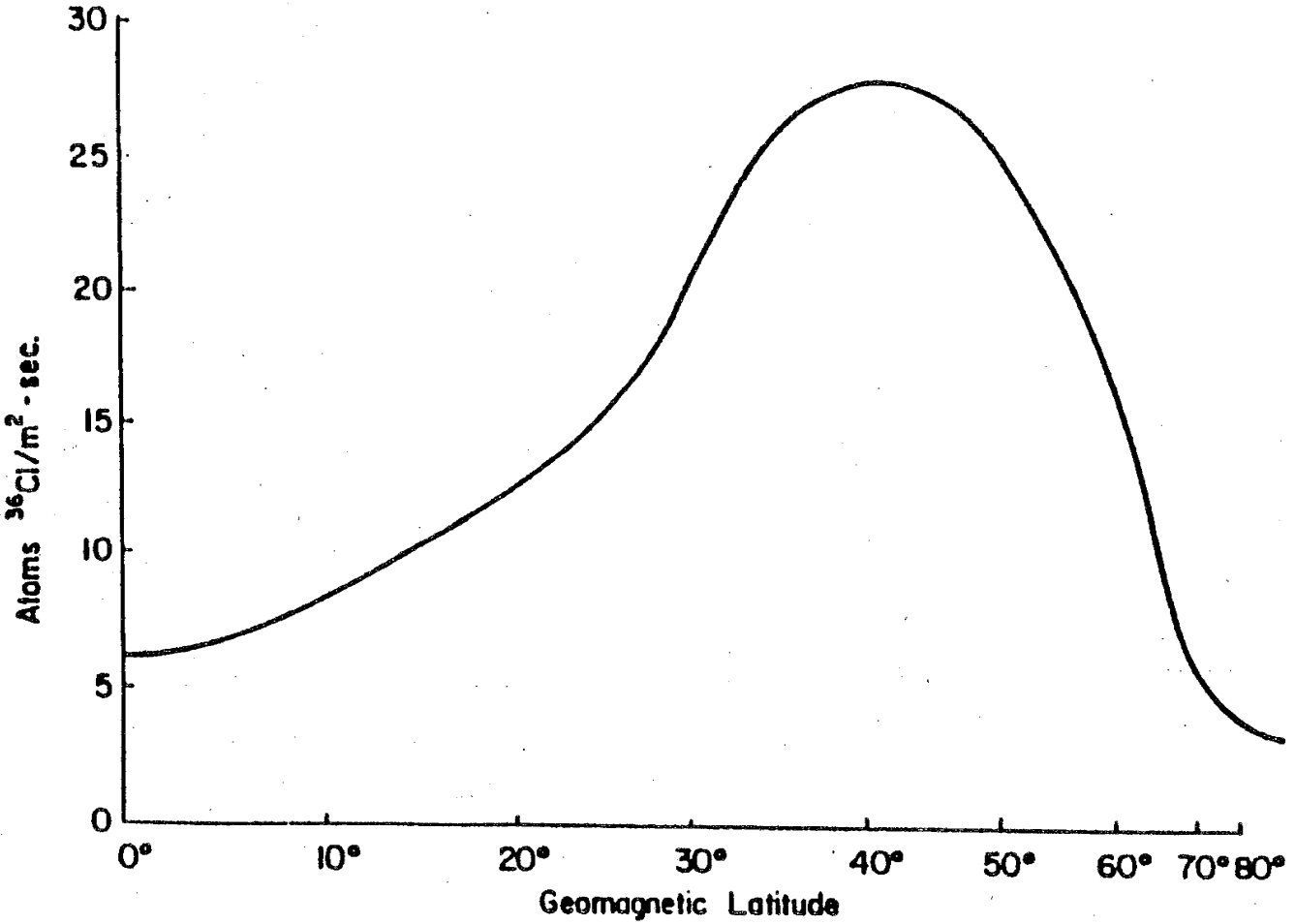

Figure 3.7: Meteoric ^{36}Cl deposition as a function of latitude. (Bentley et al., 1986a)

World-wide measurements of ^{36}Cl deposition (concentrated in the United States and Australia) are provided in Table 3.1 and compared to the Lal and Peters (1967) calculation of latitude-dependent ^{36}Cl deposition, as well as the more recent calculation by Parrat et al. (1996), in Figure 3.8(a). There is significant scatter around the calculated distribution. Sites with ^{36}Cl deposition in excess of the calculated amount typically receive high annual precipitation while those below predicted values are located in more arid regions (Table 3.1). Lal and Peters (1967) noted that ^{36}Cl fallout would be proportional to the amount of local precipitation (within a latitude belt) and data from Knies (1994) illustrates a significant linear correlation between monthly precipitation and monthly ^{36}Cl deposition at West Lafayette, Indiana. Using a simple linear correlation, Phillips (1999) postulates a relation between latitude, precipitation, and ^{36}Cl deposition as

$$D_{36}(P,\lambda) = D_{36}(\lambda) + S_P(P - \overline{P}(\lambda)) \qquad \text{Eqn 3.3}$$

where $D_{36}(\lambda)$ is the average ^{36}Cl deposition rate as a function of geographic latitude, $\overline{P}(\lambda)$ is the average precipitation rate for each latitudinal belt, and S_P is the precipitation / deposition correlation, normalized for the latitude. The precipitation / deposition correlation (S_P) was determined using (1) six sites from Table 3.1 within the latitude range of the broad deposition maximum, and (2) average monthly ^{36}Cl deposition and precipitation values (converted to annual values) from Knies (1994) (Figure 3.9). The slopes of these regressions were 0.047±0.006 and 0.052±0.006 atoms m^{-2} s^{-1}(mm yr^{-1})$^{-1}$, respectively. The dependence of deposition on precipitation was normalized for latitude using (Phillips, 1999):

Table 3.1: Summary of ^{36}Cl atmospheric deposition measurements. Asterisks designate long-term sites (>1 kyr). Taken from Phillips (1999).

Location	Latitude	Measured ^{36}Cl flux (atoms m^{-2} s^{-1})	Precipitation (mm yr^{-1})	Reference
Camp Century*	77°N	24±8	300	Conard (1986)
Summit*	72°N	19±3	230	Baumgartner *et al.* (1997)
Milcent*	70°N	24±7	500	Synal *et al.* (1994)
Dye 3*	65°N	20±6	500	Synal *et al.* (1994)
Worksop (UK)*	56°N	31±2	650	Andrews *et al.* (1994)
Weiss Fluhjoch (SW)	46°N	42±5	850	Baltensperger *et al.* (1993)
Hanford (WA, USA)*	46°N	19±4	160	Murphy *et al.* (1996)
Victor (NY, USA)	43°N	64±3	800	Hainsworth (1994)
Laingsburg (MI,USA)	43°N	63±13	700	Hainsworth (1994)
Black Hills (SD,USA)	43°N	75±7	350	Hainsworth (1994)
Lafayette (IN, USA)	41°N	68±5	1060	Knies (1994)
Elms (MD, USA)	38°N	59±8	1160	Hainsworth (1994)
Lewes (DE,USA)	38°N	47±4	1150	Hainsworth (1994)
Guliya Ice Cap (Tibet)*	35°N	17±1.5	200	Thompson *et al.* (1997)
Socorro (NM, USA)*	34°N	18±1.5	250	Phillips *et al.* (1988)
North. Terr. (AUS) 33	12°S	20±2	1200	Keywood *et al.* (1998)
North. Terr. (AUS) 32	14°S	27±2	1000	Keywood *et al.* (1998)
North. Terr. (AUS) 31	17°S	26±2	700	Keywood *et al.* (1998)
North. Terr. (AUS) 30	20°S	10±1.5	330	Keywood *et al.* (1998)
North. Terr. (AUS) 29	23°S	10±0.8	300	Keywood *et al.* (1998)
West. Aust. (AUS) 23-25	26°S	12±1.5	200	Keywood *et al.* (1998)
West. Aust. (AUS) 19-21	28°S	13±3	220	Keywood *et al.* (1998)
South Aust. (AUS) 28	28°S	18±1.5	150	Keywood *et al.* (1998)
West Aust. (AUS) 16-18	29°S	15±2.5	400	Keywood *et al.* (1998)
South Aust. (AUS) 27	32°S	22±1.5	300	Keywood *et al.* (1998)
South Aust. (AUS) 26	34°S	23±2.5	400	Keywood *et al.* (1998)

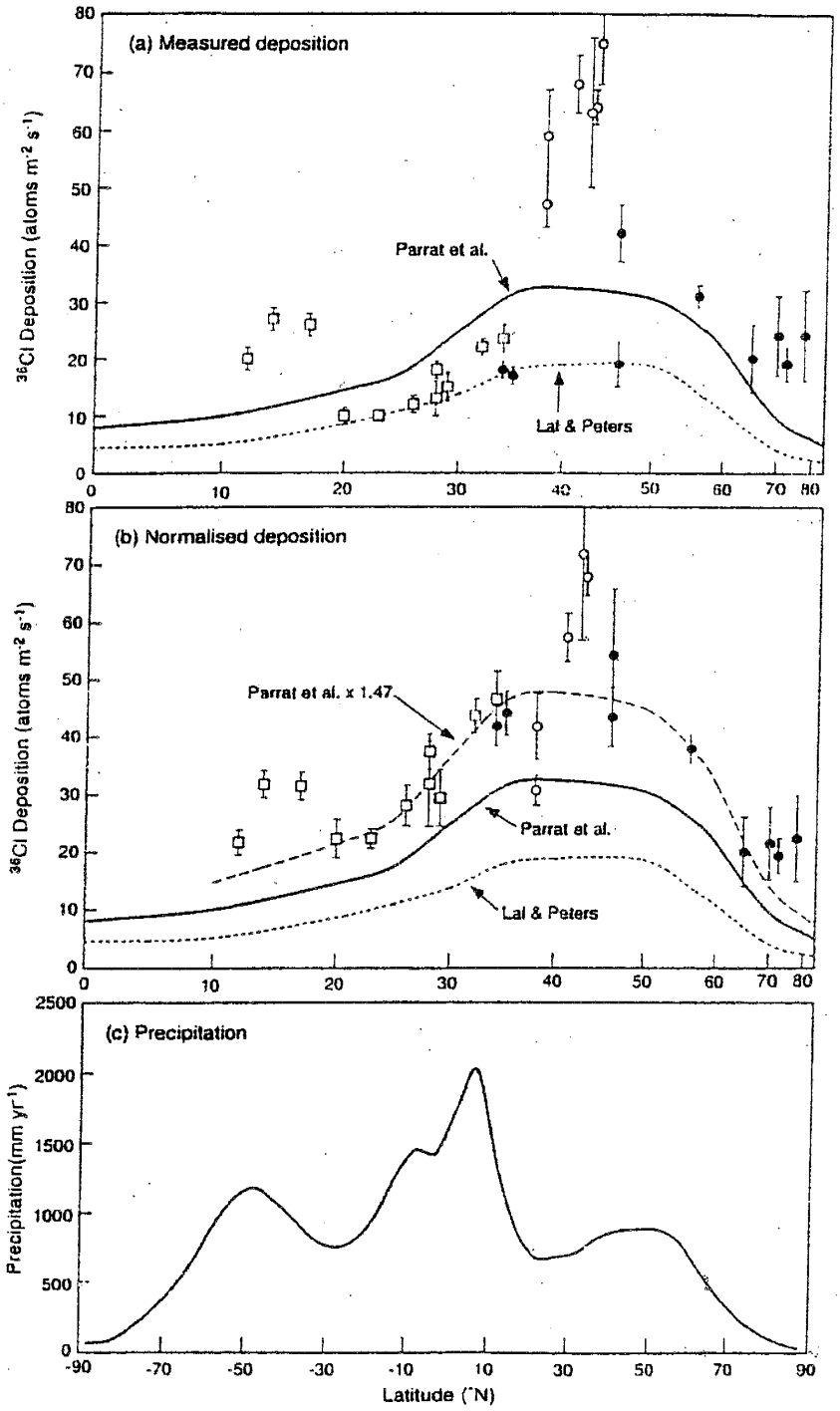

Figure 3.8: Comparison of predicted latitudinal distribution of ^{36}Cl fallout by Lal and Peters (1967) and Parrat et al. (1996) with measured fallout from Table 3.1, Normalized ^{36}Cl fallout distribution, and latitudinal distribution of global precipitation. (a) Measured deposition compared with predicted latitudinal distributions. (b) Deposition corrected for annual precipitation using Equation 4.4. (c) Latitudinal distribution of global precipitation, from Baumgartner and Reichel (1975). Circles denote northern hemisphere data, and squares southern hemisphere. Solid symbols represent long-term natural archives (>1000 yr); open symbols represent short-term precipitation collection (one to several yr). (Phillips, 1999)

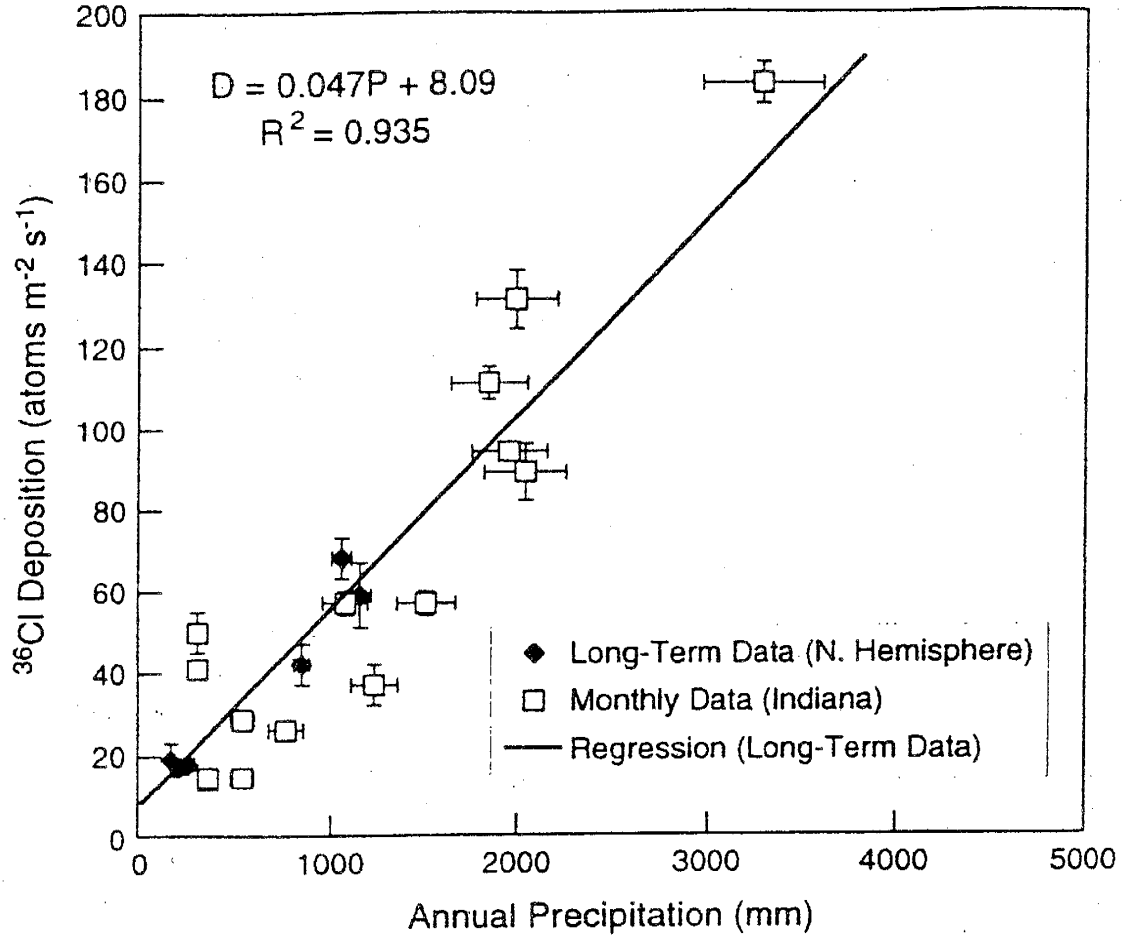

Figure 3.9: Correlation between ^{36}Cl deposition and annual precipitation. Long-term data is from selected sites in Table 3.1 (Weiss Fluhjoch, Handford, Lafayette, Elms, Guliya, and Socorro). Monthly deposition measured at West Lafayette, Indiana by Knies (1994) and monthly Lafayette precipitation was converted to annual equivalent. (Phillips, 1999)

$$S_P(\lambda) = \frac{D_{calc}(\lambda)}{D_{calc}(\lambda_o)} S_P(\lambda_o) \qquad \text{Eqn 3.4}$$

where $D_{calc}(\lambda)$ is the latitudinal dependence of cosmogenic fallout from Parrat et al. (1996) and λ_o is the latitude at which the slope was determined.

Phillips (1999) used Equation 3.4 to normalize the measured ^{36}Cl deposition rates

$$D_{36}^{norm} = D_{36}^{m} - S_P(\lambda)(P - \overline{P}(\lambda)) \qquad \text{Eqn 3.5}$$

where D_{36}^{m} is the measured ^{36}Cl deposition rate. Normalized values of ^{36}Cl deposition are provided in Figure 3.8(b) and exhibit much less scatter. Mean latitudinal precipitation values were taken from Baumgartner and Reichel (1975), as illustrated in Figure 3.8(c). The normalized values in Figure 3.8(b) are greater than those predicted by either Lal and Peters (1967) or Parrat et al. (1996). Phillips (1999) performed a linear scaling of the Parrat et al. (1996) curve which minimized the weighted chi-squared residuals with the measured values and found a curve yielding a globally-averaged deposition rate 47±5 percent higher than the prediction (dashed line in Figure 3.8(b)). The most likely explanation for the current theoretical underestimation of ^{36}Cl deposition is an additional, unquantified cosmic-ray reaction (Phillips, 1999). The proton spallation of ^{40}Ar at the energy range of solar cosmic rays has been suggested, after the measurement of high cross-sections for this reaction (Parrat et al., 1996).

Phillips (1999) derived a model for the geographical distribution of meteoric ^{36}Cl fallout by substituting Equation 3.4 into 3.3

$$D_{36}(P,\lambda) = D_{36}(\lambda)\left\{1+\frac{S_P(\lambda_o)}{D_{36}(\lambda_o)}\left[P-\overline{P}(\lambda)\right]\right\} \qquad \text{Eqn 3.6}$$

The value of the ratio $S_P(\lambda_o)/D_{36}(\lambda_o)$ is suggested to be 1.11 x 10^{-3} year mm^{-1}, $\overline{P}(\lambda)$ can be taken from Figure 3.8(c), and $D_{36}(\lambda)$ can be taken from the dashed curve in Figure 3.8(b).

3.3 The ^{36}Cl/Cl Ratio

The presence of ^{36}Cl in water (meteoric or otherwise) is commonly reported by one of two measures. One measure is the concentration expressed as the number of ^{36}Cl atoms per unit volume (typically one liter) of water. The second is the ratio of the number of ^{36}Cl atoms to the number of stable chlorine atoms (Davis et al., 1998). Each measure has advantages and disadvantages. Measures of ^{36}Cl as concentration are not affected by the addition of stable chloride to the system, but are highly sensitive to variations induced by evapotranspiration. The opposite is true of measures using the ratio; the ratio is insensitive to evapotranspiration but highly sensitive to the addition of stable chloride. Both measures are affected by the introduction of ^{36}Cl to the system (i.e. in situ production) and by radioactive decay (Davis et al., 1998). In previous studies, atmospheric deposition of ^{36}Cl has been expressed using the ratio of atoms of ^{36}Cl to atoms of stable chloride, and this convention is continued here. Typical ^{36}Cl/Cl ratios for atmospheric deposition are on the order of 100 to 1000 x 10^{-15}.

CHAPTER 4 – ^{36}Cl/Cl SPATIAL DISTRIBUTION MODELING

The main purpose of this study was to construct a statistical model to estimate the chloride and ^{36}Cl deposition over the conterminous United States. The model is intended to incorporate important climatic factors that influence atmospheric deposition. Analysis of the relationship between climatic factors, geography, and deposition allows estimation of deposition based on easily measured parameters. If a model based on simple climatic and geographic parameters can be constructed to match measured deposition values, then the model represents a powerful improvement over models based on interpolation of measurements alone, in that the effect of parameter changes on the deposition pattern can be assessed. For example, the parameter-based model can be used to estimate past deposition patterns by incorporating known past climatic conditions. A model based on modern measurements alone cannot be used in this way.

The primary factors controlling continental deposition of stable chloride are amount of precipitation and distance inland from the coastal source (Simpson and Herczeg, 1994). Figure 2.1 illustrates the nearly exponential decrease of chloride concentration in precipitation with increasing distance from the coast. Chloride is positively correlated to the amount of precipitation and will be shown to exhibit a linear relation with rainfall. In Chapter 3, ^{36}Cl deposition was shown to depend on both latitude and the amount of precipitation. A model for ^{36}Cl deposition based on these parameters was developed by Phillips (1999).

The spatial distribution of ^{36}Cl/Cl ratios over the United States was modeled by combining the Phillips (1999) model for ^{36}Cl deposition with a newly developed model of stable chloride deposition based on precipitation and distance from the coast. The stable

chloride distribution model was constructed using correlation of chloride deposition with these two parameters developed from precipitation chemistry analyses of the National Atmospheric Deposition Program / National Trends Network (NADP/NTN). A model of precipitation over the United States was used as a base model for stable chloride deposition. Precipitation from the Parameter-elevation Regressions on Independent Slopes Model (PRISM) was converted to chloride deposition using the relationships found from the NADP/NTN. The stable chloride distribution model is the first of its kind to incorporate measured dry deposition values throughout the country. Previous models have either multiplied the wet deposition component by a uniform value (typically 1.3) or have ignored the dry deposition component completely. This chapter discusses the construction of the $^{36}Cl/Cl$ ratio distribution model. First, three previous models of this distribution are described. Next, a description of the NADP/NTN network and precipitation-chloride deposition correlations is given, followed by a description of the PRISM model and its use to calculate the wet stable chloride distribution. The distribution of dry deposition measured by the NADP/NTN is then added to arrive at the total deposition of stable chloride across the country. The new stable chloride model is combined with the Phillips (1999) model of ^{36}Cl deposition to calculate $^{36}Cl/Cl$ ratios for the United States.

4.1 Previous Investigations

The spatial distribution of atmospheric $^{36}Cl/Cl$ ratios across the United States has been described by three previous models (Bentley et al., 1986a; Hainsworth, 1994; Moysey, 1999). These models combined the separate estimation of the ^{36}Cl and stable chloride distributions to determine the spatial distribution of the $^{36}Cl/Cl$ ratio. The two

earlier models used differing methods of calculating the ^{36}Cl deposition distribution, but both relied on nationwide observations of precipitation chemistry to evaluate the stable chloride contribution. The Moysey (1999) model used measured $^{36}Cl/Cl$ ratios from shallow groundwater recharged between ~10,000 and ~50 years ago as a surrogate to the meteoric input.

The first model of $^{36}Cl/Cl$ distribution was developed by Bentley, Phillips, and Davis in 1986. The spatial variability of ^{36}Cl deposition was developed by modifying the latitude-dependent fallout of long-lived cosmogenic nuclides proposed by Lal and Peters (1967; Figure 3.3) using the global average production rate of ^{36}Cl. The latitude dependence of ^{36}Cl fallout was shown in Figure 3.7. As previously discussed, the peak at 40^{o} is due to stratospheric / tropospheric mixing processes in the mid-latitudes. Stable chloride deposition was taken from calculations of chloride in precipitation made by Eriksson (1960) using precipitation data combined with rainfall concentration data measured by Junge and Werby (1958). The collectors used by Junge and Werby (1958) were closed between precipitation events and only measured wet deposition. Bentley et al. (1986a) corrected for the addition of dry deposition by multiplying the stable chloride distribution from Eriksson (1960) by 1.3. Figure 4.1 shows the $^{36}Cl/Cl$ ratios in precipitation as calculated by the Bentley et al. (1986a) model.

Hainsworth (1994) employed a substantially different method to estimate the ^{36}Cl deposition. Atmospheric fallout from the stratosphere and troposphere were treated separately and were summed to determine the total fallout. The model assumed that 70% of the mean global ^{36}Cl was produced within the stratosphere.

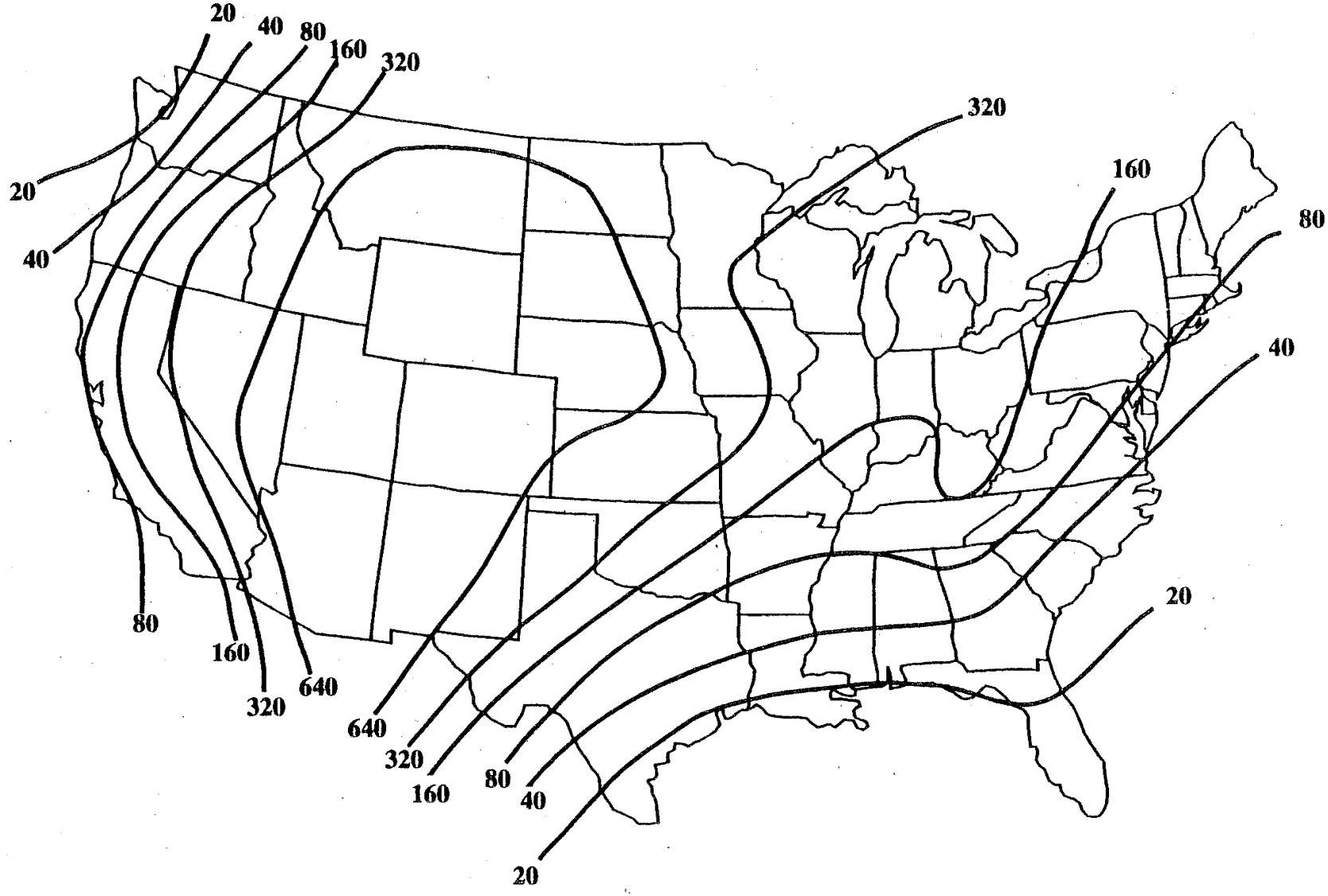

Figure 4.1: Distribution of $^{36}Cl/Cl$ ratios across the U.S. as calculated by Bentley et al. (1986a)

Hainsworth (1994) recognized that longitudinal variations in ^{36}Cl deposition were important, in addition to the latitudinal variation shown in Figure 3.7. The longitudinal variability arises from the affect of landforms, such as mountain ranges, on meteorological processes. The deposition pattern of ^{90}Sr provided evidence for the longitudinal variability of cosmogenic nuclide fallout. Strontium-90 was injected directly into the stratosphere by weapons testing during the 1950's and 1960's. Potential adverse health effects of ^{90}Sr led to the careful monitoring of its deposition across North America. Contours of ^{90}Sr concentration in soils are shown in Figure 4.2 and can be seen to follow the Rocky Mountain range. This indicates that this range has an effect on stratospheric / tropospheric mixing. Hainsworth (1994) used the measured ^{90}Sr data to predict the deposition of stratospheric ^{36}Cl by multiplying the mean stratospheric ^{36}Cl production by a focusing factor. The focusing factor was defined as local ^{90}Sr concentration divided by the mean northern hemispheric ^{90}Sr concentration. Tropospheric deposition was calculated with the assumption that ^{36}Cl produced in the upper troposphere was immediately available to be scavenged and deposited. Tropospheric deposition was a function of local precipitation compared with the mean zonal precipitation (i.e. a precipitation focusing factor). The stratospheric and tropospheric components of fallout were combined to determine the total ^{36}Cl deposition.

The stable chloride flux was determined using chloride concentrations from the National Atmospheric Deposition Program / National Trends Network (NADP/NTN) for the year 1989. The NADP/NTN data is more complete and reliable than that used in the Bentley et al. (1986a) model but, as with Junge and Werby's 1958 measurements, only assess wet deposition. Hainsworth (1994) did not correct for dry deposition, and noted that

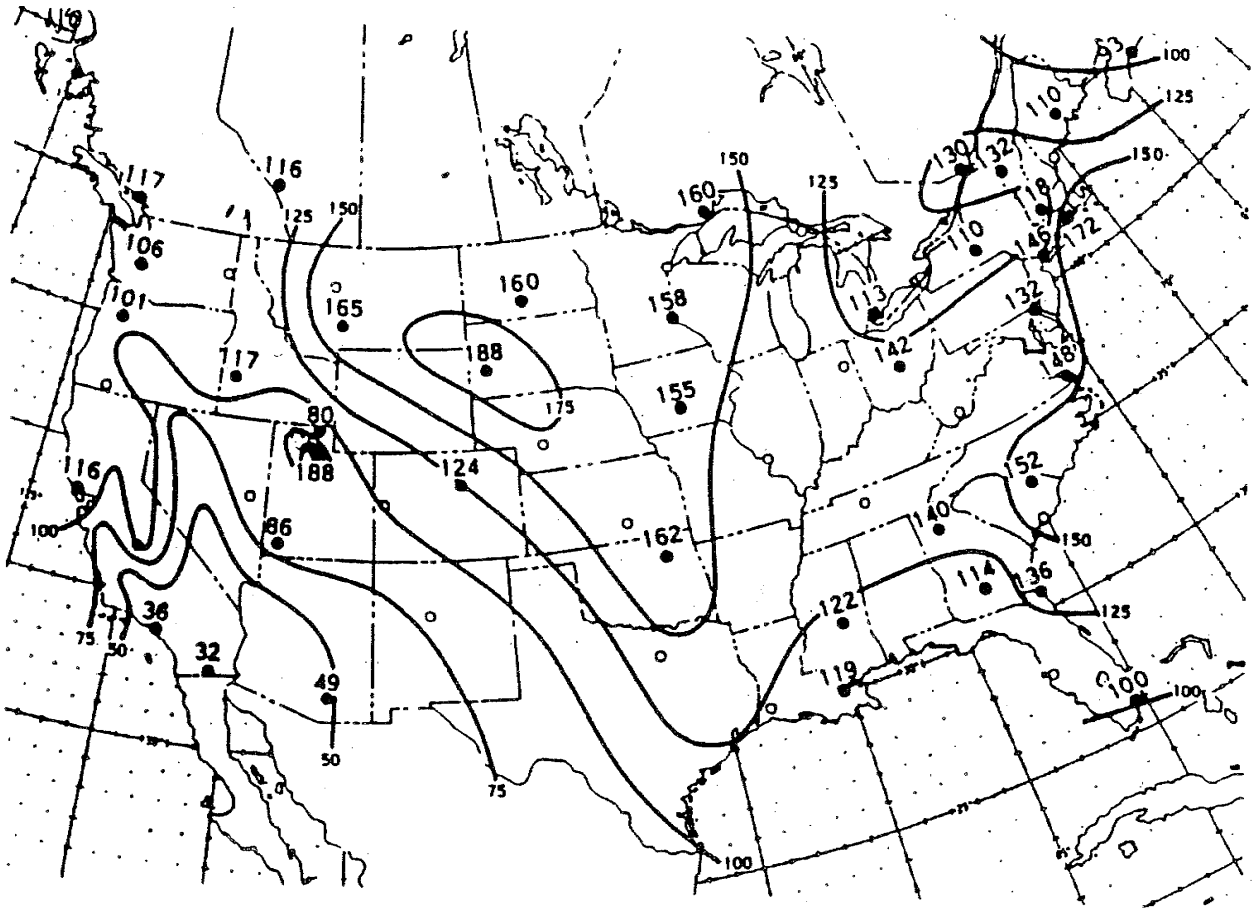

Figure 4.2: Distribution of ^{90}Sr in soils across the U.S. following thermonuclear weapons testing. Measurements from 1963 and 1964 in millicuries/mi^2. (from Hainsworth, 1994)

stable chloride concentrations used in her model were a lower limit. The $^{36}Cl/Cl$ ratios calculated using the Hainsworth (1994) model are shown in Figure 4.3. The contour lines are similar to those from the Bentley et al. (1986a) model, but the predicted ratios are approximately a factor of two higher.

Moysey (1999) described the $^{36}Cl/Cl$ ratio distribution by measuring the ratio in shallow groundwater recharged earlier than ~50 years ago but more recently than ~10,000 years ago. Recent recharge was undesirable in order to avoid the effects of anthropogenic ^{36}Cl from thermonuclear weapons testing. Groundwater greater than ~10,000 years old was also avoided in order to provide an accurate measure of the modern $^{36}Cl/Cl$ ratio and because of evidence that ^{36}Cl production was greater prior to this time as a result of a decrease in the strength of Earth's geomagnetic field. Moysey measured the ratio of one to several groundwater samples within 37 groups across the country and incorporated numerous measurements from previous studies. These groups and the empirical distribution of $^{36}Cl/Cl$ ratios developed from them are shown in Figure 4.4. Moysey also postulated that the ^{36}Cl deposition could be considered constant across the United States, based on his measurements, with a value of 21.3 atoms m^{-2} s^{-1}. The spatial variability of the $^{36}Cl/Cl$ ratio was then dependant only upon the distribution of stable chloride.

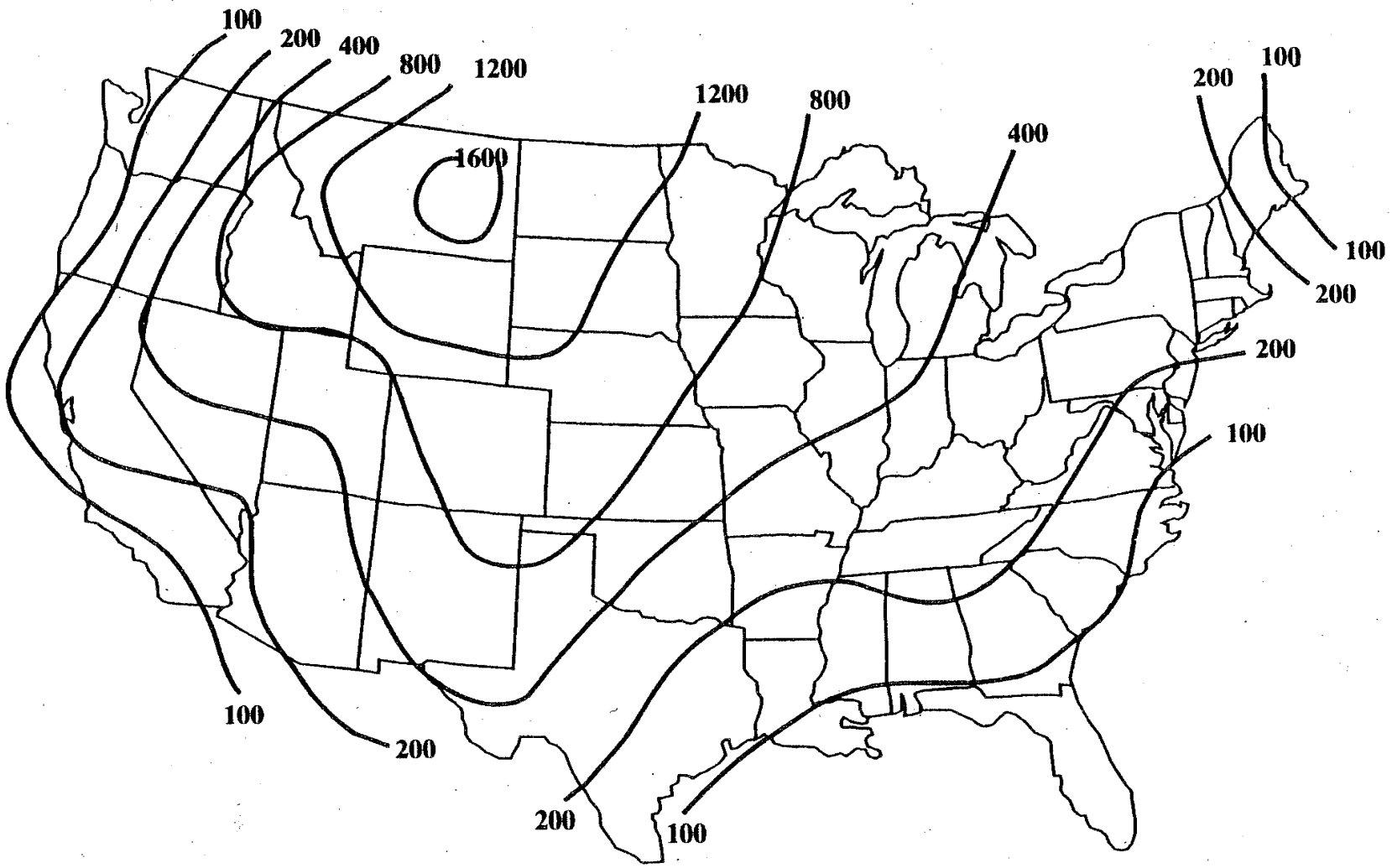

Figure 4.3: Distribution of $^{36}Cl/Cl$ ratios across the U.S. as calculated by Hainsworth (1994).

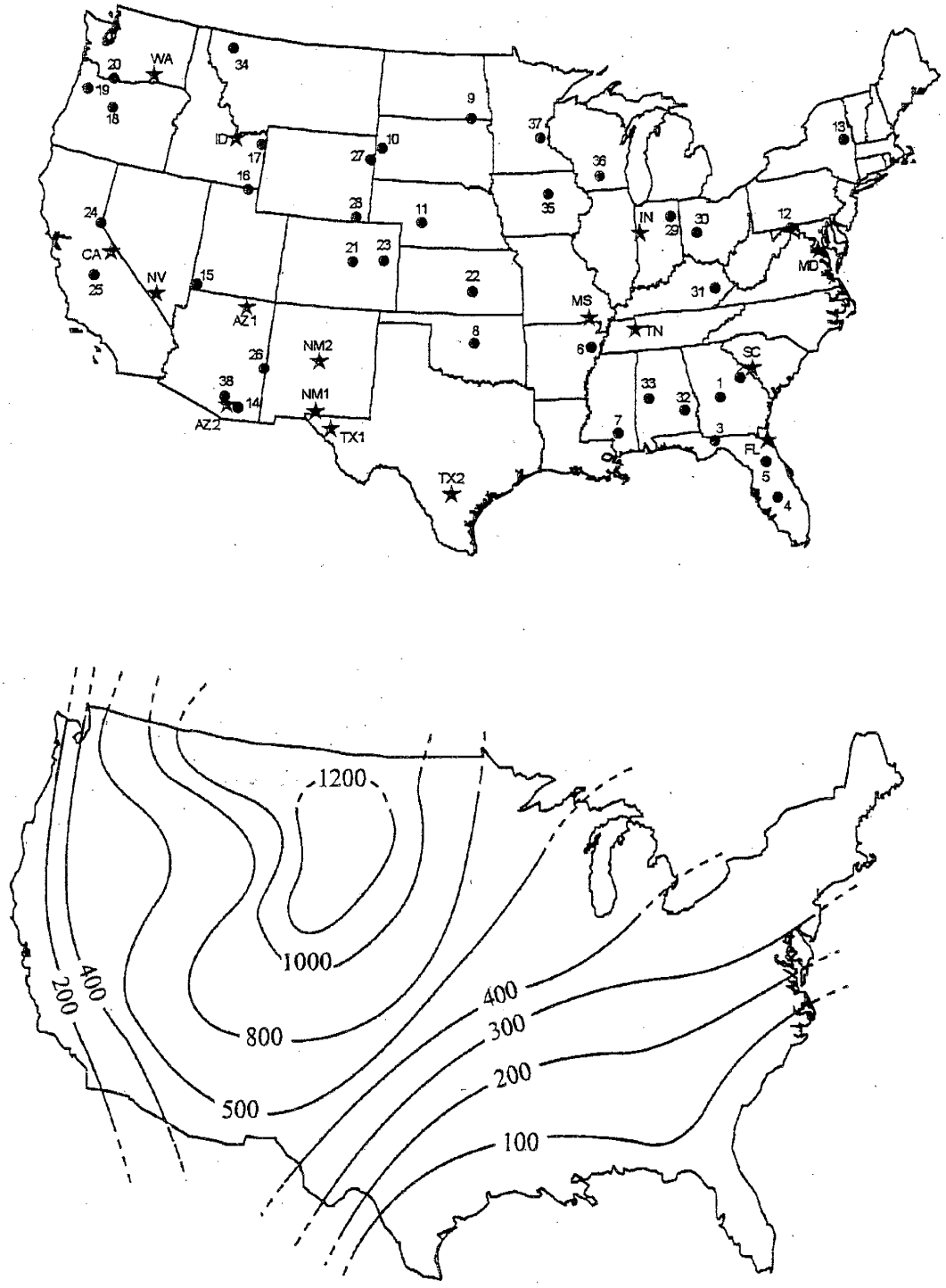

Figure 4.4: Locations of sampling groups and empirical distribution of $^{36}Cl/Cl$ ratios measured by Moysey (1999). Circles are control groups sampled by Moysey, and stars are previous studies by other authors (see Table 5.5). (Moysey, 1999)

4.2 Modeling the Stable Chloride Distribution

Analysis of precipitation chemistry from the NADP/NTN revealed a positive linear relationship between chloride deposition and precipitation, as predicted by Equation 2.2(b). The slope of the regression line changed with distance from the coast. These relationships were used to construct a model that estimated the deposition of stable chloride across the United States by combination with a pre-existing model of precipitation.

4.2.1 NADP/NTN collector network

This program is administered by the NADP/NTN Coordination Office at Colorado State University. Information on the program can be obtained through a web address, or by contacting the Coordination Office or the Program Office; addresses are provided in the bibliography. A brief summary of the program is included here.

The National Atmospheric Deposition Program (NADP) was established in 1978 as a catalyst for research addressing the problem of acidic deposition. The main objective of the network was to determine the spatial and temporal trends in chemical deposition to support research on the depositional impacts to aquatic and terrestrial ecosystems. This goal was to be met by establishing a long-term atmospheric deposition monitoring network at a national scale. The first sites were installed in July 1978, growing to 22 stations by the end of the year. The network grew to 39 stations by the end of 1979 and to 110 stations by the end of 1982. At this time the federal National Acid Precipitation Assessment Program (NAPAP) was initiated and, under the direction of the U.S. Geological Survey (USGS), additional sites were added to the NADP network to meet the 150-site design goal of the NAPAP National Trends Network (NTN). In 1983 the network was renamed NADP/NTN

and continued to grow by the addition of NTN sites; the network contained 143 stations by the end of 1983 and 204 by the end of 1986. The number of stations in the NADP/NTN network has since stabilized at approximately 200 sites. Station locations are shown in Figure 4.5.

The program characterizes regional deposition patterns on a national scale using monitoring sites located far from point sources and large urban centers. The collection network has operated continuously in order to produce the long-term data necessary to determine temporal trends in precipitation chemistry. The network was originally designed to measure total atmospheric deposition, both wet and dry. Concerns about the methodology for collecting dry deposition led to the abandonment of dry collection at many sites shortly after 1984. The available dry deposition data is discussed and evaluated in detail in a subsequent section. The network consists of AeroChem Metrics model 301 wet/dry sampling devices from which the wet-side sampling container is collected once a week. Samples are sent exclusively to the Central Analytical Laboratory (CAL), operated by the Illinois State Water Survey at the University of Illinois. Precipitation is measured on a daily basis with a 12-inch capacity recording rain gauge. Daily precipitation and weekly precipitation chemistry are provided to the Coordination Office where a database is maintained. Summary records are generated for annual, quarterly, and monthly periods and are made available on the NADP/NTN website. Precipitation and chemistry data are subject to rigid QA/QC checks and must pass certain Data Completeness Criteria for inclusion in published maps and data summary tables.

Figure 4.5: NADP/NTN station locations. Data from NADP/NTN (1998)

4.2.2 Regressions of precipitation versus chloride collection

To conduct this study, all available monthly precipitation and precipitation chemistry data (through 1998) were obtained from the NADP/NTN website and filtered to meet their Data Completeness Criteria. The relationship between chloride deposition and the amount of precipitation was assessed by plotting the mass of chloride (mg) collected each month against monthly precipitation (cm). Examples of such plots are shown in Figure 4.6. In each case, there is increasing scatter with higher precipitation, but overall there is a moderate to distinct linear trend. For each NADP/NTN station, the monthly collected mass of chloride was calculated by multiplying the volume (L) of precipitation collected during each month of record by the concentration of chloride (mg/L) measured for each corresponding month. This mass (mg) of chloride was then plotted against the measured precipitation amount (cm) for each corresponding month, as in Figure 4.6. These plots represent the relationship between chloride collection and precipitation for a generic month, at a particular station. I say 'generic' month because the data in Figure 4.6 were not plotted with regard to a specific month (such as only all Januaries), but rather represent the typical relationship between chloride collection and precipitation over any one-month period, at a particular station. The plots in Figure 4.6 do not account for seasonality, and the possibility that the relationship changes at different times of the year. The issue of seasonality will be discussed in greater detail below.

The relationship between monthly chloride collection and monthly precipitation (again, for a one-month period, not a specific month) was analyzed by fitting the data with a least squares linear regression line. The wet side of each NADP/NTN collector is closed between precipitation events, so the mass of chloride collected when there is no

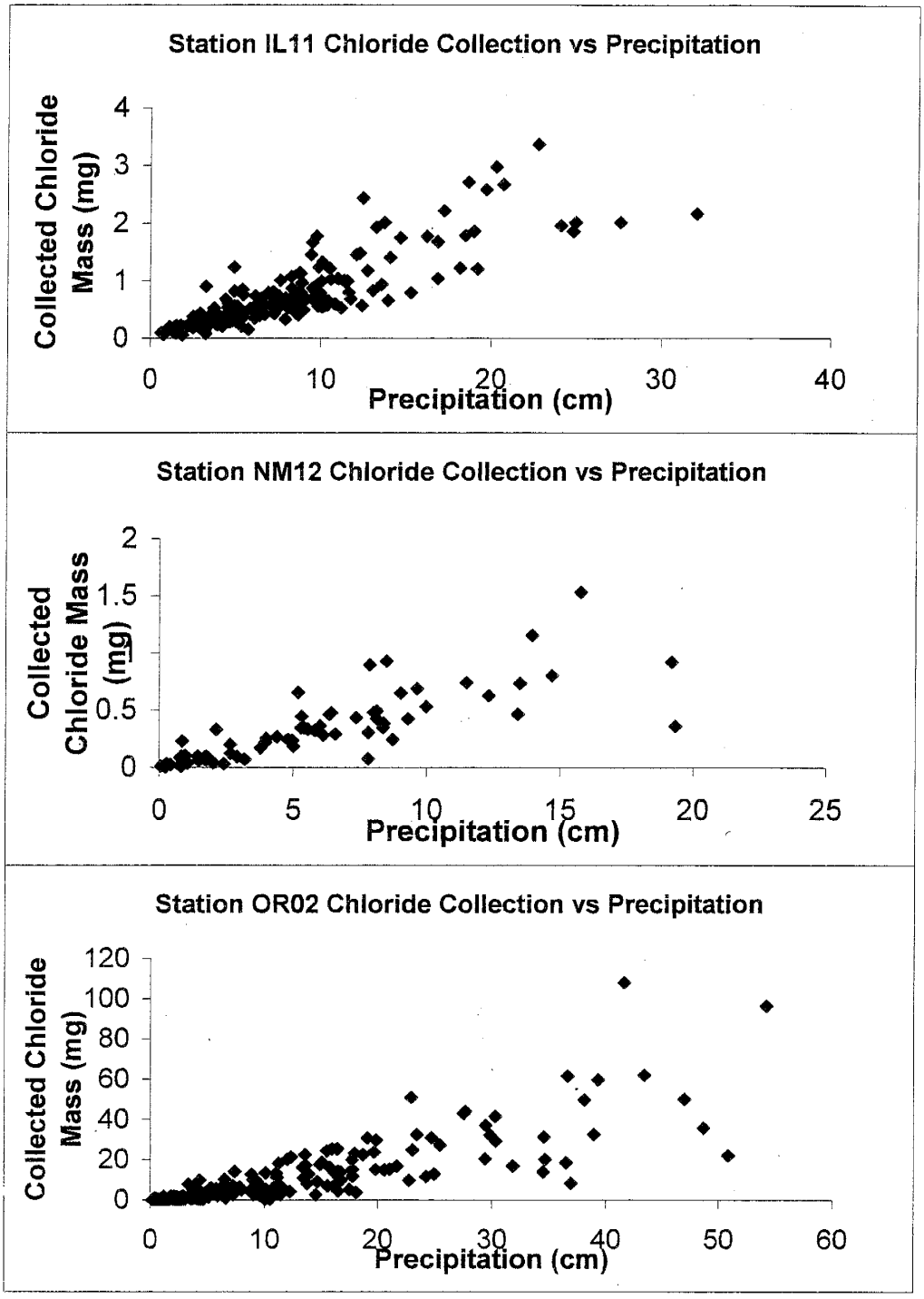

Figure 4.6: Chloride collection versus precipitation at selected NADP/NTN stations. Data from NADP/NTN (1998).

precipitation should be zero. Thus, the linear regression line was forced through zero. Figure 4.7 shows the linear regression for the data from each station in Figure 4.6, and includes the slope of the regressions. The slope of the least squares linear regression line for each of the NADP/NTN stations is provided in Table 4.1. Careful inspection of the table reveals that the slope of the regression changes depending on the distance of the station from the coastal chloride source. This behavior is better illustrated in Figure 4.8, which was created by interpolating (using an inverse distance weighting scheme) the regression slopes measured at each NADP/NTN station. The slope decreases with increasing inland distance due to decreasing chloride concentrations in precipitation. For equal precipitation, chloride deposition is lower in the continental interior than along the coast, leading to reduced regression slopes. One major exception is the region near the Great Salt Lake, Utah where entrainment of evaporite deposits may provide an additional local source of atmospheric chloride, and increased regression slopes.

The initial regression of chloride collection against precipitation (Figure 4.7) did not account for seasonality and only provided an estimate of the average chloride collection over any one-month time period. A more rigorous analysis of the relationship between chloride collection and precipitation was performed by subdividing the data at each station into individual months (January through December). For instance, all data for a particular station during only January were plotted as in Figure 4.6. In this manner, the relationship between chloride collection and precipitation during a particular month could be determined, allowing for the possibility that the relationship changes during different times of the year. In New Mexico, approximately 60 percent of annual precipitation falls during the summer months (June through September) which represent only one-third of the

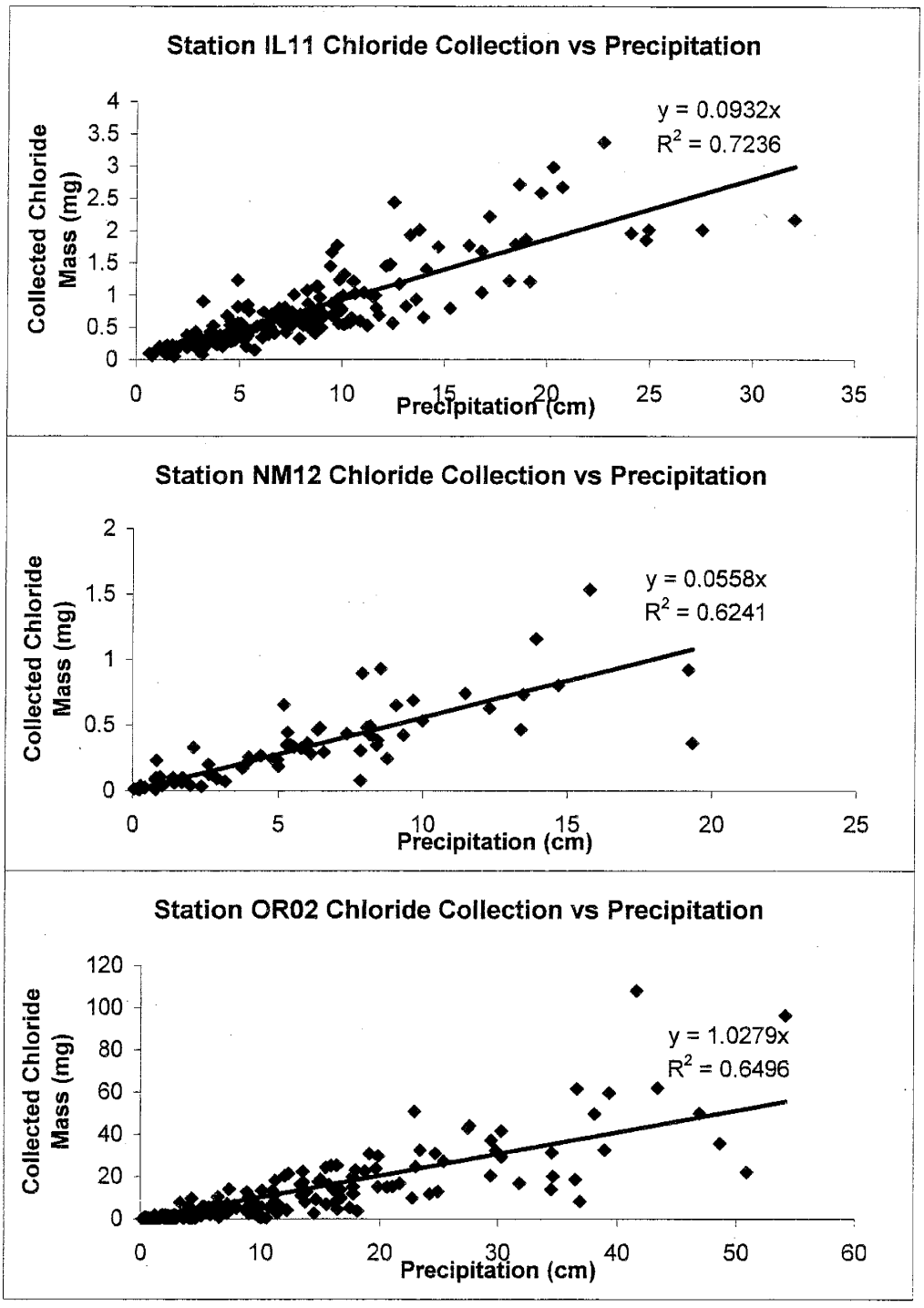

Figure 4.7: Sample linear regressions of chloride collection versus precipitation. Data from NADP/NTN (1998).

Table 4.1: Least squares linear regression slopes for NADP/NTN stations

Site ID	Latitude (°N)	Longitude (°W)	Cl Deposition/ Precipitation Regression Slope (mg/cm)*	Site ID	Latitude (°N)	Longitude (°W)	Cl Deposition/ Precipitation Regression Slope (mg/cm)*
AL10	32.4583	-87.2422	0.174	IL99	38.7100	-88.7492	0.079
AL99	34.2878	-85.9689	0.136	IN20	40.8400	-85.4639	0.080
AR02	33.6050	-92.0972	0.157	IN22	38.7408	-87.4856	0.117
AR03	34.1794	-93.0986	0.146	IN34	41.6325	-87.0878	0.093
AR16	36.0839	-92.5869	0.108	IN41	40.4753	-86.9922	0.092
AR27	36.1006	-94.1733	0.100	KS07	37.6511	-94.8036	0.084
AZ01	31.7089	-110.0572	0.096	KS31	39.1022	-96.6092	0.075
AZ03	36.0717	-112.1550	0.071	KS32	38.6717	-100.9164	0.064
AZ06	31.9506	-112.8000	0.203	KY03	37.7047	-85.0489	0.115
AZ99	33.0714	-109.8647	0.077	KY22	37.0778	-82.9936	0.077
CA34	37.3708	-118.3664	0.070	KY35	38.1183	-83.5469	0.076
CA42	34.2072	-117.7611	0.198	KY38	36.7906	-88.0672	0.106
CA45	39.0047	-123.0847	0.405	KY99	36.9014	-88.0136	0.111
CA68	33.3089	-116.8539	0.362	LA06	32.7514	-93.0506	0.172
CA75	36.5669	-118.7772	0.063	LA12	29.9297	-91.7153	0.353
CA76	41.7664	-122.4783	0.031	LA30	30.8114	-90.1808	0.313
CA88	38.5353	-121.7750	0.278	MA01	41.9758	-70.0247	1.561
CA98	34.8061	-119.0114	0.059	MA08	42.3925	-72.3444	0.140
CA99	37.7961	-119.8581	0.073	MA13	42.3839	-71.2147	0.402
CO00	37.4414	-105.8653	0.058	MD03	39.4089	-76.9953	0.187
CO01	38.1178	-103.3161	0.066	MD13	38.9131	-76.1525	0.274
CO02	40.0553	-105.5883	0.057	ME00	46.8689	-68.0131	0.069
CO08	39.4031	-107.3411	0.049	ME02	44.1075	-70.7289	0.204
CO15	40.5075	-107.7019	0.065	ME09	45.4892	-69.6653	0.088
CO19	40.3642	-105.5819	0.057	ME97	46.6547	-68.0089	0.071
CO21	39.1011	-105.0919	0.059	ME98	44.3739	-68.2606	0.761
CO22	40.8064	-104.7547	0.058	ME99	44.4083	-68.2461	0.608
CO91	37.4686	-106.7903	0.034	MI09	45.5608	-84.6783	0.055
CO92	39.4272	-107.3797	0.055	MI22	47.2269	-88.6308	0.063
CO93	40.5347	-106.7800	0.041	MI25	47.9153	-89.1525	0.057
CO94	39.9939	-105.4800	0.042	MI26	42.4103	-85.3928	0.073
CO95	37.6597	-107.7992	0.052	MI53	44.2242	-85.8186	0.063
CO96	37.7514	-107.6853	0.049	MI97	48.0575	-88.6342	0.038
CO97	40.5383	-106.6747	0.036	MI98	46.3742	-84.7414	0.047
CO98	40.2878	-105.6628	0.049	MI99	47.1047	-88.5514	0.043
CO99	37.1981	-108.4903	0.050	MN01	45.4125	-93.2125	0.045
FL00	29.7603	-82.1989	0.282	MN05	46.7131	-92.5108	0.034
FL03	29.9747	-82.1981	0.253	MN08	47.8472	-89.9625	0.034
FL05	28.7494	-82.5542	0.482	MN16	47.5311	-93.4686	0.045
FL11	25.3900	-80.6800	0.516	MN18	47.9464	-91.4961	0.045
FL14	30.5481	-84.6008	0.288	MN23	46.2494	-94.4972	0.037
FL41	27.3800	-82.2839	0.363	MN27	44.2372	-95.3006	0.055
FL99	28.5428	-80.6444	0.821	MN28	46.1208	-93.0042	0.036
GA09	30.7403	-82.1286	0.249	MN99	47.3875	-91.1958	0.035
GA20	32.1411	-81.9714	0.244	MO03	38.7536	-92.1989	0.078
GA23	31.2253	-81.3922	0.466	MO05	36.9108	-90.3186	0.130
GA41	33.1778	-84.4061	0.155	MO50	37.3986	-93.0425	0.107
GA50	31.4731	-83.5331	0.197	MS10	32.3067	-90.3183	0.192
GA99	31.5183	-83.5483	0.169	MS14	32.3344	-88.7450	0.188
IA08	42.9097	-91.4700	0.056	MS19	32.3347	-89.1658	0.144
IA23	40.9631	-93.3925	0.056	MS30	34.0025	-89.8000	0.136
ID03	43.4614	-113.5547	0.078	MT00	45.5686	-107.4375	0.051
ID04	46.6278	-115.8194	0.043	MT05	48.5103	-113.9958	0.033
ID11	43.2053	-116.7492	0.053	MT07	46.4850	-112.0647	0.041
ID15	44.2978	-116.0636	0.041	MT13	48.4886	-105.2083	0.041
IL11	40.0533	-88.3719	0.093	MT97	45.6917	-113.9656	0.024
IL18	41.8414	-88.8511	0.074	MT98	48.4992	-109.7975	0.036
IL19	41.7011	-87.9953	0.108	MT99	48.7411	-113.4300	0.028
IL35	37.7100	-89.2689	0.109	NC03	36.1325	-77.1714	0.268
IL47	38.6433	-88.9669	0.099	NC11	35.9025	-78.8700	0.120
IL63	37.4356	-88.6719	0.123	NC25	35.0606	-83.4306	0.125
IL78	40.9333	-90.7231	0.067	NC33	35.8964	-78.8606	0.132
NC34	35.6969	-80.6225	0.164	SC18	34.6239	-82.7342	0.107

Table 4.1: Least squares linear regression slopes for NADP/NTN stations

NC35	35.0258	-78.2783	0.301	SD00	44.3842	-98.2206	0.055
NC36	34.9708	-79.5283	0.210	SD08	43.9492	-101.8583	0.039
NC41	35.7283	-78.6803	0.215	SD99	44.3550	-98.2908	0.051
NC45	35.7353	-82.2861	0.057	TN00	35.9614	-84.2872	0.130
ND07	47.6014	-103.2642	0.042	TN11	35.6644	-83.5903	0.068
ND08	48.7825	-97.7542	0.038	TN14	35.4678	-89.1586	0.117
ND11	47.1256	-99.2369	0.046	TN98	35.1825	-87.1964	0.114
NE15	41.1531	-96.4928	0.079	TN99	35.2847	-86.9033	0.103
NE99	41.0592	-100.7464	0.046	TX02	33.9578	-102.7761	0.083
NH02	43.9431	-71.7033	0.107	TX03	28.4667	-97.7069	0.457
NJ29	40.3456	-74.6169	0.363	TX04	29.3022	-103.1772	0.075
NJ99	40.3150	-74.8547	0.235	TX10	29.6614	-96.2594	0.298
NM01	33.2203	-108.2347	0.064	TX16	30.2614	-100.5550	0.117
NM07	35.7817	-106.2675	0.052	TX18	33.9242	-100.0469	0.085
NM08	32.9094	-105.4706	0.042	TX21	32.3786	-94.7117	0.205
NM09	36.0408	-106.9714	0.060	TX22	31.9083	-104.8067	0.053
NM12	36.7789	-103.9814	0.056	TX38	31.5606	-94.8608	0.219
NV00	36.1358	-115.4256	0.054	TX51	33.2733	-99.2153	0.126
NV01	41.2853	-115.8522	0.072	TX53	28.8453	-96.9203	0.454
NV03	38.7992	-119.2567	0.040	TX56	33.3917	-97.6397	0.141
NV05	39.0050	-114.2158	0.098	UT01	41.6583	-111.8969	0.252
NY08	42.7339	-76.6597	0.083	UT08	41.3575	-111.0486	0.114
NY10	42.2994	-79.3964	0.085	UT98	38.9983	-110.1653	0.074
NY12	42.3783	-73.5028	0.100	UT99	37.6186	-112.1728	0.067
NY20	43.9731	-74.2231	0.060	VA00	38.0406	-78.5431	0.126
NY51	41.3500	-74.0394	0.202	VA13	37.3314	-80.5575	0.076
NY52	43.5261	-75.9472	0.088	VA28	38.5225	-78.4358	0.113
NY65	42.1064	-77.5358	0.066	VA29	36.6389	-81.6058	0.050
NY68	41.9936	-74.5036	0.099	VA33	36.7367	-81.6869	0.105
NY98	44.3933	-73.8594	0.042	VT01	42.8761	-73.1633	0.078
NY99	41.3508	-74.0486	0.259	VT99	44.5283	-72.8689	0.042
OH09	39.5314	-84.7242	0.088	WA14	47.8600	-123.9319	0.555
OH17	40.3553	-83.0661	0.097	WA15	48.8433	-117.2839	0.044
OH49	39.7928	-81.5311	0.109	WA19	48.5406	-121.4453	0.133
OH71	40.7822	-81.9200	0.090	WA21	46.8353	-122.2867	0.230
OK00	36.8053	-98.2006	0.112	WA24	46.7606	-117.1847	0.043
OK17	34.9800	-97.5214	0.104	WI09	45.7964	-88.3994	0.046
OK25	34.5297	-95.3531	0.168	WI25	45.0533	-88.3728	0.054
OK29	36.5908	-101.6175	0.076	WI28	44.6644	-89.6525	0.057
OR02	44.3856	-123.6153	1.028	WI36	46.0528	-89.6531	0.044
OR08	42.6678	-122.6831	0.093	WI37	45.8228	-91.8744	0.048
OR09	43.1217	-121.0578	0.038	WI98	43.7022	-90.5686	0.049
OR10	44.2122	-122.2558	0.206	WI99	42.5792	-88.5006	0.069
OR11	43.8994	-117.4269	0.060	WV04	37.9800	-80.9500	0.070
OR17	45.6900	-118.8378	0.093	WV18	39.0897	-79.6622	0.073
OR18	45.2244	-118.5114	0.032	WY00	41.3761	-106.2594	0.047
OR97	44.6347	-123.1900	0.443	WY02	42.7339	-108.8500	0.035
OR98	45.4478	-122.1481	0.364	WY06	42.9289	-109.7867	0.071
OR99	44.6264	-123.2139	0.413	WY08	44.9172	-110.4203	0.059
PA15	40.7883	-77.9458	0.088	WY95	41.3647	-106.2408	0.049
PA29	41.5978	-78.7675	0.094	WY96	41.3403	-106.1908	0.062
PA42	40.6575	-77.9397	0.100	WY97	42.4947	-108.8292	0.051
PA72	41.3275	-74.8203	0.129	WY98	43.2228	-109.9911	0.045
SC06	33.5394	-80.4350	0.236	WY99	43.8733	-104.1922	0.047

* Regression of monthly chloride collection (mg) versus monthly precipitation (cm)

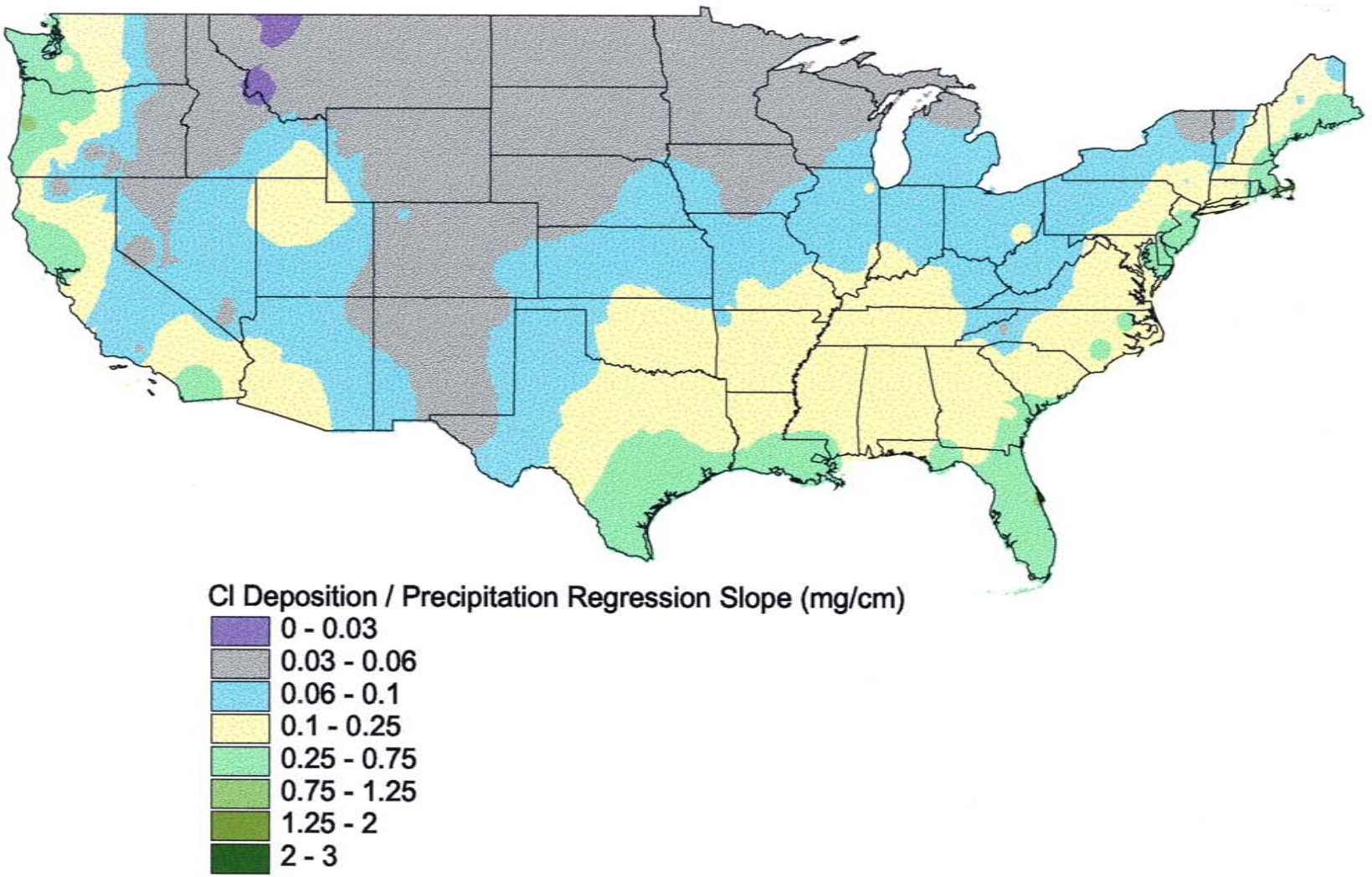

Figure 4.8: Interpolated chloride deposition / precipitation regression slopes. Values interpolated from data in Table 4.1.

year. In much of California, very little precipitation falls during the summer months, falling instead mainly during the winter months. By analyzing the chloride collection and precipitation relationship for each individual month, the potential effect of these seasonal precipitation cycles could be assessed. For each month at every NADP/NTN station, a least squares linear regression was fit through the subdivided data representing only that month. The regression slope for each month at all NADP stations is presented in Table 4.2. The slope of the regression was found to, indeed, change during the course of a year. For instance, in New Mexico the regression slope is steepest during the wet summer months, and shallowest during the winter. The change in regression slope during the course of a year is most pronounced in areas, such as New Mexico, with monsoonal climates, where precipitation is concentrated during certain months of the year. Figures 4.9 and 4.10 illustrate the change in chloride collection / precipitation regression slopes across the country over each month of the year. The overall pattern of decreasing regression slopes with increasing inland distance (as shown in Figure 4.8) is still observed, but the slope can change significantly at different times of the year throughout the midwest and southwest. One explanation for the seasonal slope variation could be seasonal weather patterns. In New Mexico, summertime monsoonal rainstorms originate from the Gulf Coast, while winter precipitation originates from the Pacific Ocean. The effective transport distance of winter precipitation is greater than that of summer precipitation and, since the chloride concentration in an air mass is dependant on the distance from the coast, more chloride can be delivered for an equal precipitation amount during the summer than in the winter.

Table 4.2: Monthly least squares linear regression slopes (Cl deposition vs precipitation) for NADP/NTN stations.

	Chloride Deposition / Precipitation Regression Slopes by Month (mg/cm)											
Station	January	February	March	April	May	June	July	August	September	October	November	December
AL10	0.239	0.261	0.205	0.272	0.229	0.137	0.108	0.103	0.101	0.163	0.180	0.165
AL99	0.157	0.173	0.124	0.152	0.161	0.079	0.095	0.110	0.065	0.084	0.183	0.184
AR02	0.142	0.150	0.160	0.199	0.183	0.123	0.137	0.092	0.099	0.123	0.181	0.234
AR03	0.170	0.199	0.139	0.148	0.189	0.173	0.127	0.096	0.094	0.099	0.150	0.153
AR16	0.099	0.077	0.152	0.151	0.093	0.085	0.083	0.099	0.066	0.103	0.122	0.107
AR27	0.052	0.078	0.098	0.110	0.112	0.094	0.094	0.099	0.102	0.087	0.116	0.113
AZ01			0.204		0.580	0.112	0.092	0.094				
AZ03	0.034	0.043	0.054	0.130	0.101	0.129	0.087	0.102	0.101	0.065	0.054	0.041
AZ06	0.270	0.314	0.585	1.296	0.320	1.246	0.135	0.117	0.116	0.259	0.890	0.140
AZ98												
AZ99	0.048	0.055	0.090	0.156	0.127	0.123	0.058	0.063	0.063	0.111	0.138	0.052
CA34		0.126	0.047	0.063	0.305			0.871		0.279		
CA42	0.085	0.215	0.260	0.345	0.655	1.281	0.044	0.168	0.216	0.187	0.231	0.182
CA45	0.371	0.435	0.437	0.382	0.143	0.189	0.084	0.043	0.254	0.293	0.441	0.351
CA68	0.307	0.204	0.811	0.563	1.597		0.519	0.346	0.286	0.570	0.326	0.140
CA75	0.065	0.047	0.055	0.075	0.105	0.097	0.179	0.204	0.060	0.073	0.057	0.090
CA76	0.028	0.023	0.032	0.049	0.047	0.054	0.068	0.042	0.068	0.041	0.034	0.030
CA85												
CA88	0.224	0.330	0.322	0.179	0.127	0.151		0.275	0.141	0.243	0.325	0.279
CA98	0.043	0.059	0.046	0.089	0.091	0.276	0.087	0.263	0.070	0.054	0.062	0.082
CA99	0.092	0.090	0.052	0.096	0.083	0.067	0.191		0.099	0.056	0.094	0.070
CO00	0.017	0.077	0.036	0.060	0.072	0.081	0.090	0.053	0.060	0.035	0.037	0.029
CO01	0.049	0.045	0.073	0.059	0.066	0.099	0.080	0.054	0.062	0.024	0.045	0.031
CO02					0.039	0.040	0.071	0.069	0.060	0.028		
CO08	0.041	0.035	0.034	0.060	0.060	0.034	0.047	0.056	0.059	0.050	0.038	0.034
CO10												
CO15	0.056	0.039	0.075	0.057	0.072	0.106	0.086	0.086	0.053	0.048	0.039	0.033
CO19	0.045	0.023	0.032	0.062	0.065	0.074	0.073	0.068	0.090	0.043	0.032	0.053
CO21	0.054	0.038	0.038	0.041	0.062	0.055	0.077	0.055	0.068	0.038	0.023	0.048
CO22	0.053	0.129	0.043	0.041	0.051	0.072	0.061	0.053	0.060	0.056	0.022	0.059
CO91			0.072	0.061	0.049	0.036	0.019	0.030	0.044		0.031	
CO92		0.055	0.031	0.060	0.062	0.066	0.079	0.059	0.047	0.057		0.042
CO93				0.036	0.035	0.041	0.070	0.062	0.037	0.035	0.040	
CO94	0.046	0.025	0.022	0.034	0.042	0.041	0.078	0.064	0.053	0.034	0.031	0.026
CO95				0.038			0.075	0.046	0.099	0.044	0.036	0.031
CO96		0.011	0.027	0.054	0.063	0.105	0.057	0.039	0.052	0.050	0.022	0.033
CO97					0.033	0.046	0.049	0.047	0.028	0.029		
CO98					0.041	0.051	0.057	0.045	0.051			
CO99	0.016	0.037	0.038	0.088	0.080	0.075	0.088	0.035	0.070	0.051	0.048	0.035
FL00	0.296	0.266	0.533		0.224	0.594	0.144	0.206	0.222	0.395	0.635	0.423

Table 4.2: Monthly least squares linear regression slopes (Cl deposition vs precipitation) for NADP/NTN stations.

	Chloride Deposition / Precipitation Regression Slopes by Month (mg/cm)											
Station	January	February	March	April	May	June	July	August	September	October	November	December
FL03	0.332	0.396	0.358	0.276	0.322	0.175	0.171	0.159	0.182	0.351	0.318	0.369
FL05	0.364	0.455		0.716				0.331	0.433		0.223	
FL11	1.024	0.851	1.157	0.973	0.389	0.331	0.512	0.463	0.508	0.852	1.103	0.657
FL14	0.321	0.191	0.345	0.342	0.239	0.210	0.190	0.185	0.151	0.528	0.253	0.275
FL23												
FL41	0.498	1.019	0.482	0.348	0.473	0.284	0.253	0.273	0.375	0.585	0.287	0.491
FL99	1.535	1.971	1.001	1.328	0.585	0.376	0.407	0.479	0.645	1.502	1.475	1.441
GA09								0.090	0.215		0.199	0.206
GA20	0.220	0.306	0.302	0.312	0.215	0.160	0.165	0.243	0.127	0.381	0.366	0.199
GA23	0.648	0.182	1.108	0.610	0.297	0.466	0.268	0.610		0.691	0.407	0.371
GA41	0.215	0.198	0.159	0.185	0.230	0.132	0.075	0.082	0.113	0.156	0.147	0.188
GA50	0.189	0.213	0.286	0.325	0.229	0.184	0.113	0.141	0.205	0.261	0.239	0.179
GA99	0.282	0.229	0.257	0.243	0.256	0.174	0.173	0.137	0.062	0.137	0.129	0.147
IA08	0.061	0.075	0.078	0.062	0.067	0.049	0.062	0.049	0.054	0.052	0.052	0.073
IA23	0.073	0.036	0.114	0.052	0.072	0.084	0.050	0.077	0.031	0.059	0.049	0.047
ID03	0.044	0.048	0.064	0.052	0.078	0.091	0.112	0.194	0.122	0.102	0.048	0.076
ID04	0.038	0.029	0.030	0.056	0.061	0.048	0.059	0.048	0.037	0.073	0.044	0.043
ID11	0.036	0.050	0.065	0.067	0.060	0.077	0.098	0.091	0.067	0.070	0.063	0.029
ID15	0.035	0.074	0.041	0.043	0.043	0.070	0.076	0.081	0.042	0.082	0.031	0.034
IL11	0.080	0.087	0.120	0.126	0.097	0.093	0.084	0.106	0.080	0.071	0.076	0.095
IL18	0.060	0.044	0.104	0.079	0.087	0.076	0.081	0.056	0.061	0.075	0.082	0.092
IL19	0.165	0.194	0.174	0.125	0.099	0.084	0.078	0.094	0.069	0.094	0.102	0.145
IL35	0.069	0.113	0.124	0.067	0.118	0.087	0.101	0.077	0.074	0.110	0.126	0.222
IL46												
IL47	0.072	0.197	0.104	0.095	0.106	0.080	0.073	0.088	0.081	0.084	0.115	0.127
IL63	0.235	0.086	0.171	0.101	0.119	0.089	0.106	0.086	0.091	0.115	0.116	0.184
IL78	0.086	0.038	0.112	0.065	0.092	0.071	0.067	0.056	0.049	0.047	0.068	0.037
IL99	0.093	0.098		0.097	0.098	0.108	0.029	0.075	0.076	0.039	0.079	0.116
IN20	0.062	0.101	0.081	0.092	0.073	0.064	0.083	0.078	0.060	0.092	0.090	0.097
IN22	0.128	0.148	0.095	0.110	0.126	0.071	0.174	0.097	0.096	0.084	0.126	0.126
IN34	0.091	0.118	0.111	0.108	0.106	0.100	0.107	0.058	0.074	0.078	0.094	0.163
IN41	0.122	0.121	0.100	0.108	0.098	0.102	0.065	0.105	0.081	0.085	0.083	0.096
KS07	0.078	0.048	0.093	0.100	0.105	0.092	0.089	0.073	0.055	0.117	0.072	0.043
KS31	0.065	0.057	0.061	0.077	0.082	0.087	0.093	0.057	0.060	0.066	0.062	0.035
KS32	0.018	0.034	0.056	0.063	0.067	0.073	0.072	0.054	0.051	0.044	0.066	0.026
KY03	0.087	0.090	0.070	0.110	0.096	0.085	0.329	0.084	0.070	0.102	0.093	0.089
KY22	0.054	0.067	0.079	0.089	0.102	0.090	0.075	0.089	0.058	0.070	0.063	0.058
KY35	0.088	0.066	0.085	0.101	0.099	0.071	0.074	0.048	0.062	0.086	0.069	0.101
KY38	0.103	0.115	0.122	0.120	0.109	0.101	0.093	0.078	0.071	0.101	0.131	0.094
KY99	0.141	0.139					0.116	0.034	0.119	0.131	0.095	0.138

Table 4.2: Monthly least squares linear regression slopes (Cl deposition vs precipitation) for NADP/NTN stations.

	Chloride Deposition / Precipitation Regression Slopes by Month (mg/cm)											
Station	January	February	March	April	May	June	July	August	September	October	November	December
LA06	0.130	0.099	0.267	0.331	0.220	0.153	0.131	0.104	0.179	0.207	0.157	0.110
LA12	0.260	0.473	0.483	0.451	0.291	0.343	0.386	0.395	0.302	0.249	0.413	0.352
LA30	0.384	0.378	0.436	0.428	0.278	0.241	0.162	0.181	0.171	0.361	0.308	0.286
MA01	2.314	2.671	1.926	2.030	1.009	0.582	0.717	0.634	1.567	1.599	2.123	
MA08	0.286	0.216	0.224	0.159	0.124	0.064	0.092	0.103	0.083	0.169	0.211	0.101
MA13	0.496	0.478	0.480	0.531	0.244	0.252	0.163	0.315	0.297	0.654	0.544	0.676
MD03	0.303	0.247	0.180	0.184	0.125	0.132	0.102	0.109	0.091	0.320	0.290	0.193
MD13	0.256	0.282	0.276	0.272	0.202	0.189	0.184	0.195	0.258	0.364	0.483	0.430
ME00	0.099	0.089	0.092	0.132	0.077	0.085	0.052	0.034	0.052	0.089	0.092	0.064
ME02	0.319	0.660	0.301	0.176	0.147	0.085	0.053	0.092	0.101	0.358	0.257	0.116
ME09	0.108	0.149	0.121	0.095	0.079	0.059	0.049	0.036	0.048	0.160	0.133	0.082
ME96												
ME97	0.136	0.077	0.190	0.107	0.067	0.062	0.054	0.057	0.060	0.138	0.100	0.098
ME98	0.710	0.745	0.570	0.730	0.317	0.303	0.134	0.347	0.322	0.660	1.394	1.383
ME99			0.801	0.724	0.237	0.193	0.106	0.309	0.498			1.497
MI09	0.064	0.068	0.065	0.060	0.061	0.061	0.059	0.047	0.044	0.052	0.057	0.063
MI22	0.039	0.104	0.092	0.042	0.052						0.110	0.085
MI25						0.063	0.058	0.055				
MI26	0.091	0.085	0.112	0.078	0.090	0.076	0.053	0.074	0.058	0.061	0.086	0.075
MI51												
MI52												
MI53	0.089	0.062	0.077	0.067	0.071	0.067	0.066	0.059	0.052	0.054	0.062	0.103
MI97						0.047	0.038	0.038	0.037			
MI98		0.058	0.067	0.054	0.046	0.047	0.048	0.055	0.039	0.038	0.069	0.037
MI99	0.081	0.070	0.048	0.051	0.033	0.052	0.042	0.038	0.047	0.032	0.044	0.048
MN01		0.097							0.054		0.064	0.104
MN05			0.055			0.037		0.037			0.024	
MN08			0.063	0.034	0.033	0.026		0.030	0.034		0.037	
MN16	0.037	0.076	0.065	0.033	0.044	0.063	0.042	0.048	0.032	0.038	0.035	0.065
MN18	0.042	0.037	0.038	0.035	0.034	0.078	0.043	0.037	0.035	0.043	0.029	0.031
MN23	0.035	0.051	0.036	0.040	0.039	0.037	0.037	0.034	0.032	0.047	0.034	0.087
MN27	0.115	0.062	0.062	0.056	0.067	0.060	0.057	0.049	0.037	0.068	0.051	0.042
MN28								0.041	0.046			
MN99		0.050	0.051			0.055		0.038	0.026			
MO03	0.085	0.070	0.074	0.087	0.096	0.085	0.072	0.066	0.065	0.069	0.066	0.095
MO05	0.175	0.088	0.139	0.140	0.102	0.110	0.079	0.075	0.086	0.138	0.145	0.169
MO50	0.284	0.057		0.044					0.072	0.126	0.139	0.031
MS10	0.178	0.181	0.344	0.254	0.157	0.126	0.109	0.123	0.110	0.190	0.187	0.218
MS14	0.179	0.176	0.196	0.202	0.201	0.129	0.077	0.126	0.093	0.231	0.251	0.281
MS19	0.132	0.184	0.199	0.125	0.157	0.106	0.075	0.062	0.064	0.132	0.261	0.202

Table 4.2: **Monthly least squares linear regression slopes (Cl deposition vs precipitation) for NADP/NTN stations.**

	Chloride Deposition / Precipitation Regression Slopes by Month (mg/cm)											
Station	January	February	March	April	May	June	July	August	September	October	November	December
MS30	0.141	0.167	0.169	0.150	0.113	0.161	0.122	0.095	0.077	0.127	0.123	0.146
MT00	0.036	0.042	0.060	0.045	0.046	0.057	0.054	0.083	0.056	0.038	0.045	0.047
MT05	0.035	0.019	0.034	0.039	0.041	0.037	0.027	0.059	0.036	0.035	0.033	0.025
MT07	0.025	0.025	0.033	0.039	0.043	0.067	0.035	0.041	0.041	0.023	0.027	0.032
MT13	0.078	0.090	0.025	0.073	0.055	0.043	0.030	0.063	0.058	0.064	0.102	0.025
MT97			0.021	0.019	0.028	0.037	0.031	0.049	0.036	0.019		
MT98	0.118	0.032	0.046	0.079	0.038	0.041	0.023	0.050	0.045	0.029	0.022	0.029
MT99		0.096		0.075	0.029	0.023	0.052	0.027	0.020	0.060	0.026	
NC03	0.347	0.457	0.544	0.360	0.212	0.141	0.104	0.083	0.316	0.404	0.444	0.323
NC06												
NC11	0.177	0.192	0.137	0.299	0.102	0.076	0.040	0.072	0.187	0.176	0.400	0.210
NC25	0.110	0.152	0.123	0.161	0.131	0.067	0.076	0.067	0.081	0.098	0.209	0.176
NC33	0.326	0.197	0.168	0.171	0.100	0.077	0.073	0.073	0.117	0.157	0.439	0.186
NC34	0.253	0.191	0.226	0.236	0.140	0.106	0.117	0.092	0.119	0.145	0.210	0.206
NC35	0.555	0.349	0.485	0.659	0.203	0.203	0.149	0.083	0.403	0.458	0.336	0.442
NC36	0.372	0.230	0.286	0.184	0.257	0.125	0.098	0.092	0.164	0.423	0.317	0.278
NC41	0.400	0.233	0.274	0.283	0.156	0.131	0.113	0.101	0.169	0.229	0.307	0.298
NC45	0.059	0.065	0.080	0.120	0.049	0.054	0.058	0.049	0.051	0.056	0.096	0.017
ND07	0.057	0.055	0.027	0.035	0.035	0.051	0.039	0.061	0.033	0.029	0.044	0.061
ND08			0.025	0.055	0.037	0.041	0.039	0.047	0.038	0.041	0.039	
ND11		0.080	0.040	0.056	0.041	0.060	0.041	0.051	0.026	0.048	0.051	0.072
NE15	0.043	0.074	0.074	0.087	0.075	0.096	0.073	0.104	0.058	0.084	0.051	0.020
NE99	0.055	0.034	0.035	0.044	0.049	0.051	0.053	0.040	0.042	0.041	0.031	0.045
NH02	0.082	0.236	0.156	0.121	0.089	0.081	0.054	0.069	0.095	0.127	0.196	0.082
NJ00												
NJ29	0.825	0.886		0.283	0.253	0.202			0.273			
NJ99	0.385	0.321	0.223	0.333	0.142	0.113	0.106	0.142	0.227	0.342	0.342	0.539
NM01	0.021	0.048	0.138	0.432	0.077	0.165	0.074	0.074	0.057	0.059	0.062	0.016
NM07	0.026	0.055	0.062	0.079	0.067	0.073	0.062	0.054	0.040	0.052	0.036	0.038
NM08	0.041	0.061	0.149	0.102	0.060	0.030	0.059	0.039	0.035	0.042	0.084	0.048
NM09	0.028	0.033	0.064	0.071	0.066	0.147	0.075	0.062	0.061	0.040	0.041	0.033
NM12	0.104	0.271	0.049	0.101	0.063	0.090	0.063	0.051	0.026	0.141	0.032	0.030
NV00	0.042	0.051	0.042	0.134	0.165	0.206	0.087	0.145	0.055	0.045	0.068	0.067
NV01		0.017	0.093	0.061	0.074	0.101	0.062	0.209	0.133	0.044	0.074	0.048
NV03	0.041	0.022	0.037	0.042	0.069	0.092	0.124	0.136	0.052	0.036	0.038	0.032
NV05	0.345	0.101	0.087	0.126	0.091	0.131	0.108	0.109	0.104	0.077	0.050	0.057
NY08	0.071	0.091	0.096	0.085	0.076	0.090	0.084	0.089	0.083	0.091	0.080	0.079
NY10	0.045	0.099	0.103	0.106	0.090	0.084	0.091	0.107	0.072	0.081	0.076	0.104
NY12	0.201	0.101	0.097	0.100	0.096	0.074	0.082	0.136	0.103	0.095	0.113	0.208
NY20	0.041	0.103	0.074	0.111	0.059	0.056	0.054	0.048	0.052	0.055	0.053	0.051

Table 4.2: Monthly least squares linear regression slopes (Cl deposition vs precipitation) for NADP/NTN stations.

Station	Chloride Deposition / Precipitation Regression Slopes by Month (mg/cm)											
	January	February	March	April	May	June	July	August	September	October	November	December
NY51	0.214	0.777	0.155	0.200	0.133	0.079	0.102	0.077	0.198	0.194	0.210	0.746
NY52	0.149	0.204	0.108	0.085	0.063	0.080	0.092	0.083	0.068	0.079	0.087	0.121
NY65	0.047	0.085	0.079	0.081	0.075	0.058	0.073	0.064	0.067	0.059	0.059	0.056
NY68	0.148	0.133	0.096	0.136	0.078	0.070	0.067	0.071	0.081	0.168	0.093	0.072
NY98	0.032	0.054	0.052	0.055	0.046	0.048	0.042	0.038	0.038	0.041	0.039	0.041
NY99	0.359	0.467	0.240	0.367	0.179	0.130	0.135	0.136	0.298	0.283	0.322	0.456
OH09	0.113	0.094	0.098	0.095	0.093	0.080	0.078	0.082	0.074	0.082	0.108	0.080
OH15												
OH17	0.172	0.179	0.140	0.103	0.089	0.084	0.078	0.092	0.064	0.087	0.099	0.120
OH49	0.191	0.126	0.120	0.131	0.103	0.113	0.098	0.077	0.083	0.120	0.112	0.135
OH54												
OH71	0.101	0.135	0.134	0.126	0.091	0.084	0.075	0.090	0.054	0.103	0.085	0.109
OK00	0.080	0.067	0.093	0.088	0.124	0.130	0.161	0.107	0.097	0.059	0.093	0.092
OK17	0.062	0.064	0.162	0.087	0.147	0.103	0.099	0.139	0.110	0.053	0.121	0.085
OK25	0.027	0.124	0.222	0.174	0.161	0.088	0.128	0.150	0.081	0.174	0.184	0.400
OK29	0.052	0.047	0.059	0.087	0.096	0.078	0.081	0.077	0.060	0.033	0.040	0.028
OR02	1.280	0.844	0.886	1.221	0.507	0.426	0.215	0.197	0.867	0.764	1.407	0.745
OR08	0.093	0.067	0.091	0.048	0.035	0.066	0.085	0.071	0.140	0.030	0.129	0.117
OR09	0.027	0.017	0.032	0.042	0.060	0.045	0.075	0.076	0.075	0.065	0.032	0.026
OR10	0.203	0.163	0.170	0.186	0.105	0.088	0.066	0.082	0.196	0.275	0.269	0.196
OR11	0.052	0.041	0.053	0.076	0.052	0.080	0.098	0.081	0.062	0.059	0.060	0.079
OR17	0.104	0.115	0.196	0.091	0.142	0.039	0.152		0.049	0.262	0.008	0.069
OR18	0.045	0.018	0.035	0.030	0.040	0.038	0.041	0.058	0.043	0.031	0.030	0.026
OR97	0.414	0.302	0.427	0.373	0.164	0.182	0.152	0.122	0.280	0.387	0.643	0.438
OR98	0.347	0.284	0.381	0.378	0.266	0.211	0.153	0.216	0.303	0.368	0.433	0.427
OR99	0.603	0.320	0.493	0.791	0.145	0.285	0.235		0.330	0.506	0.520	0.333
PA00												
PA15	0.121	0.098	0.093	0.079	0.088	0.115	0.108	0.079	0.083	0.067	0.087	0.098
PA29	0.090	0.106	0.094	0.104	0.083	0.073	0.078	0.230	0.076	0.076	0.085	0.084
PA42	0.122	0.114	0.099	0.110	0.094	0.094	0.124	0.074	0.121	0.093	0.097	0.103
PA72	0.217	0.160	0.161	0.140	0.089	0.121	0.086	0.098	0.143	0.117	0.157	0.162
SC06	0.254	0.347	0.411	0.370	0.278	0.130	0.131	0.147	0.139	0.179	0.575	0.220
SC18	0.127	0.205	0.297	0.217	0.219	0.101	0.136	0.117	0.103	0.141	0.221	0.273
SD00						0.036	0.121	0.038		0.068		
SD08		0.014	0.051	0.029	0.047	0.037	0.042	0.041	0.028	0.018	0.039	0.031
SD99		0.055	0.058	0.058	0.044	0.061	0.050	0.049	0.040	0.041	0.094	
TN00	0.133	0.155	0.134	0.129	0.154	0.095	0.106	0.112	0.081	0.127	0.136	0.152
TN04												
TN11	0.051	0.079	0.069	0.078	0.089	0.051	0.068	0.049	0.061	0.062	0.062	0.063
TN14	0.120	0.137	0.135	0.130	0.120	0.080	0.098	0.062	0.075	0.107	0.134	0.161

Table 4.2: Monthly least squares linear regression slopes (Cl deposition vs precipitation) for NADP/NTN stations.

	Chloride Deposition / Precipitation Regression Slopes by Month (mg/cm)											
Station	January	February	March	April	May	June	July	August	September	October	November	December
TN98	0.126	0.122	0.116	0.198	0.099	0.088	0.114	0.072	0.072	0.094	0.106	0.113
TN99	0.138	0.113	0.159	0.114		0.092	0.102	0.088	0.063	0.040	0.131	0.223
TX02	0.052	0.071	0.108	0.095	0.114	0.100	0.105	0.072	0.076	0.049	0.063	0.024
TX03	0.439	0.442	0.443	0.523	0.413	0.542	0.131	0.393	0.416	0.650	0.559	0.904
TX04	0.026	0.067	0.049	0.056	0.097	0.104	0.076	0.069	0.069	0.060	0.059	0.077
TX10	0.263	0.404	0.323	0.491	0.311	0.262	0.202	0.282	0.270	0.361	0.412	0.339
TX16	0.067	0.115	0.259	0.153	0.182	0.137	0.101	0.223	0.110	0.147	0.119	0.052
TX18	0.019	0.047	0.069	0.085	0.128	0.115	0.041	0.151	0.068	0.063	0.047	0.067
TX21	0.216	0.151	0.240	0.242	0.195	0.128	0.235	0.110	0.124	0.198	0.267	0.270
TX22	0.090	0.056	0.106	0.053	0.072	0.050	0.060	0.051	0.049	0.045	0.069	0.027
TX38	0.165	0.232	0.258	0.303	0.252	0.090	0.187	0.127	0.169	0.170	0.344	0.292
TX51	0.111	0.070	0.181	0.074	0.155	0.181	0.113	0.161	0.147	0.077	0.080	0.142
TX53	0.567	0.634	0.616	0.433	0.461	0.477	0.153	0.433	0.515	0.431	0.513	0.619
TX56	0.163	0.096	0.179	0.115	0.182	0.170	0.094	0.114	0.106	0.188	0.159	0.079
UT01	0.220	0.759	0.364	0.210	0.205	0.237	0.236	0.321	0.363	0.199	0.198	0.280
UT02		0.027		0.324								
UT08			0.071	0.355	0.129	0.163	0.178	0.112	0.091	0.049		0.125
UT09												0.019
UT98	0.045	0.085	0.053	0.098	0.078	0.377	0.159	0.125	0.094	0.045	0.042	0.048
UT99	0.159	0.046	0.057	0.220	0.113	0.163	0.078	0.089	0.050	0.042	0.054	0.027
VA00	0.462	0.128	0.114	0.142	0.104	0.121	0.057	0.096	0.094	0.132	0.232	0.091
VA13	0.074	0.076	0.073	0.089	0.078	0.080	0.076	0.068	0.073	0.095	0.080	0.080
VA24												
VA28	0.603	0.057	0.104	0.098	0.061	0.075	0.068	0.077	0.138	0.114	0.083	0.040
VA29	0.054	0.055	0.089	0.061	0.067	0.048	0.064	0.060	0.033	0.041		0.055
VA33			0.176	0.086	0.072	0.096						0.191
VT01	0.123	0.122	0.101	0.125	0.078	0.068	0.063	0.042	0.063	0.087	0.067	0.095
VT99	0.054	0.074	0.063	0.058	0.050	0.046	0.035	0.034	0.045	0.043	0.036	0.052
WA14	0.583	0.247	0.540	0.722	0.460	0.466	0.302	0.097	0.728	0.504	0.660	0.602
WA15		0.029	0.033		0.040	0.082	0.050	0.041	0.052	0.043	0.036	0.035
WA19	0.119	0.101	0.129	0.158	0.119	0.086	0.057	0.073	0.139	0.207	0.127	0.190
WA21	0.239	0.131	0.225	0.196	0.152	0.167	0.082	0.121	0.170	0.353	0.385	0.238
WA24	0.040	0.035	0.052	0.042	0.043	0.058	0.060	0.048	0.041	0.041	0.046	0.041
WI09	0.056	0.067	0.074	0.048	0.052	0.054	0.048	0.046	0.036	0.046	0.047	0.040
WI25	0.095	0.068	0.078	0.045	0.054	0.060	0.057	0.049	0.049	0.058	0.054	0.052
WI28	0.117	0.087	0.091	0.053	0.069	0.067	0.055	0.055	0.043	0.062	0.058	0.081
WI35												
WI36	0.046	0.055	0.051	0.042	0.046	0.052	0.049	0.047	0.040	0.039	0.031	0.039
WI37	0.043	0.074	0.058	0.045	0.050	0.056	0.052	0.043	0.044	0.040	0.048	0.053
WI98	0.061	0.079	0.069	0.046	0.057	0.048	0.048	0.055	0.042	0.059	0.051	0.057

Table 4.2: Monthly least squares linear regression slopes (Cl deposition vs precipitation) for NADP/NTN stations.

	Chloride Deposition / Precipitation Regression Slopes by Month (mg/cm)											
Station	January	February	March	April	May	June	July	August	September	October	November	December
WI99	0.114	0.070	0.100	0.068	0.076	0.063	0.073	0.070	0.054	0.062	0.074	0.075
WV04	0.065	0.077	0.075	0.092	0.068	0.066	0.065	0.060	0.056	0.071	0.073	0.080
WV05												
WV18	0.088	0.071	0.076	0.089	0.075	0.081	0.081	0.069	0.052	0.066	0.068	0.075
WY00					0.038	0.045	0.057	0.054	0.033			
WY02	0.026	0.027	0.035	0.030	0.034	0.042	0.076	0.062	0.047	0.019	0.033	0.017
WY06	0.043	0.023	0.057	0.056	0.066	0.080	0.160	0.117	0.051	0.029	0.062	0.046
WY08	0.035	0.023	0.043	0.047	0.070	0.068	0.079	0.085	0.080	0.046	0.033	0.029
WY95					0.036	0.049	0.066	0.059	0.050			0.024
WY96					0.054	0.062	0.063	0.087	0.059	0.017		
WY97		0.061	0.069	0.040	0.045	0.064	0.084	0.065	0.058	0.033	0.035	0.081
WY98	0.098	0.098	0.065	0.040	0.035	0.059	0.071	0.073	0.047	0.067	0.069	0.060
WY99	0.135	0.033	0.050	0.039	0.055	0.041	0.044	0.064	0.045	0.037	0.037	0.044

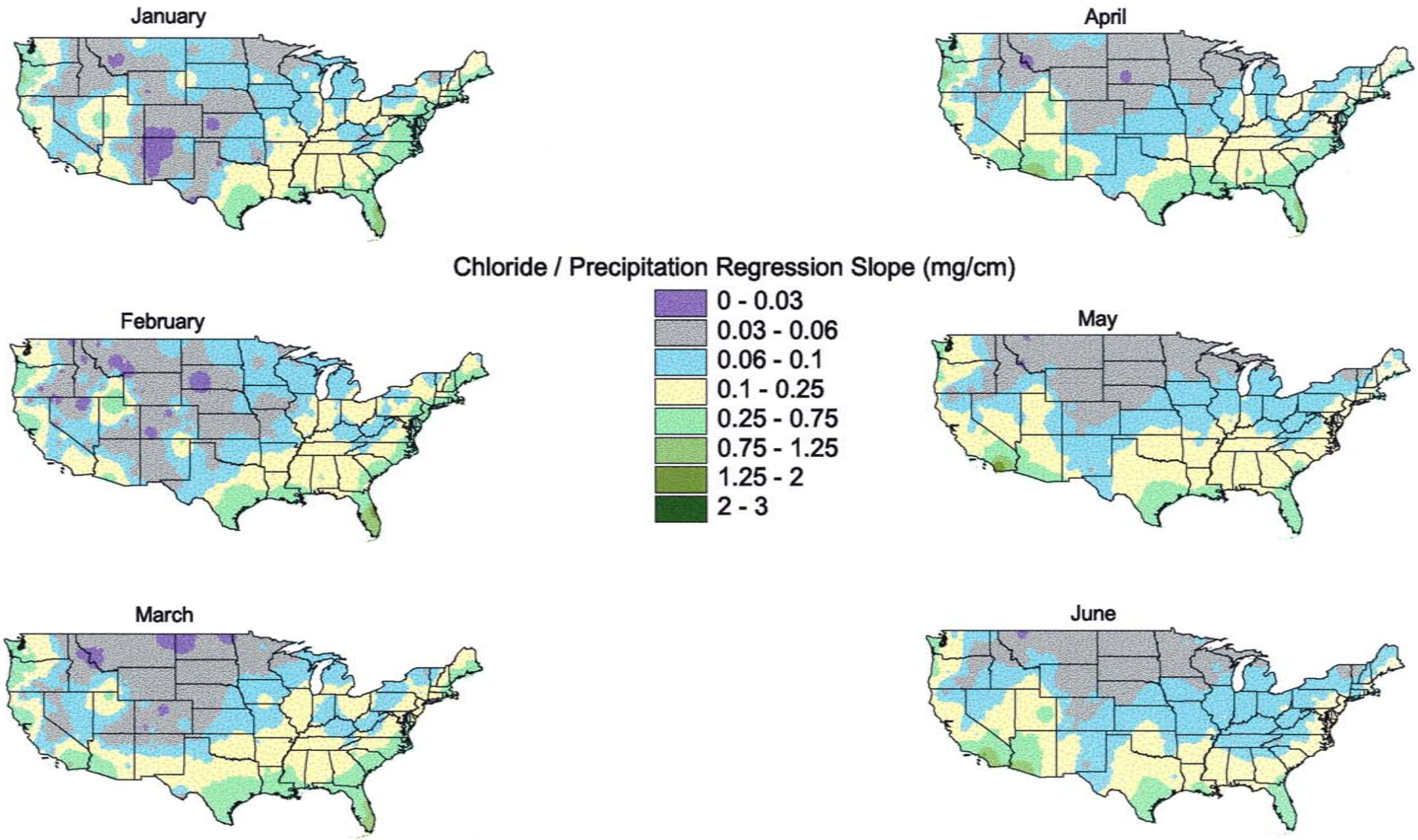

Figure 4.9: Monthly interpolatedchloride collection / precipitation regression slopes; January to June.
Values interpolated from data in Table 4.2.

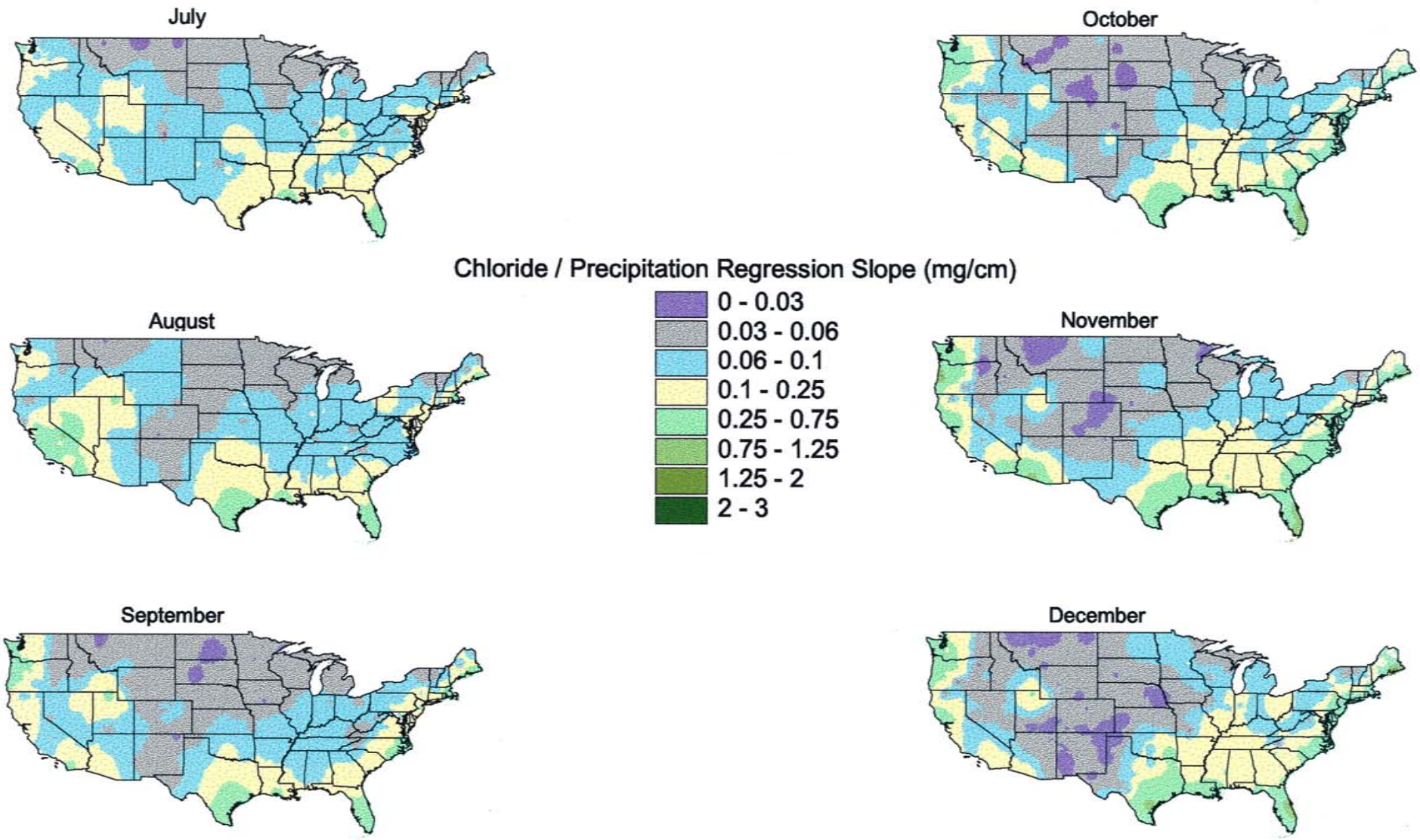

Figure 4.10: Monthly interpolated chloride collection / precipitation regression slopes; July to December.
Values interpolated from data in Table 4.2.

Both the seasonal and 'generic monthly' regression analyses were used to construct two separate models of wet chloride deposition. As both models will be discussed in subsequent sections, a naming convention must be applied. In the first case, a linear regression was fit through all monthly data, without regard to the relationship during a particular month. The same regression slope was then used for every month throughout the year. Since the same regression slope was applied over the entire year, the model based on such 'generic monthly' data is termed the "annual wet deposition model". In the second case, the data were subdivided into each month, with a separate regression performed for each month in order to assess seasonal variability in the regression slope. Here, the regression slope changes for each month of the year, and the model based on this seasonal data is termed the "monthly wet deposition model". The "annual" and "monthly" wet deposition models will later be compared to each other, and to the measured deposition values during an evaluation of the models' performance.

This study was concerned only with long-term average chloride deposition, rather than prediction of deposition associated with individual precipitation events, and thus data within precipitation intervals were averaged at a few selected stations in order to assess the long-term correlation of chloride deposition with precipitation. For a selected station, the monthly precipitation was subdivided into the intervals 0-2 cm, 2-4 cm, 4-6 cm, 6-8 cm, 8-10 cm, 10-15 cm, and every 10 cm thereafter up to the maximum monthly precipitation measured. Smaller intervals were used in the lower range because more data were available. Within each precipitation interval, the average mass of collected chloride was calculated over all months with precipitation within the range. This reduced the data to individual average chloride collection values for each precipitation interval, revealing

long-term trends. An example of this analysis is shown in Figure 4.11, where the average chloride within each interval is plotted against the median precipitation of each interval. A distinct linear trend is evident over the majority of the precipitation range. This linear trend offers significant support for the use of a linear chloride / precipitation regression to model long-term average chloride deposition. At precipitation amounts approaching the maximum recorded value, a ceiling value of chloride collection is apparent. This ceiling suggests that all available chloride within the atmosphere above a collector is effectively removed during months of extreme precipitation. Any additional precipitation does not add appreciable amounts of chloride. Typically, only one to five percent of recorded months at any station have precipitation values within the range producing a ceiling value for chloride collection. Thus, the linear chloride / precipitation relation applies for the great majority of time, and is the most appropriate measure of the average long-term correlation. An alternative to the linear correlation would only be required for a few exceptionally high precipitation areas and to model the chloride / precipitation relationship at the scale of individual precipitation events, where precipitation amounts exceeding the ceiling value of chloride collection would be important for extreme events.

The average chloride collection within precipitation intervals analysis was performed purely to assess long-term average behavior, and to verify whether a linear relationship was justified. This approach was not used in the chloride deposition model. The complete data (either all monthly data or data subdivided into specific months) were fit with least squares linear regressions as discussed in the preceding paragraphs. The continental distribution of stable chloride could then be estimated from precipitation using a linear relation with rainfall amount whose slope varied with inland distance. This

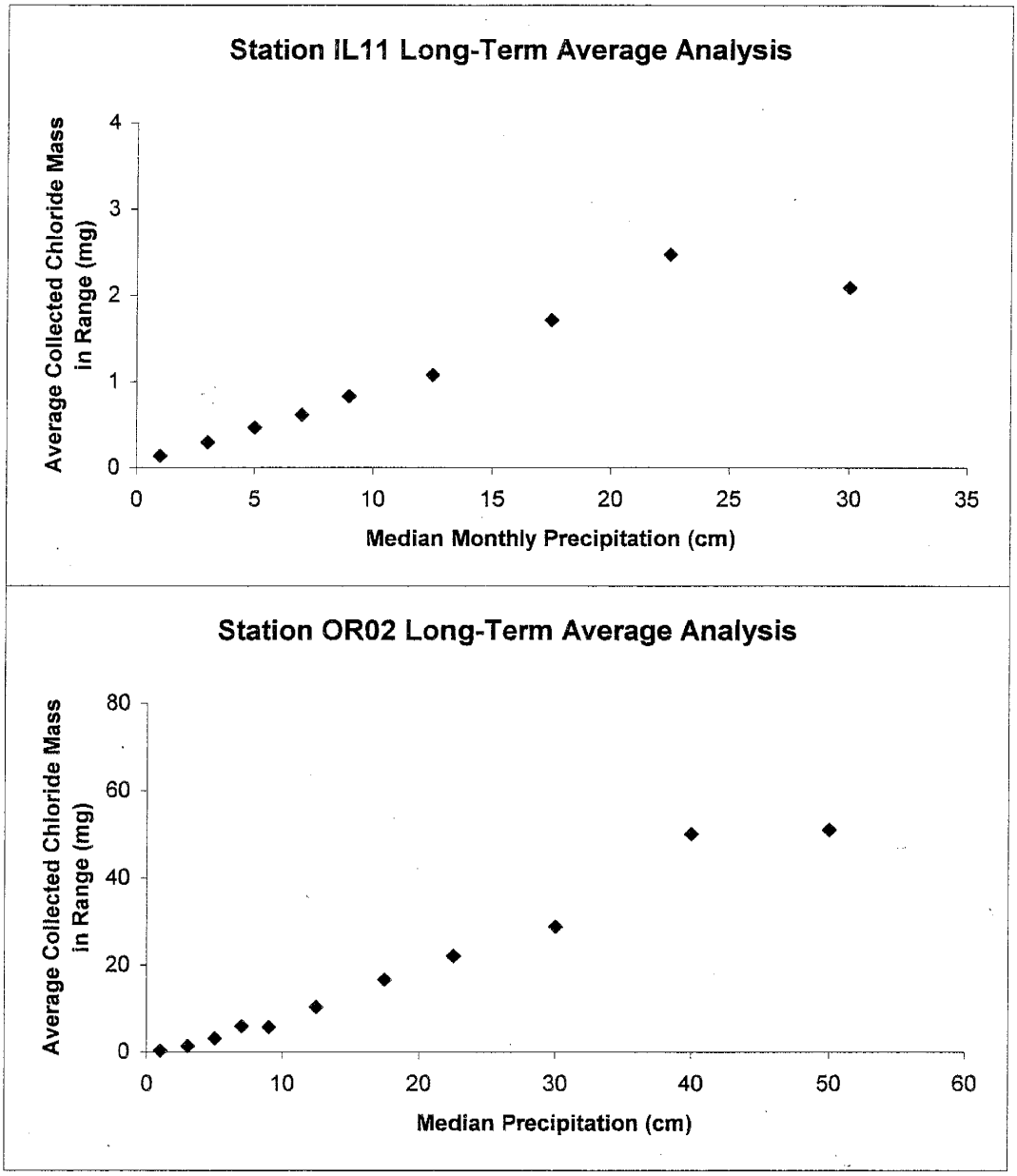

Figure 4.11: Long-term average relationship between chloride collection and precipitation.
Data from NADP/NTN (1998).

required a suitable map of monthly precipitation and the regression slope for stations throughout the country. For this study, a digital form of precipitation map was desired. The PRISM precipitation model was chosen because it was based on 30 years of measured precipitation and has undergone extensive peer review. The PRISM model output was also easily accessible from the internet.

4.2.3 Discussion of the PRISM precipitation model

The Parameter-elevation Regressions on Independent Slopes Model (PRISM) is a linear-interpolation precipitation model developed by the combined efforts of Oregon State University (OSU) and the United States Department of Agriculture Natural Resource Conservation Service's (USDA-NRCS) National Water and Climate Center in Portland, Oregon. The main objective of the project is to produce base climate layers for the multitude of climate-related projects administered by the USDA. The PRISM modeling approach is described by Daly et al. (1994 and 1997) and Daly and Johnson (1999). PRISM data sets were freely available on the internet at the time of this writing (http://www.ocs.orst.edu/prism). The data sets used in this study were monthly precipitation maps at 4 km by 4 km resolution over the United States. The PRISM precipitation model underlies the new model of chloride and ^{36}Cl deposition developed in this study, and is therefore described in some detail here.

The PRISM model utilizes point data, a digital elevation model (DEM), and other spatial data sets to estimate climatic elements, such as precipitation or temperature. The model is based on the premise that numerous climatic elements show a strong correlation with elevation. For instance, local temperature is inversely related to elevation while

precipitation is generally greater at the peak of local topographic features than at lower elevations. In modeling precipitation, the PRISM model utilizes a linear regression of precipitation with elevation. Other non-linear methods such as polynomial regression, or curve-fitting functions such as splining, are avoided because: (1) altitudinal variations of precipitation often approximate a linear form; (2) the linear function can be extrapolated in a stable fashion far beyond the elevational range of the data; and (3) the linear function is easily manipulated to compensate for data inadequacies (Daly and Johnson, 1999). Elevation is not the only factor influencing the spatial distribution of precipitation. Other important factors include coastal proximity and the orientation of local topography (such as west-facing slopes versus north-facing slopes). A multiple regression incorporating many factors is rejected in favor of a simple regression involving only elevation due to difficulties in controlling and interpreting the complex relationship among multiple independent variables. Additional influences on precipitation are accounted for using weighting factors.

The simple linear regression used in PRISM has the form

$$Y = J_1X + J_o \qquad \text{Eqn 4.1}$$

where Y is the predicted precipitation (or other climate element), X is the DEM elevation at the target grid cell, and J_1 and J_o are the regression slope and intercept, respectively (Daly and Johnson, 1999). As the regression function is evaluated, each station is assigned a weight, W, based on

$$W = f\{W_d, W_z, W_c, W_l, W_f, W_p, W_e\} \quad \text{Eqn 4.2}$$

where W_d, W_z, W_c, W_l, W_f, W_p, and W_e are the distance, elevation, cluster, vertical layer, topographic facet, coastal proximity, and effective terrain weights, respectively (Daly and Johnson, 1999). Weighting based on distance, elevation, and cluster is relatively straightforward; a station is down-weighted when it is relatively distant or at a much different elevation than the target grid cell, or when it is near several other stations (preventing over-representation). Vertical layer weighting accounts for the fact that precipitation at a local topographic peak is not always greater than at the base or midslope. Near mid-latitude coastal areas with a relatively thin, moist marine layer, orographic precipitation resulting from uplift of this layer can cause midslope precipitation maxima, with drying at higher elevations. PRISM divides stations entering the regression into two vertical layers, a boundary layer and a free atmosphere layer. Stations within the same layer as the target grid cell receive full weight, while those in the adjacent layer receive lower weighting. This weighting limits over-estimation of precipitation at high elevations (resulting from steep regression slopes within the moist boundary layer) in areas where midslope maxima are likely to occur. Topographic orientation can dramatically influence local precipitation. The most common example is the rain shadow, which occurs on the lee sides of many mountain ranges in the western U.S. Mixing of windward and leeward local-station data would produce very inaccurate estimates of precipitation based on elevation (a clear, linear relationship would not likely exist). PRISM accounts for this by dividing the terrain into major topographic orientations, or facets, based on an eight-point compass. Facets can be defined at multiple scales in order to incorporate a sufficient

number of stations on similar facets. Stations on the same facet as the target grid cell receive the highest weight, while others are down-weighted accordingly. Coastal proximity affects both temperature and precipitation gradients. For example, summer maximum-temperature gradients can exceed 20 °C within thin coastal strips, and coastal precipitation can be different from adjacent inland areas (Daly and Johnson, 1999). In coastal areas, PRISM preferentially weights stations with similar inland distance (measured as the shortest distance to water) as the target grid cell, reducing sensitivity to relative differences in the density and location of coastal and inland stations. The effective terrain weighting accounts for the variable orographic precipitation enhancement of different terrain features. Orographic precipitation enhancement depends on the ability of a landform to block and uplift moisture-bearing air. PRISM compares the elevation of the target cell (from the DEM) with the elevation of the cell given a smoothed, large-scale representation of the terrain. Features rising well above the background elevation are assumed to have a significant effect on precipitation. In areas of orographically-effective terrain, PRISM operates in a full 3D fashion, while acting as a 2D interpolator in regions of non-effective terrain. Only distance, clustering, and coastal proximity weighting factors are used within non-effective terrain. Figure 4.12 shows those regions where PRISM operates in full 3D mode, and those where it acts as an interpolator.

The point data used in the PRISM model were collected from observations from the National Weather Service (NWS) cooperative network, the National Resource Conservation Service (NRCS) SNOTEL network, storage gauges, snow courses, and estimated 'pseudo' stations at monthly or annual resolution for the time period 1961 to 1990. Annual-only precipitation data (from storage gauges, snow courses, and 'pseudo'

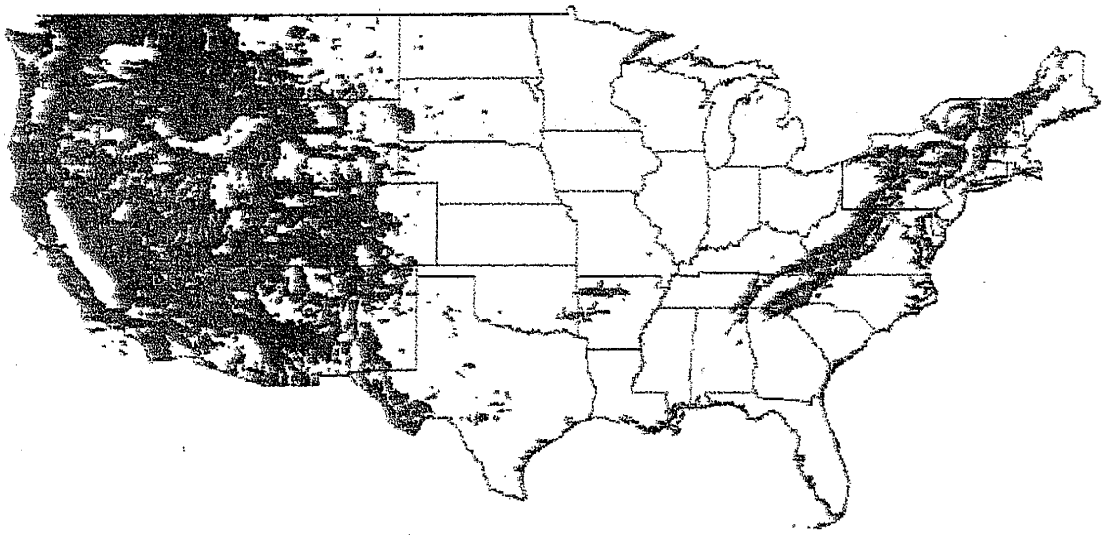

Figure 4.12: Orographically effective terrain distribution used by the PRISM model. Shaded areas denote terrain features that are expected to produce significant terrain-induced (3D) precipitation patterns. 2D interpolation of station data used in unshaded areas. (Daly and Johnson, 1999)

stations) were processed into mean monthly values based on subjectively chosen, nearby monthly stations. 'Pseudo' station data were estimated by state climatologists or Oregon State University (OSU) personnel when station data were deemed insufficient in an area. The 'pseudo' station data were typically based on vegetation type, short-term observations, or streamflow records. Approximately 8,500 stations from the NWS cooperative network are used in the PRISM model; the station distribution is shown in Figure 4.13. A 15-second DEM was degraded in resolution using a Gaussian filter to create a 2.5-minute DEM gridded base coverage. PRISM operates using a moving-window approach in which a separate regression is calculated for each cell in the domain. Stations located within the local window surrounding a cell are weighted as previously discussed as they are incorporated into the regression.

The PRISM model has undergone extensive peer review since 1993 when a committee of climatologists and hydrologists (from several state and federal agencies) was formed to evaluate the PRISM methodology in four test states (Oregon, Idaho, Nevada, and Utah) chosen for their spatially complex precipitation regimes. Committee members were asked to evaluate draft PRISM mean annual precipitation maps within their area of expertise by: (1) inspecting precipitation patterns for accuracy, reasonableness, and detail; (2) inspecting high and low precipitation amounts and their locations; (3) inspecting the interrelationships between extremes; and (4) producing factual evidence supporting major differences between the PRISM model and member viewpoints (Daly and Johnson, 1999). This review lasted two years and concluded with all members sanctioning the PRISM model as able to produce precipitation maps of equivalent or superior quality to those prepared manually by expert climatologists. Improvements to the PRISM model, in

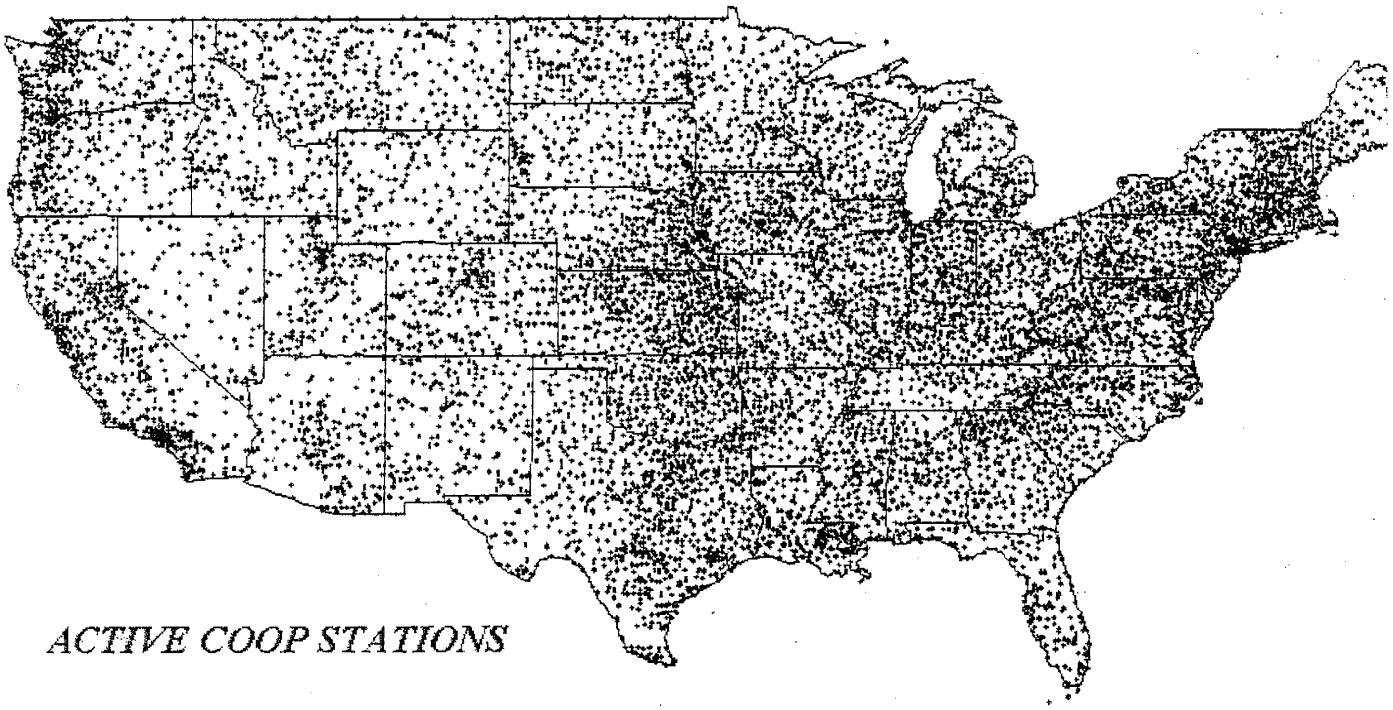

Figure 4.13: Distribution of National Weather Service cooperative network precipitation stations used in the PRISM precipitation model. (PRISM, 1998)

response to the initial review, included increasing the grid resolution from 5-minutes to 2.5-minutes and delineating topographic facet orientation on an eight-point compass rather than four. Draft monthly and annual precipitation maps for the entire U.S. were then generated, with a mean annual map for each state sent to climatologists for further review. This review took two additional years and resulted in improvements including the effective terrain height and coastal proximity weighting factors. Final precipitation grids were produced in 1997, and updated in 1998 at higher numerical precision. Figure 4.14 shows mean annual precipitation (in cm) in the conterminous United States calculated by the PRISM model, while Figures 4.15 and 4.16 show the PRISM precipitation each month.

4.2.4 Calculation of the wet stable chloride deposition

The calculation of the wet component of stable chloride deposition (and other components of this model) was performed using the Geographic Information Systems (GIS) software package ArcView® (version 3.0) and the extension Spatial Analyst® (version 1.0), distributed by the Environmental Systems Research Institute, Inc. (ESRI). The PRISM output is made available for direct use within GIS applications and consists of gridded precipitation data (or coverages) at a 4 km by 4 km resolution. The monthly gridded coverages available on the website were in the awkward units of mm times 100. The data were first converted to precipitation in cm, to match the units used for the regressions of collected chloride mass versus monthly precipitation. The high-resolution PRISM coverage has a value within every grid cell of the coverage, while the regressions were performed at approximately 200 point locations across the country. In order to calculate the chloride flux within each PRISM grid cell, the regression slope point data had

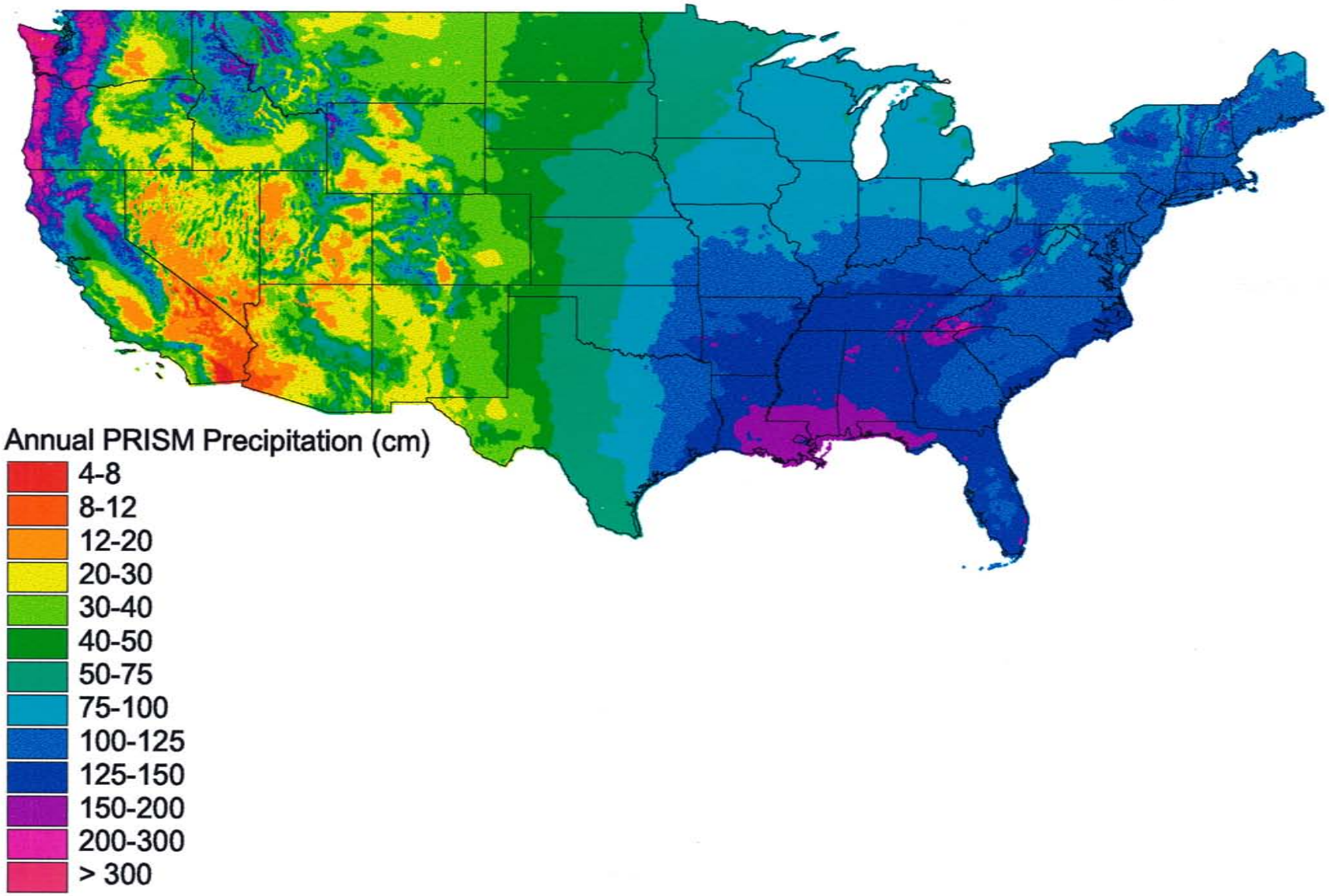

Figure 4.14: Mean annual precipitation over the U.S. as calculated by the PRISM (1998) model.
Average calculated over the period 1961 to 1990.

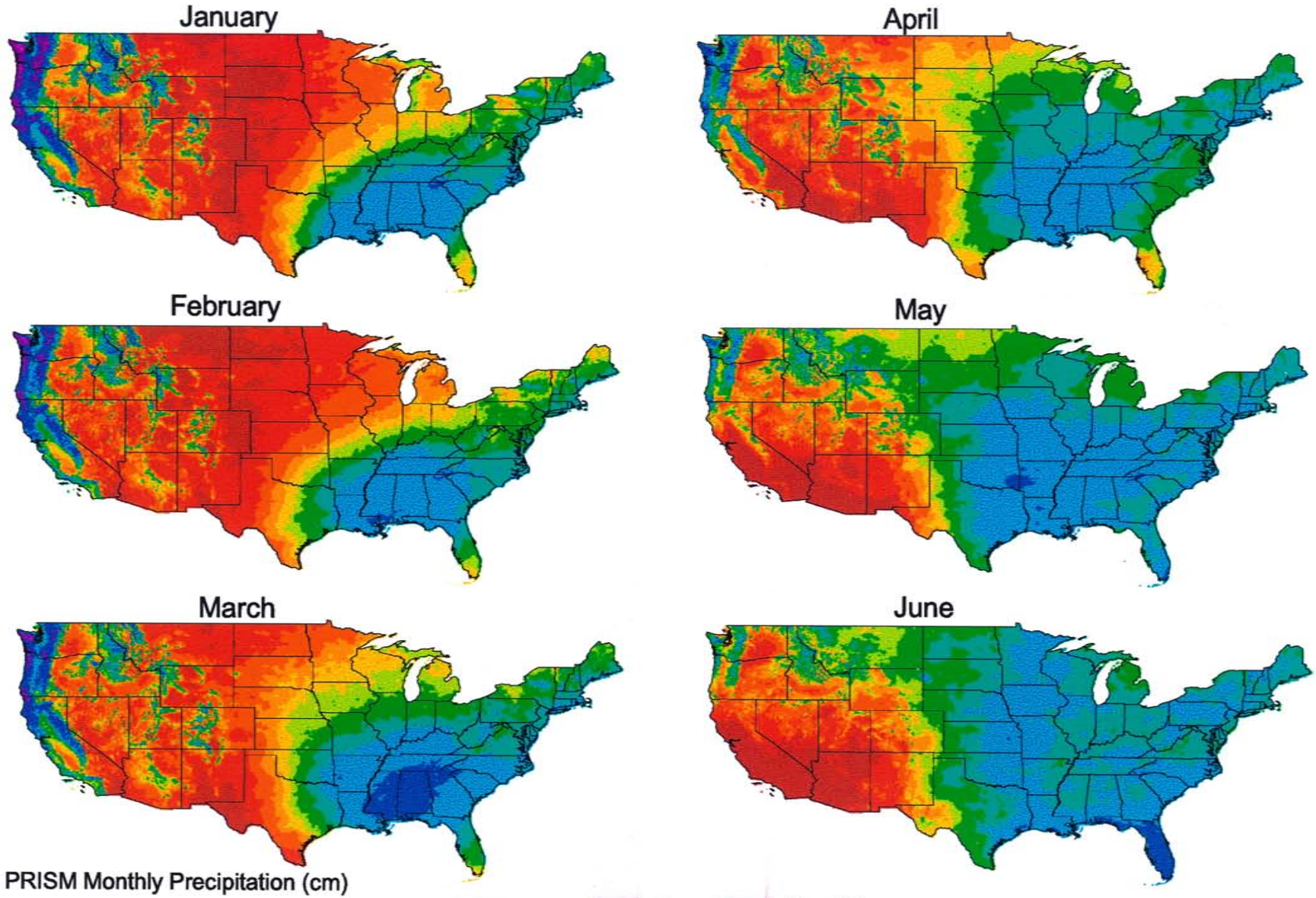

Figure 4.15: Average precipitation by month over the U.S. as calculated by the PRISM (1998) model; January through June.

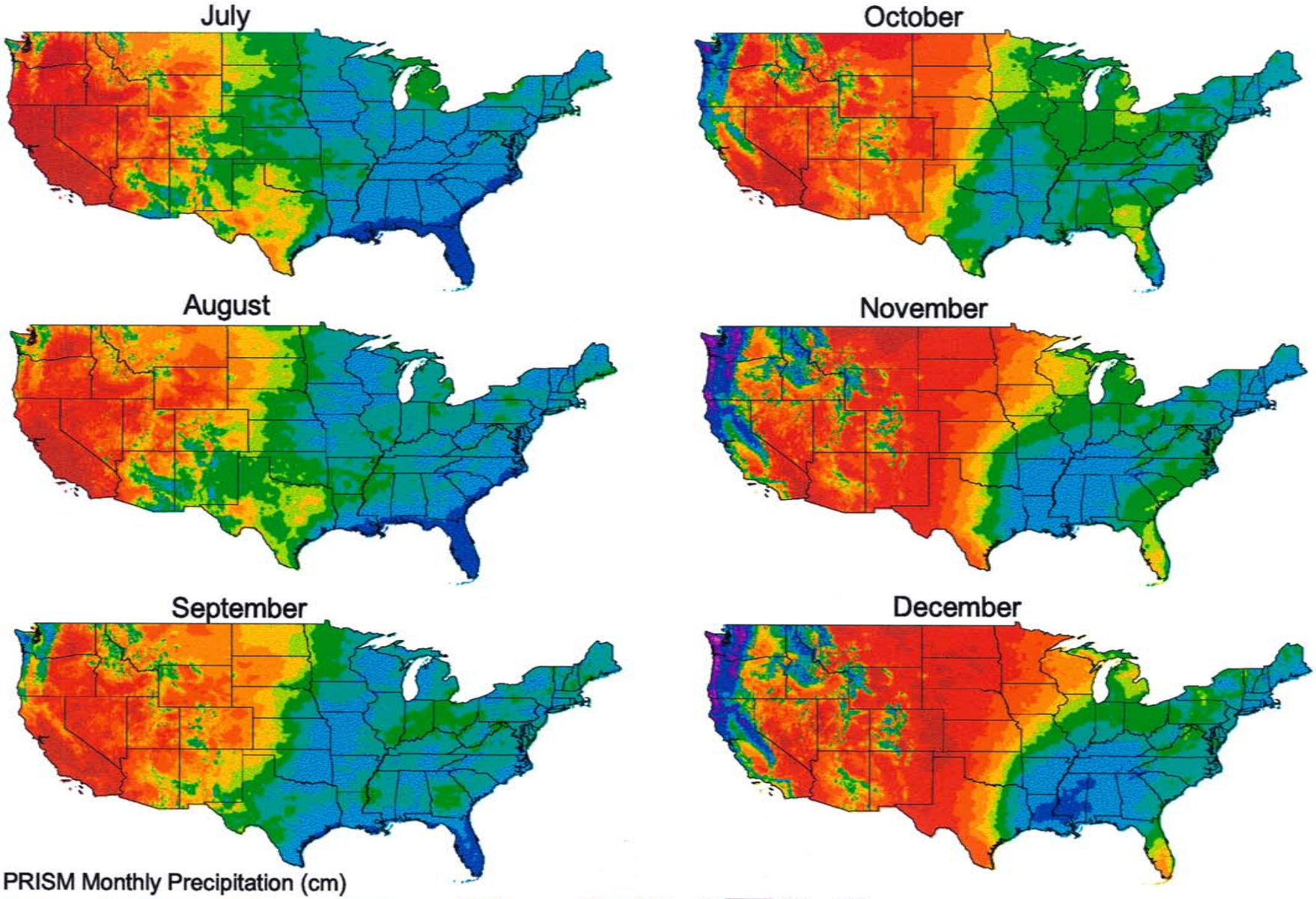

Figure 4.16: Average precipitation by month over the U.S. as calculated by the PRISM (1998) model; July through December.

to be remapped to the same resolution as the precipitation grid. This was done by interpolating the regression slopes using an inverse distance weighting scheme. The regressions were performed using all undifferentiated monthly data (the "annual" approach) and for each specific month (the "monthly" approach), as discussed previously. The interpolated regression slope field for the annual approach was shown in Figure 4.8, while the interpolated regression slope fields for each individual month were shown in Figures 4.9 and 4.10. With the monthly PRISM precipitation grids and the interpolated regression slope fields at the same scale and resolution, they were combined to calculate the wet chloride deposition each month using

$$Deposition = \frac{P * S}{A} \qquad \text{Eqn 4.3}$$

where P is the monthly precipitation (cm $month^{-1}$) in a PRISM grid cell, S is the slope of the chloride collection / precipitation regression (mg cm^{-1}) in a grid cell, and A is the collection area of each NADP/NTN collector (678.9 cm^2). The monthly depositions were summed to calculate the annual wet chloride deposition. The "annual" wet chloride deposition model used the same regression slope field each month (Figure 4.8) multiplied by each monthly PRISM gridded coverage (using Equation 4.3). The "monthly" wet chloride deposition model used individual monthly regression slope fields (Figures 4.9 and 4.10) multiplied by each corresponding monthly PRISM gridded coverage. The annual distribution of wet chloride deposition calculated using both the "annual" and "monthly" wet deposition models is shown in Figure 4.17 in units of mg m^{-2} yr^{-1}. The two models calculate nearly identical deposition over the eastern United States, and in the Pacific

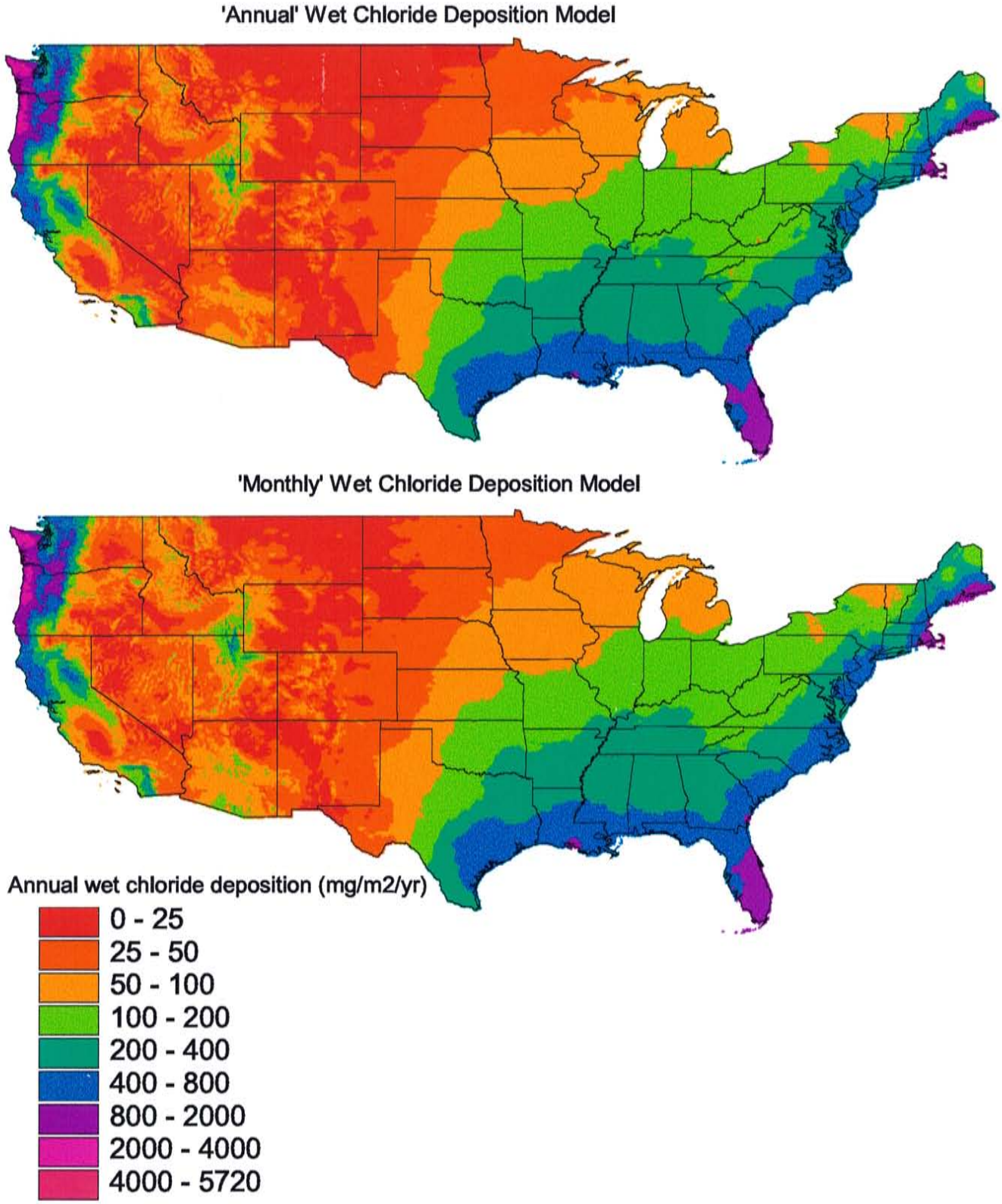

Figure 4.17: Annual wet chloride deposition over the U.S. calculated using the "annual" and "monthly" wet deposition models.

Northwest. The major difference between the models is within the Southwest, particularly in Arizona, Utah, and Nevada. The "monthly" model predicts higher wet deposition in these states due to increased regression slopes during the rainy summer months.

4.3 Incorporation of Dry Deposition

An aspect distinctly lacking from previous models of the $^{36}Cl/Cl$ ratio distribution has been the incorporation of dry deposition. Both Bentley et al. (1986a) and Moysey (1999) accounted for the dry deposition component by multiplying the wet component by 130 percent. Hainsworth (1994) did not address dry deposition directly. While the dry component has not been actively studied, it is commonly hypothesized to account for the lack of agreement between modeled and measured results. A goal of this study was to determine the availability of dry deposition measurements from across the country and, if available, to incorporate them directly into a new model of the $^{36}Cl/Cl$ distribution.

4.3.1 NADP/NTN dry deposition measurements

The NADP/NTN collector network was used to assess the wet deposition component as previously discussed. When reviewing the specifics of the network design, it was noted that the samplers used for the network are AeroChem Metrics (model 301) wet/dry collectors. While only wet deposition data are posted and available on the NADP/NTN website, one might assume that the use of a wet/dry collector meant that dry deposition was also measured, though perhaps not made readily available. Scotty R. Dossett of the NADP Program Office (Illinois State Water Survey) was contacted to determine whether the dry-side collection buckets were ever sampled, whether chemical

analyses were performed, and if dry-side data could be obtained. Dossett responded that, yes, the dry-side buckets had been analyzed, but the data had not been reported. According to Dossett, field collection of the dry-side bucket was a required protocol at all NADP/NTN stations until the summer of 1984 when it became optional. The reason for the change was the increasing controversy on the use of surrogate surface techniques to measure dry deposition. This issue is discussed in more detail below. The dry-side bucket was rinsed with a 250 ml charge of reagent grade water, with the rinse water analyzed for the same chemical parameters as the wet bucket sample. The dry-side bucket was not sampled as frequently as the wet-side bucket (weekly); the typical sampling interval was every one to two months. After 1984, the number of stations participating in dry deposition collection fell rapidly. Approximately 24 stations continued measurements through 1986, and only about 12 stations continued until the fall of 1998 when all measurements of the dry-side samples were discontinued.

All available dry-side analytical data were requested and received from the NADP Program Office. The data included qualifiers denoting the presence of various contaminants found in the dry-side bucket at the time of collection, including insects, grass clippings, and water. The data were culled to include only those samples for which the sample volume was less than or equal to 260 ml, 10 ml more than the volume of rinse water used. The data culling criterion was not lowered to 250 ml in order to maintain an adequate number of stations in the database. The 10 ml of additional water was assumed not to add an appreciable amount of chloride to the sample. This assumption was supported by the lack of significant concentration differences between samples over and at the 250 ml volume, measured at the same station. All data with a sample volume of 260

ml or less were used, regardless of other potential contaminants, in order to maintain as many measurements as possible. The potential effect of insect and vegetation contamination on chloride concentration was not assessed, but was assumed to be negligible.

The annual sum of dry-bucket chloride collection (mg) was calculated for all stations in which a complete year of consecutive measurements was available. If several years with complete data were available, an average annual value was calculated. Prior to the data culling discussed above, 113 stations had at least one complete year of consecutive measurements. After the data were culled, this number dropped to only 53 stations. Figure 4.18(a) shows the location of stations for which at least one complete year of measurement was available, both before and after the data culling. Overall, there is broad coverage of the entire United States, but there are areas which do not have adequate representation after the data culling. In an effort to fill data gaps, an additional station, and stations with only partial-year data were added. A station in the Sevilleta National Wildlife Refuge (SNWR) near Socorro, New Mexico was added to the dry deposition dataset. As part of the Long Term Ecological Research (LTER) project, in connection with the University of New Mexico's (UNM) Biology Department, the SNWR contains numerous atmospheric deposition collectors. Data from one of the wet/dry collectors has been collected for more than five consecutive years, and is considered to provide a highly reliable estimate of the local dry deposition (Moore, 1998). Contact information for the SNWR is provided in the bibliography. Many of the NADP/NTN stations with only a partial year of consecutive measurements were added, after correction to an annual amount. For instance, if a station contained 9-months of consecutive data, those data were

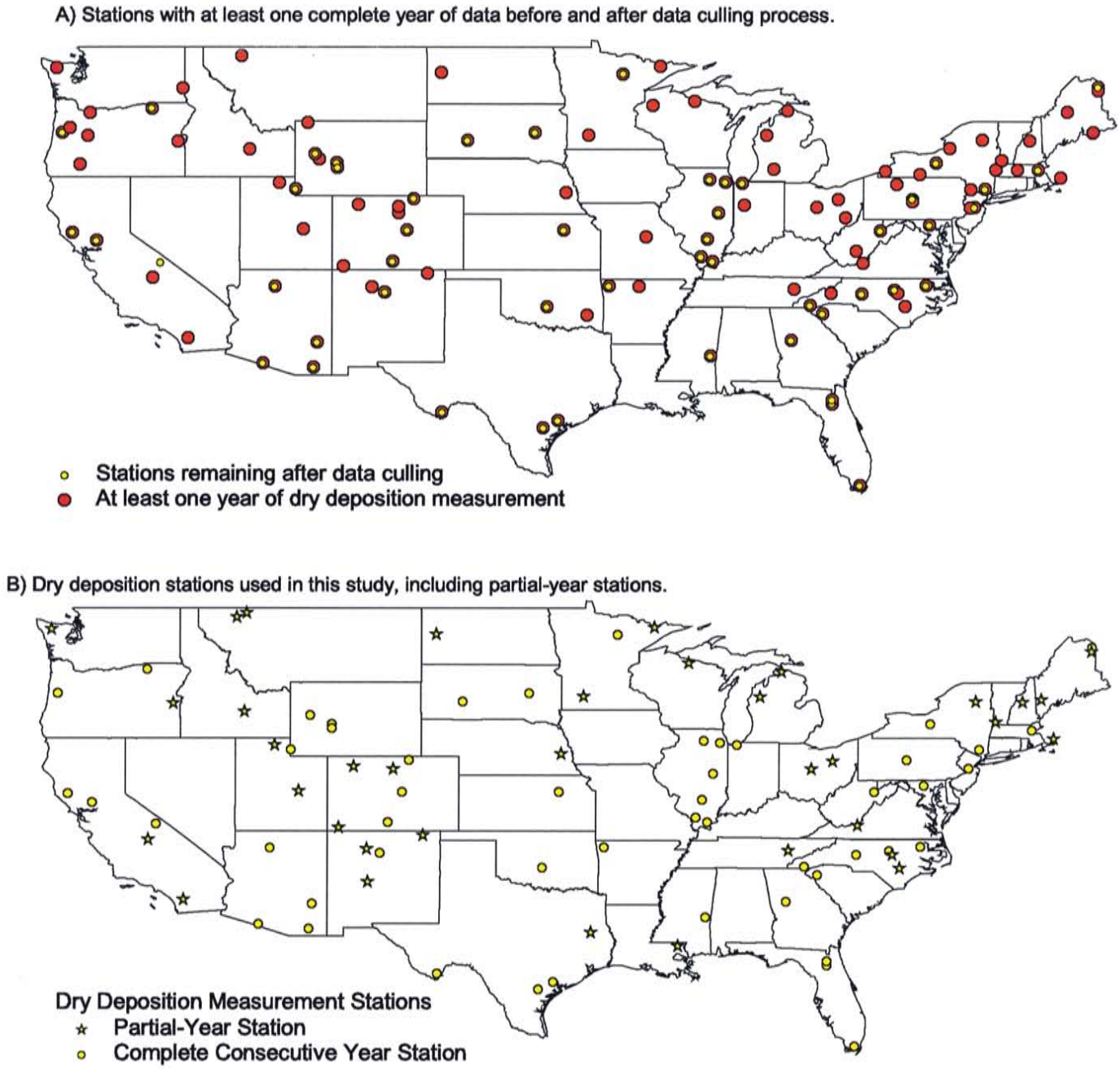

Figure 4.18: Location of dry deposition measurement stations.

summed and multiplied by 1.33 (twelve-ninths) to calculate the annual total. This approach could produce erroneous annual totals if seasonal variation is important to dry deposition, and periods of lower or higher deposition are not accounted for. The approach was deemed appropriate for a general average, though, and was thought better than not having an annual estimate whatsoever. Figure 4.18(b) highlights the location of stations with only partial-year records.

The dry deposition pattern is generally similar to the wet deposition pattern, with elevated values along the coasts and lower values in the continental interior. The data from Figure 4.18(b) were interpolated in ArcView® (using an inverse distance weighting scheme) to the same resolution as the PRISM precipitation and wet chloride deposition data, as illustrated in Figure 4.19.

It is important to note the uncertainties involved with using these dry deposition data. There has been increasing controversy regarding the ability of a surrogate surface (such as a collector funnel) to emulate the capture characteristics of the native ground surface. Indeed, this led to the lifting of mandatory dry-side bucket analyses for NADP/NTN stations in 1984, and the complete elimination of such analyses in 1998. Further, it is well documented that different collector geometries can lead to highly variable deposition measurements. Dolske and Gatz (1984) compared measured dry deposition of sulfate using numerous sampling surfaces and geometries. They found that flux measurements in petri dishes were twice as high as on flat plates, and that dry-collection bucket measurements were five times higher. The sampling bias may be due to aerodynamic turbulence produced by air moving across the sampler, which can enhance or discourage capture by the collector. Presently, it is unknown which method (or geometry)

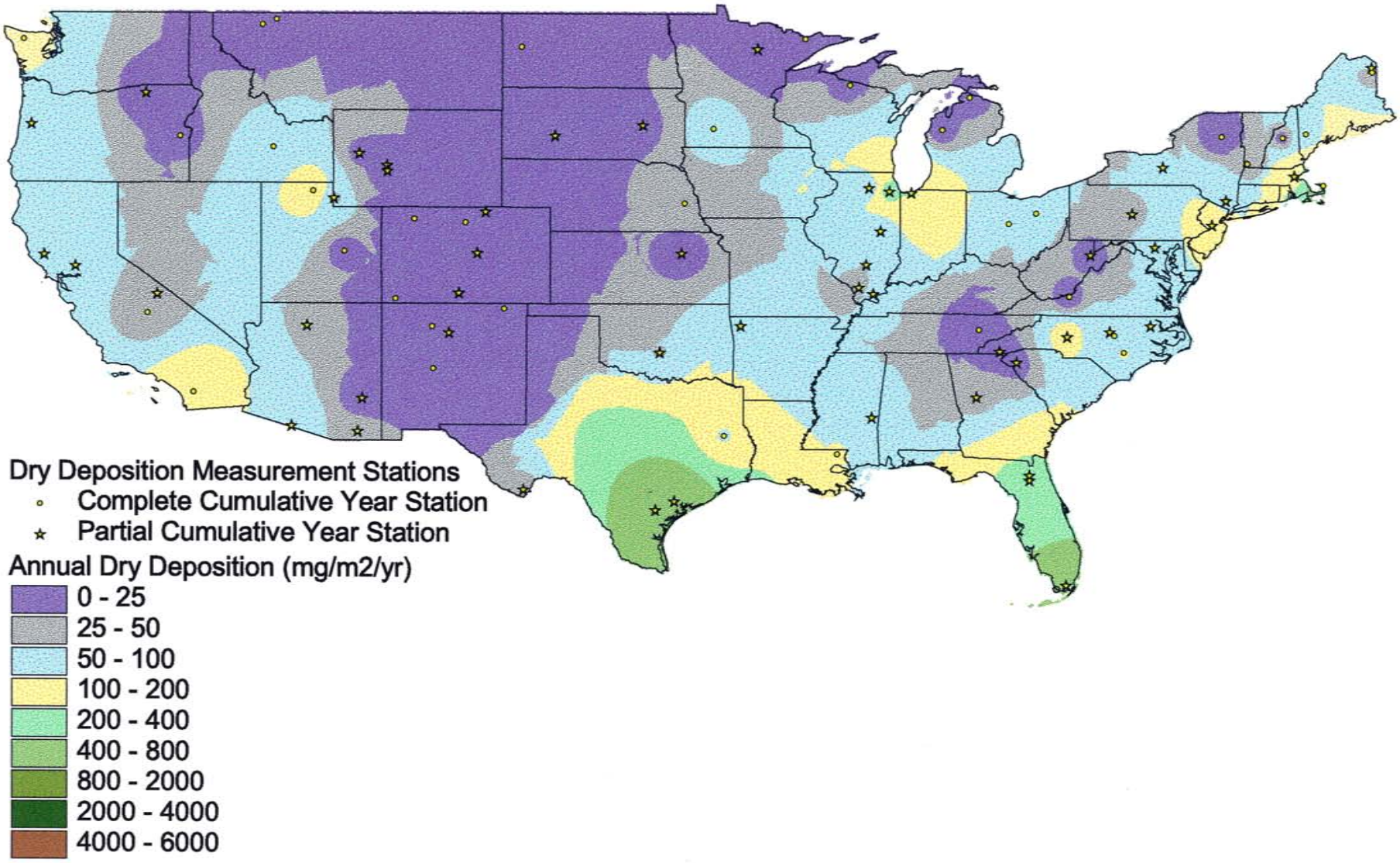

Figure 4.19: Distribution of dry deposition over the U.S. Interpolated from data in Figure 4.18(b).

most accurately represents natural dry deposition. While it is uncertain whether the NADP/NTN data over- or underestimate the actual dry deposition flux, they provide essentially the only available continental-scale measurement of such flux, and provide an important contribution to the study of atmospheric deposition. The advantage of the NADP/NTN network over a compilation of individual site measurements made by different investigators is the use of a common collector and common sampling methodology which allows more direct comparison of values measured at different locations.

4.3.2 Total stable chloride deposition

The wet and dry deposition components were summed to calculate the total atmospheric chloride deposition over the conterminous United States. This was done using both the "annual" wet deposition model output and the "monthly" wet deposition model output. Total atmospheric stable chloride deposition is shown in Figure 4.20, for both wet deposition models. The map of the dry deposition component was divided by the total deposition map to determine the percent of the total deposition due to dryfall. The dry deposition component typically accounts for between 15 to 60 percent of the total deposition, as illustrated in Figure 4.21. These values are in agreement with the ranges reported or estimated by Eriksson (1960; 25%), Hainsworth (1994; 25%), Bentley et al. (1986a; 30%), Li (1992; ~50%), Whitehead and Feth (1964; ~50%), and at the SNWR (40%).

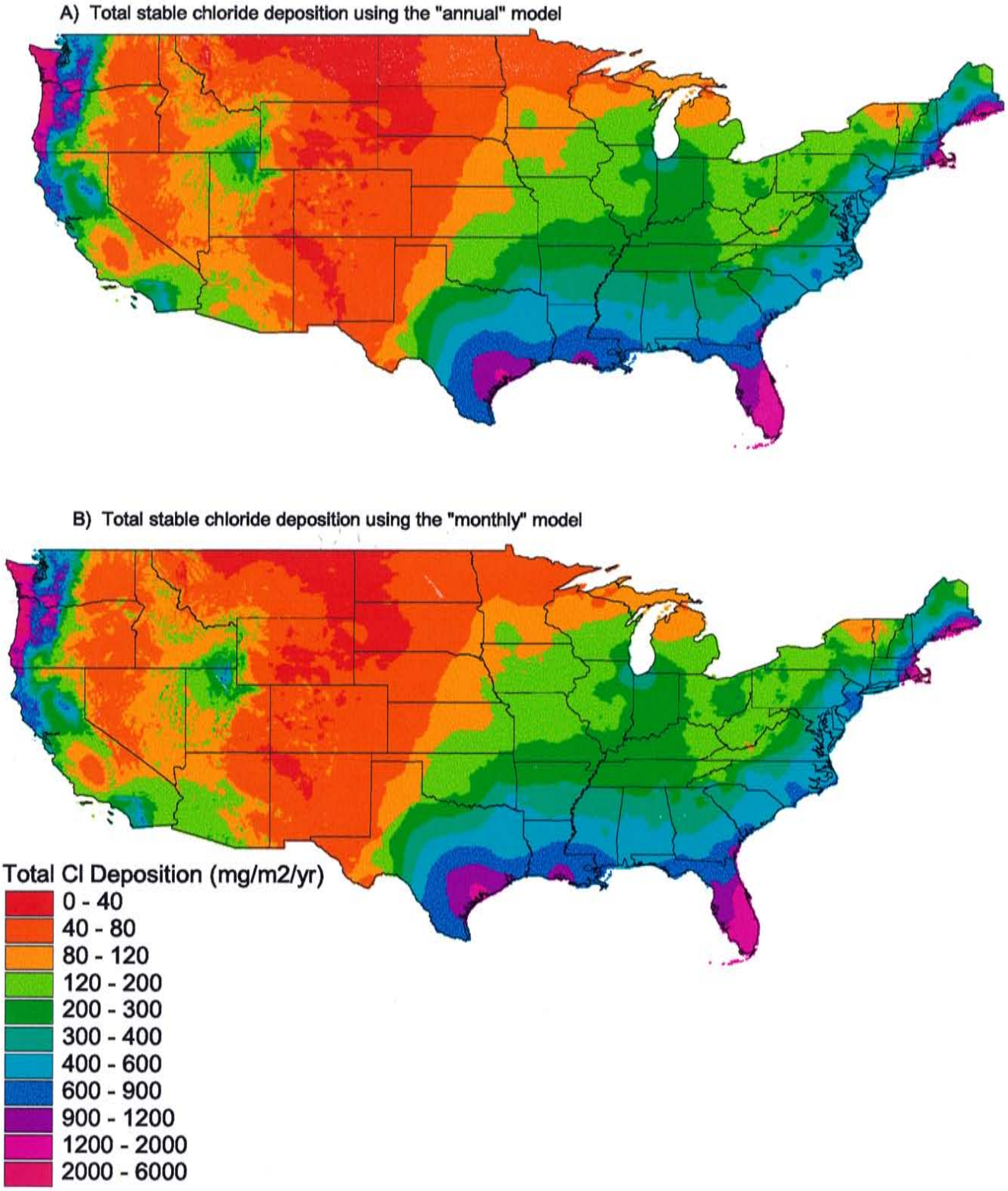

Figure 4.20: Total atmospheric stable chloride deposition over the U.S. using both the "annual" and "monthly" wet deposition models.

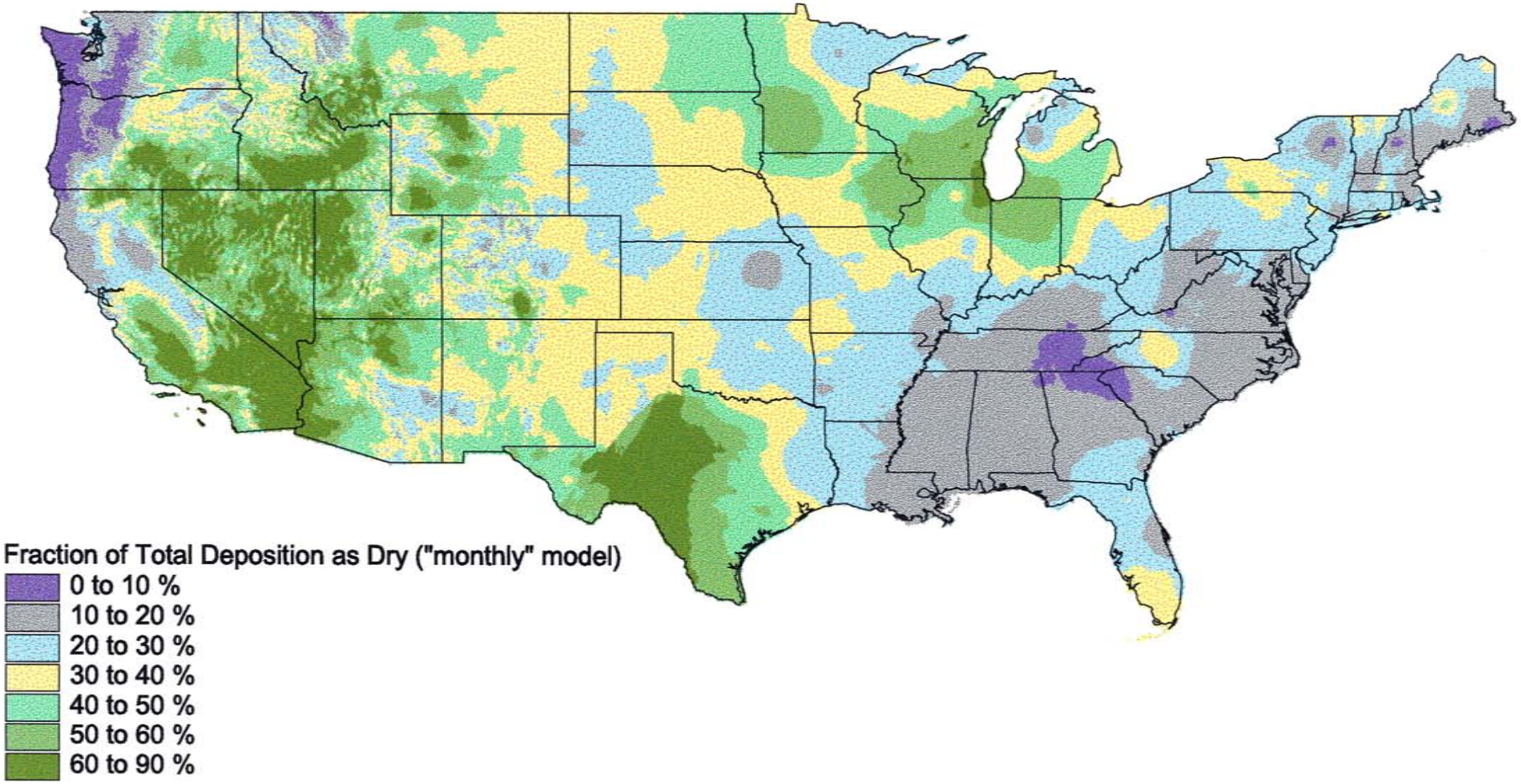

Figure 4.21: Percent of total deposition due to dryfall throughout the U.S.

4.4 Modeling the ^{36}Cl Deposition

The recent model of ^{36}Cl deposition proposed by Phillips (1999) was incorporated into this study. As previously discussed in Chapter 3, the ^{36}Cl deposition is dependent on both latitude and the amount of precipitation, and is described by Equation 4.6. Solution of Equation 4.6 requires knowledge of the local mean precipitation ($\overline{P}$), the mean latitudinal precipitation ($\overline{P}(\lambda)$), the latitude dependence of ^{36}Cl deposition ($D_{36}(\lambda)$), and the value of the ratio $S_p(\lambda_o)/D_{36}(\lambda_o)$ (suggested as 1.11 x 10^{-3} yr mm^{-1}). The terms $\overline{P}(\lambda)$ and $D_{36}(\lambda)$ are taken from Figure 3.8(c) and the dashed line in Figure 3.8(b), respectively. In order to apply Equation 4.6 at all locations across the country, the curves representing the $\overline{P}(\lambda)$ and $D_{36}(\lambda)$ terms were fit by polynomial expressions, to facilitate calculation of these parameters at any latitude over the United States. The mean latitudinal precipitation ($\overline{P}(\lambda)$) was described between 25°N and 65°N by the third-order polynomial

$$\overline{P}(\lambda) = -0.0309\lambda^3 + 3.3967\lambda^2 - 110.25\lambda + 1783.1 \qquad \text{Eqn 4.4}$$

where λ is the latitude. The latitude dependence of ^{36}Cl deposition was described between 25°N and 60°N by the third-order polynomial

$$D_{36}(\lambda) = 0.00075112\lambda^3 - 0.1613\lambda^2 + 9.5848\lambda - 125.05 \qquad \text{Eqn 4.5}$$

The ^{36}Cl deposition across the country was calculated using ArcView® at the same resolution as the PRISM precipitation gridded coverage using the precipitation value

within each grid cell, the latitude of each grid cell, equations 4.5 and 4.6, and the suggested value for the term $S_p(\lambda_o)/D_{36}(\lambda_o)$. Figure 4.22 illustrates the result of the calculation.

4.5 Spatial Distribution of the ^{36}Cl/Cl Ratio

A new model of the spatial distribution of the ^{36}Cl/Cl ratio was constructed by combining the recent model of ^{36}Cl deposition proposed by Phillips (1999) with the new model of stable chloride deposition developed as part of this study. Using ArcView®, the model output shown in Figure 4.22 was divided by each of the total stable chloride outputs shown in Figure 4.20. Two different maps of the ^{36}Cl/Cl ratio are shown in Figure 4.23, one using the "annual" wet deposition model to calculate total stable chloride deposition and the other incorporating the "monthly" wet deposition model. The two ^{36}Cl/Cl ratio distributions share the same overall distribution pattern, but the map incorporating the "monthly" wet deposition model shows generally lower ratios within the southwestern United States. The pattern of the ^{36}Cl/Cl ratio distribution is also similar to that from previous models, although this new model produces steeper gradients along the coasts. An analysis of the measured errors of the new ^{36}Cl/Cl model and its components is presented in Chapter 5.

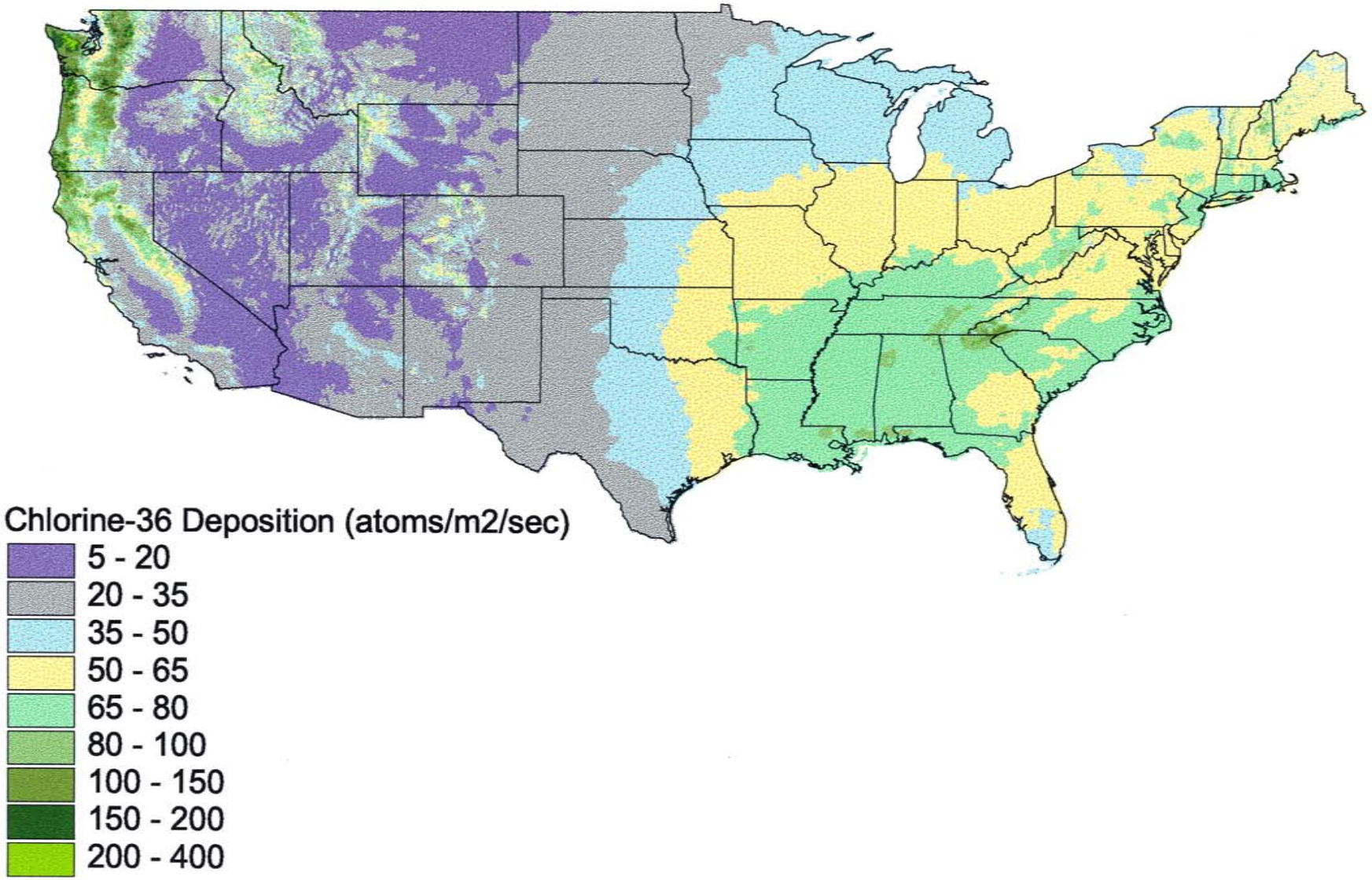

Figure 4.22: Distribution of 36Cl deposition over the U.S. calculated using the Phillips (1999) model of 36Cl deposition and the PRISM precipitation model.

A) 36Cl/Cl ratio distribution using 'annual' wet deposition model, dry deposition interpolation, and modeled 36Cl deposition

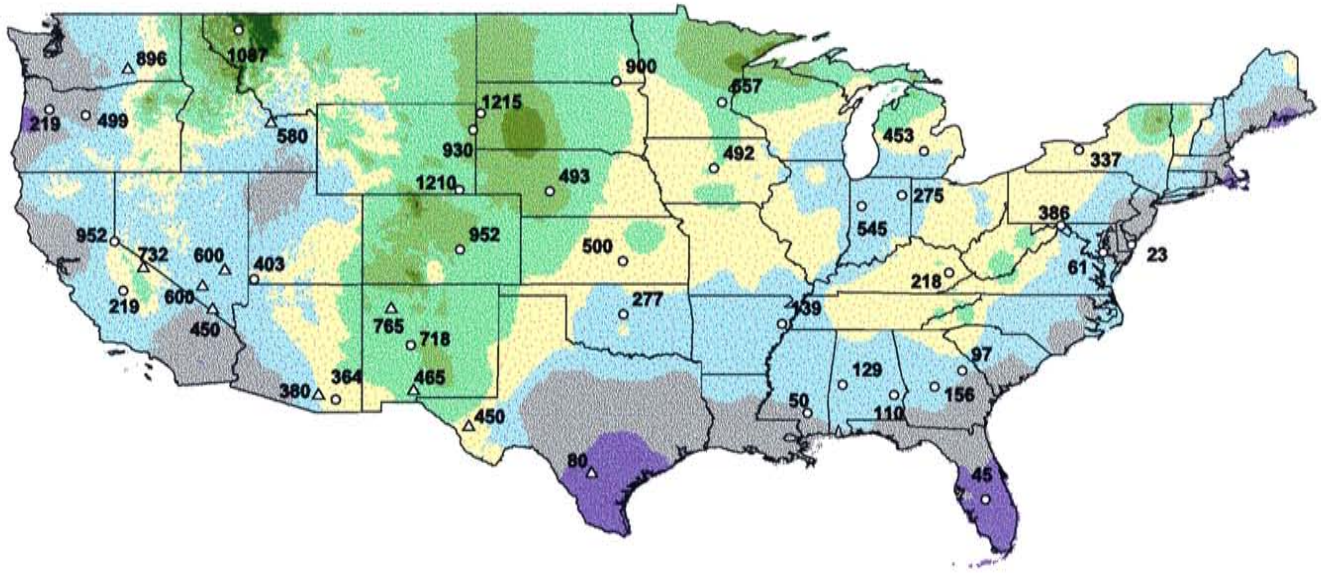

B) 36Cl/Cl ratio distribution using 'monthly' wet deposition model, dry deposition interpolation, and modeled 36Cl deposition

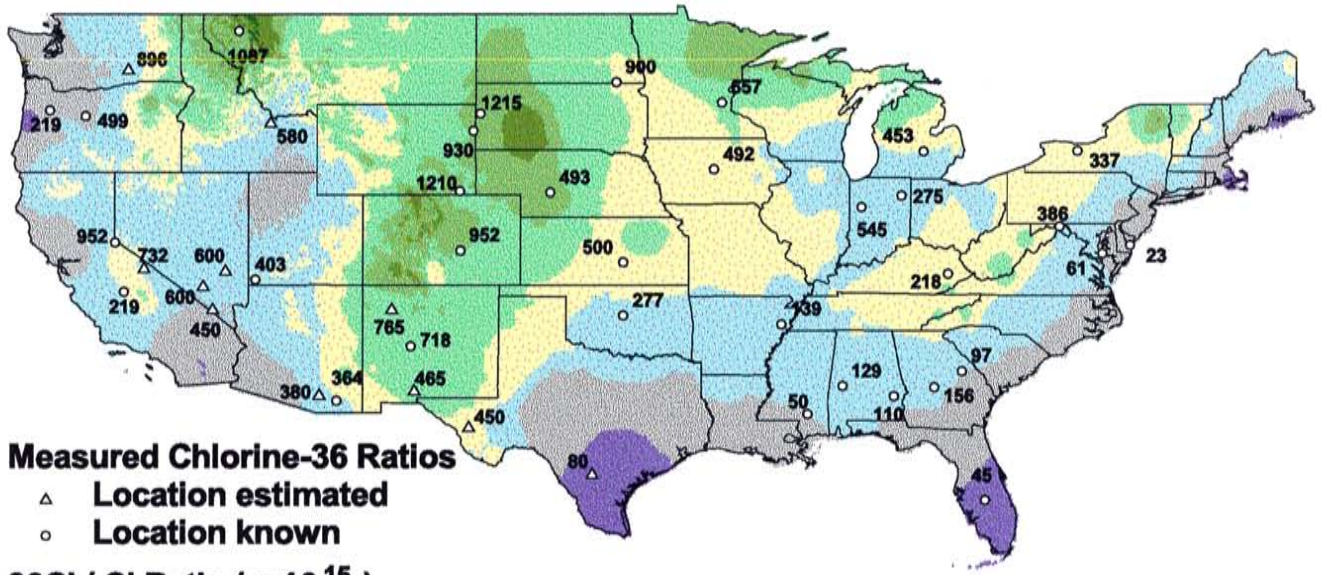

Measured Chlorine-36 Ratios

△ Location estimated

○ Location known

36Cl / Cl Ratio (x 10^{15})

- 0 - 100
- 100 - 250
- 250 - 500
- 500 - 750
- 750 - 1000
- 1000 - 1250
- 1250 - 1500
- > 1500

Figure 4.23: Distribution of 36Cl/Cl ratios over the U.S. calculated using the new model developed in this study.

CHAPTER 5 - MODEL ERROR ASSESSMENT

The $^{36}Cl/Cl$ model constructed for this study represents a new approach to the modeling of the spatial distribution of chloride and ^{36}Cl across the country. The model and its components were compared with measurements throughout the country to assess the performance of the new model, and to determine whether it offered improvement over previous modeling efforts. The major components of the $^{36}Cl/Cl$ model were the PRISM precipitation model, the new wet chloride deposition model, the dry deposition component, and the ^{36}Cl deposition model. Each of these components of the $^{36}Cl/Cl$ model was assessed independently, and is discussed in the following sections. The identification and quantification of the modeling errors reveals the current weaknesses in the modeling approach, and the areas where improvements should be pursued.

5.1 PRISM Precipitation Model Errors

The PRISM model is the base model on which the new wet deposition model and the ^{36}Cl deposition distributions are based. Errors in the PRISM model would thus have a significant effect on the modeling results of this study. The PRISM model, however, has undergone extensive peer review by expert climatologists in each state, and is probably one of the smaller sources of error in the models presented in this study.

5.2 Errors in the Wet Chloride Deposition Model

The wet chloride deposition model developed in this study was based on a linear relationship between chloride deposition and precipitation, determined using measurements from the NADP/NTN. Two versions of the wet deposition model were

constructed, the "annual" version and the "monthly" version. The "annual" model used a single regression at each NADP/NTN station based on all available monthly chloride and precipitation data; the same regression was used with each month of PRISM data to calculate the wet deposition each month. The "monthly" model used twelve separate regressions at each NADP/NTN station, one for each month of the year. Each monthly regression was used with the corresponding monthly PRISM data to calculate the wet deposition each month. In both models, the monthly wet deposition values were summed to obtain the annual wet chloride deposition over the United States, as shown in Figure 4.17.

The two wet deposition models were compared to the measured data at each of the NADP/NTN stations to assess which one more closely matched the observations. The percent difference between the model predictions and the measured values was calculated at each NADP/NTN station using

$$\text{Percent difference} = \frac{[Model] - [Measured]}{[Measured]} * 100 \qquad \text{Eqn 5.1}$$

A positive percent difference indicates model overprediction, while a negative percent difference indicates model underprediction. The distribution of the percent difference for each of the two models is shown in Figure 5.1, and Table 5.1 summarizes the errors calculated at each station. The "monthly" wet chloride deposition model offers a much better fit to the measured data than does the "annual" model. This indicates that the change in chloride / precipitation regression slopes throughout the year is significant. The "monthly" wet deposition model is within ±20% of the measured data over most of the

Table 5.1: Calculated errors for the "annual" and "monthly" wet deposition models

Site ID	Latitude (°N)	Longitude (°W)	Measured Wet Cl Deposition ($mg/m^2/yr$))	"Annual" Model Predicted Deposition ($mg/m^2/yr$)	"Annual" Model Error	"Annual" Absolute Error	"Monthly" Model Predicted Deposition ($mg/m^2/yr$)	"Monthly" Model Error	"Monthly" Absolute Error
AL10	32.4583	-87.2422	357.66	354.40	-0.01	0.01	378.54	0.06	0.06
AL99	34.2878	-85.9689	263.68	281.29	0.07	0.07	278.98	0.06	0.06
AR02	33.6050	-92.0972	364.16	319.63	-0.12	0.12	317.36	-0.13	0.13
AR03	34.1794	-93.0986	326.87	290.12	-0.11	0.11	291.45	-0.11	0.11
AR16	36.0839	-92.5869	180.93	178.89	-0.01	0.01	173.07	-0.04	0.04
AR27	36.1006	-94.1733	182.96	164.83	-0.10	0.10	164.04	-0.10	0.10
AZ03	36.0717	-112.1550	52.58	28.75	-0.45	0.45	31.97	-0.39	0.39
AZ06	31.9506	-112.8000	153.87	76.41	-0.50	0.50	109.85	-0.29	0.29
AZ99	33.0714	-109.8647	43.39	39.04	-0.10	0.10	38.19	-0.12	0.12
CA42	34.2072	-117.7611	291.23	236.69	-0.19	0.19	255.66	-0.12	0.12
CA45	39.0047	-123.0847	513.05	570.00	0.11	0.11	535.90	0.04	0.04
CA75	36.5669	-118.7772	107.68	87.14	-0.19	0.19	93.28	-0.13	0.13
CA76	41.7664	-122.4783	22.88	15.35	-0.33	0.33	17.98	-0.21	0.21
CA98	34.8061	-119.0114	46.30	31.87	-0.31	0.31	35.01	-0.24	0.24
CO01	38.1178	-103.3161	36.54	29.48	-0.19	0.19	29.68	-0.19	0.19
CO08	39.4031	-107.3411	43.54	50.11	0.15	0.15	46.41	0.07	0.07
CO15	40.5075	-107.7019	36.27	39.46	0.09	0.09	37.80	0.04	0.04
CO19	40.3642	-105.5819	39.10	41.83	0.07	0.07	43.27	0.11	0.11
CO21	39.1011	-105.0919	35.96	44.29	0.23	0.23	40.53	0.13	0.13
CO22	40.8064	-104.7547	31.48	29.02	-0.08	0.08	28.22	-0.10	0.10
CO94	39.9939	-105.4800	37.02	29.24	-0.21	0.21	30.66	-0.17	0.17
CO99	37.1981	-108.4903	44.12	33.26	-0.25	0.25	34.62	-0.22	0.22
FL03	29.9747	-82.1981	583.60	500.04	-0.14	0.14	503.28	-0.14	0.14
FL11	25.3900	-80.6800	1334.10	1084.40	-0.19	0.19	1230.31	-0.08	0.08
FL14	30.5481	-84.6008	566.49	616.50	0.09	0.09	546.60	-0.04	0.04
FL41	27.3800	-82.2839	761.15	724.67	-0.05	0.05	779.60	0.02	0.02
FL99	28.5428	-80.6444	1866.04	1598.05	-0.14	0.14	1691.75	-0.09	0.09
GA20	32.1411	-81.9714	422.40	432.17	0.02	0.02	421.44	0.00	0.00
GA41	33.1778	-84.4061	300.97	298.48	-0.01	0.01	306.12	0.02	0.02
GA50	31.4731	-83.5331	388.11	337.85	-0.13	0.13	366.16	-0.06	0.06
GA99	31.5183	-83.5483	398.27	313.37	-0.21	0.21	352.61	-0.11	0.11
IA08	42.9097	-91.4700	84.76	69.24	-0.18	0.18	72.69	-0.14	0.14

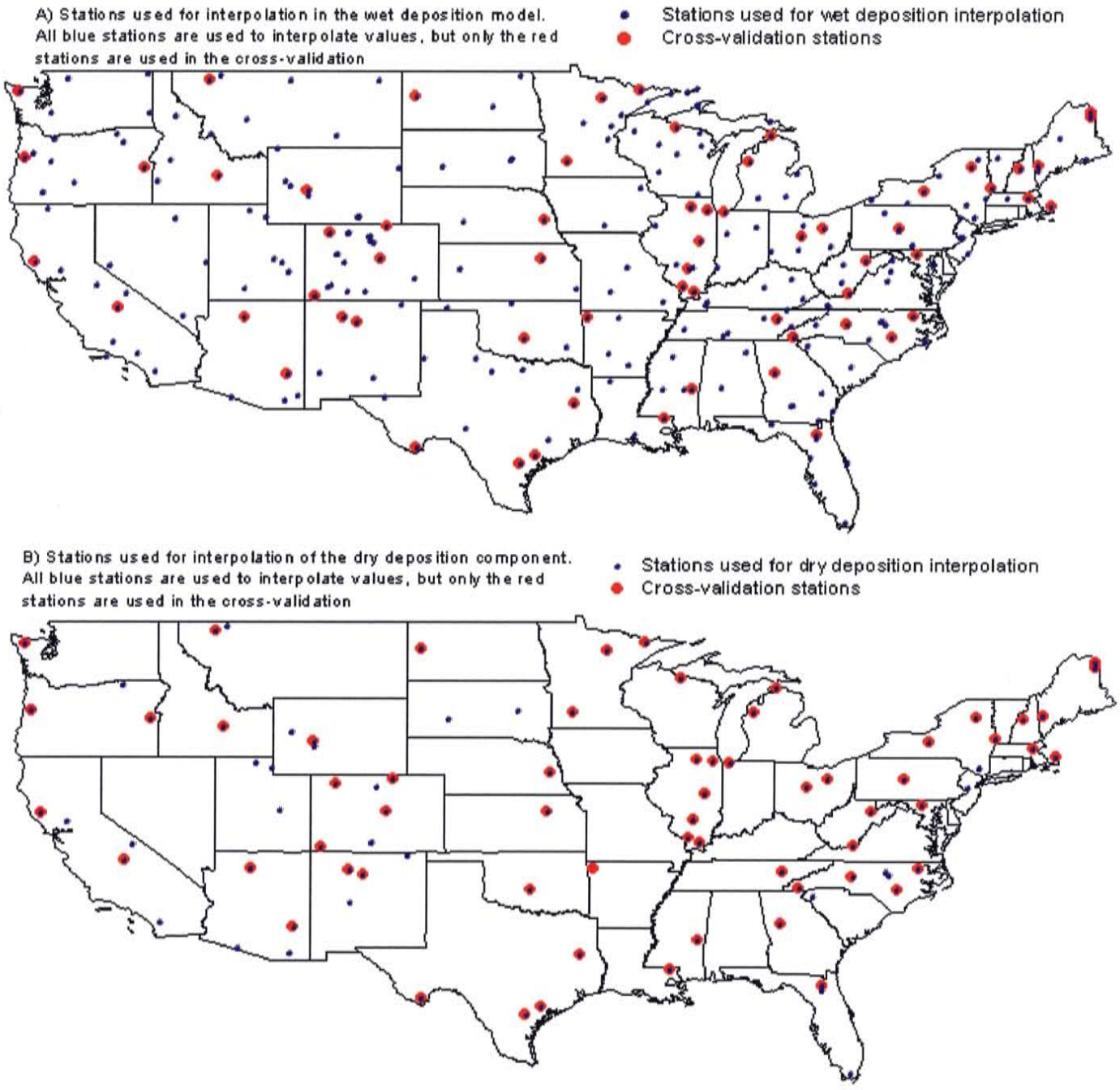

Figure 5.3: Distribution of stations available for the analysis of interpolation errors for the wet deposition model and the dry deposition distribution.

Table 5.1: Calculated errors for the "annual" and "monthly" wet deposition models

Site ID	Latitude (°N)	Longitude (°W)	Measured Wet Cl Deposition ($mg/m^2/yr$))	"Annual" Model Predicted Deposition ($mg/m^2/yr$)	"Annual" Model Error	"Annual" Absolute Error	"Monthly" Model Predicted Deposition ($mg/m^2/yr$)	"Monthly" Model Error	"Monthly" Absolute Error
IA23	40.9631	-93.3925	91.44	75.57	-0.17	0.17	84.70	-0.07	0.07
ID03	43.4614	-113.5547	46.13	44.89	-0.03	0.03	45.21	-0.02	0.02
ID04	46.6278	-115.8194	67.67	63.10	-0.07	0.07	66.16	-0.02	0.02
ID11	43.2053	-116.7492	29.18	21.78	-0.25	0.25	25.09	-0.14	0.14
ID15	44.2978	-116.0636	54.75	41.80	-0.24	0.24	49.71	-0.09	0.09
IL11	40.0533	-88.3719	127.33	136.55	0.07	0.07	138.63	0.09	0.09
IL18	41.8414	-88.8511	106.41	100.62	-0.05	0.05	103.41	-0.03	0.03
IL19	41.7011	-87.9953	150.19	147.75	-0.02	0.02	149.68	0.00	0.00
IL35	37.7100	-89.2689	179.43	181.93	0.01	0.01	182.86	0.02	0.02
IL47	38.6433	-88.9669	150.73	150.35	0.00	0.00	153.38	0.02	0.02
IL63	37.4356	-88.6719	236.42	218.42	-0.08	0.08	222.21	-0.06	0.06
IL78	40.9333	-90.7231	86.73	91.27	0.05	0.05	91.19	0.05	0.05
IN20	40.8400	-85.4639	113.62	108.85	-0.04	0.04	109.83	-0.03	0.03
IN22	38.7408	-87.4856	189.93	189.65	0.00	0.00	187.09	-0.01	0.01
IN34	41.6325	-87.0878	150.96	129.97	-0.14	0.14	138.13	-0.08	0.08
IN41	40.4753	-86.9922	135.42	124.38	-0.08	0.08	128.90	-0.05	0.05
KS07	37.6511	-94.8036	153.35	134.05	-0.13	0.13	135.10	-0.12	0.12
KS31	39.1022	-96.6092	95.16	93.44	-0.02	0.02	90.13	-0.05	0.05
KS32	38.6717	-100.9164	52.04	47.26	-0.09	0.09	44.32	-0.15	0.15
KY03	37.7047	-85.0489	191.03	208.34	0.09	0.09	204.43	0.07	0.07
KY22	37.0778	-82.9936	142.57	123.06	-0.14	0.14	120.24	-0.16	0.16
KY35	38.1183	-83.5469	143.86	131.71	-0.08	0.08	137.15	-0.05	0.05
KY38	36.7906	-88.0672	194.83	201.87	0.04	0.04	198.90	0.02	0.02
LA12	29.9297	-91.7153	919.23	796.47	-0.13	0.13	822.35	-0.11	0.11
LA30	30.8114	-90.1808	770.14	742.40	-0.04	0.04	720.39	-0.06	0.06
MA01	41.9758	-70.0247	2695.49	2563.19	-0.05	0.05	2493.94	-0.07	0.07
MA08	42.3925	-72.3444	278.40	242.44	-0.13	0.13	259.86	-0.07	0.07
MA13	42.3839	-71.2147	687.63	684.56	0.00	0.00	747.19	0.09	0.09
MD03	39.4089	-76.9953	282.27	294.57	0.04	0.04	291.07	0.03	0.03
MD13	38.9131	-76.1525	433.46	438.20	0.01	0.01	445.32	0.03	0.03
ME00	46.8689	-68.0131	118.16	95.40	-0.19	0.19	106.04	-0.10	0.10
ME02	44.1075	-70.7289	285.40	349.14	0.22	0.22	375.58	0.32	0.32

Table 5.1: Calculated errors for the "annual" and "monthly" wet deposition models

Site ID	Latitude (°N)	Longitude (°W)	Measured Wet Cl Deposition ($mg/m^2/yr$))	"Annual" Model Predicted Deposition ($mg/m^2/yr$)	"Annual" Model Error	"Annual" Absolute Error	"Monthly" Model Predicted Deposition ($mg/m^2/yr$)	"Monthly" Model Error	"Monthly" Absolute Error
ME09	45.4892	-69.6653	148.84	145.14	-0.02	0.02	150.14	0.01	0.01
ME97	46.6547	-68.0089	108.49	94.30	-0.13	0.13	118.60	0.09	0.09
ME98	44.3739	-68.2606	1392.15	1385.49	0.00	0.00	1337.45	-0.04	0.04
MI09	45.5608	-84.6783	71.49	65.99	-0.08	0.08	68.91	-0.04	0.04
MI26	42.4103	-85.3928	103.39	99.22	-0.04	0.04	104.17	0.01	0.01
MI53	44.2242	-85.8186	105.73	78.57	-0.26	0.26	83.52	-0.21	0.21
MN16	47.5311	-93.4686	55.72	44.60	-0.20	0.20	46.15	-0.17	0.17
MN18	47.9464	-91.4961	41.76	47.41	0.14	0.14	45.93	0.10	0.10
MN23	46.2494	-94.4972	43.98	36.38	-0.17	0.17	38.72	-0.12	0.12
MN27	44.2372	-95.3006	61.62	52.74	-0.14	0.14	54.70	-0.11	0.11
MO03	38.7536	-92.1989	128.81	113.14	-0.12	0.12	113.60	-0.12	0.12
MO05	36.9108	-90.3186	215.97	228.63	0.06	0.06	214.02	-0.01	0.01
MS10	32.3067	-90.3183	391.03	399.83	0.02	0.02	398.64	0.02	0.02
MS14	32.3344	-88.7450	416.29	399.82	-0.04	0.04	388.78	-0.07	0.07
MS19	32.3347	-89.1658	339.94	305.99	-0.10	0.10	312.86	-0.08	0.08
MS30	34.0025	-89.8000	304.41	287.07	-0.06	0.06	286.68	-0.06	0.06
MT00	45.5686	-107.4375	26.76	30.14	0.13	0.13	30.26	0.13	0.13
MT05	48.5103	-113.9958	46.04	33.11	-0.28	0.28	34.80	-0.24	0.24
MT07	46.4850	-112.0647	26.88	22.42	-0.17	0.17	21.66	-0.19	0.19
MT13	48.4886	-105.2083	25.57	18.53	-0.28	0.28	23.88	-0.07	0.07
MT98	48.4992	-109.7975	23.82	16.21	-0.32	0.32	20.11	-0.16	0.16
NC03	36.1325	-77.1714	523.32	469.52	-0.10	0.10	510.36	-0.02	0.02
NC11	35.9025	-78.8700	235.50	205.01	-0.13	0.13	270.57	0.15	0.15
NC25	35.0606	-83.4306	322.53	341.85	0.06	0.06	338.03	0.05	0.05
NC33	35.8964	-78.8606	268.07	205.66	-0.23	0.23	269.56	0.01	0.01
NC34	35.6969	-80.6225	299.51	273.61	-0.09	0.09	279.62	-0.07	0.07
NC35	35.0258	-78.2783	542.19	552.74	0.02	0.02	609.15	0.12	0.12
NC36	34.9708	-79.5283	409.46	371.96	-0.09	0.09	395.42	-0.03	0.03
NC41	35.7283	-78.6803	376.94	359.32	-0.05	0.05	365.74	-0.03	0.03
NC45	35.7353	-82.2861	157.76	127.15	-0.19	0.19	140.44	-0.11	0.11
ND07	47.6014	-103.2642	26.35	24.37	-0.08	0.08	24.76	-0.06	0.06
NE15	41.1531	-96.4928	84.02	87.30	0.04	0.04	85.47	0.02	0.02

Table 5.1: Calculated errors for the "annual" and "monthly" wet deposition models

Site ID	Latitude (°N)	Longitude (°W)	Measured Wet Cl Deposition ($mg/m^2/yr$))	"Annual" Model Predicted Deposition ($mg/m^2/yr$)	"Annual" Model Error	"Annual" Absolute Error	"Monthly" Model Predicted Deposition ($mg/m^2/yr$)	"Monthly" Model Error	"Monthly" Absolute Error
NE99	41.0592	-100.7464	35.11	33.45	-0.05	0.05	32.93	-0.06	0.06
NH02	43.9431	-71.7033	195.31	196.91	0.01	0.01	212.88	0.09	0.09
NJ99	40.3150	-74.8547	422.08	405.24	-0.04	0.04	441.64	0.05	0.05
NM01	33.2203	-108.2347	49.07	38.82	-0.21	0.21	46.05	-0.06	0.06
NM07	35.7817	-106.2675	39.64	28.91	-0.27	0.27	31.95	-0.19	0.19
NM08	32.9094	-105.4706	54.65	29.60	-0.46	0.46	40.26	-0.26	0.26
NM09	36.0408	-106.9714	35.67	30.14	-0.16	0.16	30.85	-0.14	0.14
NM12	36.7789	-103.9814	48.61	38.33	-0.21	0.21	49.45	0.02	0.02
NV00	36.1358	-115.4256	26.94	12.67	-0.53	0.53	22.46	-0.17	0.17
NV03	38.7992	-119.2567	16.15	12.32	-0.24	0.24	16.23	0.00	0.00
NV05	39.0050	-114.2158	63.23	48.28	-0.24	0.24	54.81	-0.13	0.13
NY08	42.7339	-76.6597	113.33	108.44	-0.04	0.04	110.92	-0.02	0.02
NY10	42.2994	-79.3964	148.48	148.42	0.00	0.00	154.60	0.04	0.04
NY12	42.3783	-73.5028	147.43	169.89	0.15	0.15	195.46	0.33	0.33
NY20	43.9731	-74.2231	96.97	94.00	-0.03	0.03	96.82	0.00	0.00
NY51	41.3500	-74.0394	479.33	419.72	-0.12	0.12	478.66	0.00	0.00
NY52	43.5261	-75.9472	195.02	162.92	-0.16	0.16	187.07	-0.04	0.04
NY65	42.1064	-77.5358	84.27	82.09	-0.03	0.03	83.40	-0.01	0.01
NY68	41.9936	-74.5036	198.53	204.12	0.03	0.03	205.93	0.04	0.04
NY98	44.3933	-73.8594	78.89	63.58	-0.19	0.19	65.60	-0.17	0.17
NY99	41.3508	-74.0486	500.54	422.29	-0.16	0.16	479.58	-0.04	0.04
OH09	39.5314	-84.7242	146.18	133.37	-0.09	0.09	135.41	-0.07	0.07
OH17	40.3553	-83.0661	144.53	136.47	-0.06	0.06	144.87	0.00	0.00
OH49	39.7928	-81.5311	180.00	156.95	-0.13	0.13	163.53	-0.09	0.09
OH71	40.7822	-81.9200	130.03	122.65	-0.06	0.06	130.76	0.01	0.01
OK00	36.8053	-98.2006	147.22	118.67	-0.19	0.19	112.89	-0.23	0.23
OK17	34.9800	-97.5214	172.32	141.97	-0.18	0.18	146.85	-0.15	0.15
OK25	34.5297	-95.3531	383.19	310.10	-0.19	0.19	292.57	-0.24	0.24
OK29	36.5908	-101.6175	53.42	48.18	-0.10	0.10	46.53	-0.13	0.13
OR02	44.3856	-123.6153	2205.74	3271.32	0.48	0.48	3087.69	0.40	0.40
OR08	42.6678	-122.6831	115.65	112.04	-0.03	0.03	108.02	-0.07	0.07
OR09	43.1217	-121.0578	21.07	13.79	-0.35	0.35	15.85	-0.25	0.25

Table 5.1: Calculated errors for the "annual" and "monthly" wet deposition models

Site ID	Latitude (°N)	Longitude (°W)	Measured Wet Cl Deposition ($mg/m^2/yr$))	"Annual" Model Predicted Deposition ($mg/m^2/yr$)	"Annual" Model Error	"Annual" Absolute Error	"Monthly" Model Predicted Deposition ($mg/m^2/yr$)	"Monthly" Model Error	"Monthly" Absolute Error
OR10	44.2122	-122.2558	648.55	550.52	-0.15	0.15	522.06	-0.20	0.20
OR11	43.8994	-117.4269	20.68	20.55	-0.01	0.01	21.91	0.06	0.06
OR18	45.2244	-118.5114	31.75	29.13	-0.08	0.08	31.15	-0.02	0.02
OR97	44.6347	-123.1900	592.06	704.67	0.19	0.19	711.93	0.20	0.20
OR98	45.4478	-122.1481	1013.60	1052.31	0.04	0.04	1011.55	0.00	0.00
OR99	44.6264	-123.2139	651.75	685.27	0.05	0.05	728.76	0.12	0.12
PA15	40.7883	-77.9458	155.49	126.10	-0.19	0.19	133.85	-0.14	0.14
PA29	41.5978	-78.7675	194.57	159.64	-0.18	0.18	166.87	-0.14	0.14
PA42	40.6575	-77.9397	169.08	140.95	-0.17	0.17	145.35	-0.14	0.14
PA72	41.3275	-74.8203	246.40	207.63	-0.16	0.16	216.36	-0.12	0.12
SC06	33.5394	-80.4350	458.76	408.55	-0.11	0.11	425.58	-0.07	0.07
SC18	34.6239	-82.7342	326.63	209.67	-0.36	0.36	358.88	0.10	0.10
TN00	35.9614	-84.2872	255.12	258.25	0.01	0.01	253.63	-0.01	0.01
TN11	35.6644	-83.5903	155.40	143.30	-0.08	0.08	137.52	-0.12	0.12
TN14	35.4678	-89.1586	249.81	230.35	-0.08	0.08	231.87	-0.07	0.07
TN98	35.1825	-87.1964	254.36	236.27	-0.07	0.07	233.42	-0.08	0.08
TX02	33.9578	-102.7761	61.52	55.71	-0.09	0.09	56.17	-0.09	0.09
TX03	28.4667	-97.7069	553.95	548.68	-0.01	0.01	566.30	0.02	0.02
TX04	29.3022	-103.1772	40.69	36.62	-0.10	0.10	36.46	-0.10	0.10
TX10	29.6614	-96.2594	609.80	461.63	-0.24	0.24	499.18	-0.18	0.18
TX16	30.2614	-100.5550	132.78	101.81	-0.23	0.23	126.39	-0.05	0.05
TX18	33.9242	-100.0469	90.88	75.65	-0.17	0.17	76.63	-0.16	0.16
TX21	32.3786	-94.7117	387.48	358.49	-0.07	0.07	351.84	-0.09	0.09
TX22	31.9083	-104.8067	53.11	37.13	-0.30	0.30	43.19	-0.19	0.19
TX38	31.5606	-94.8608	428.56	361.01	-0.16	0.16	361.65	-0.16	0.16
TX51	33.2733	-99.2153	141.53	128.81	-0.09	0.09	132.68	-0.06	0.06
TX53	28.8453	-96.9203	819.83	635.64	-0.22	0.22	660.48	-0.19	0.19
TX56	33.3917	-97.6397	196.96	180.49	-0.08	0.08	182.56	-0.07	0.07
UT01	41.6583	-111.8969	215.76	170.02	-0.21	0.21	200.27	-0.07	0.07
UT98	38.9983	-110.1653	26.55	16.98	-0.36	0.36	23.53	-0.11	0.11
UT99	37.6186	-112.1728	50.90	39.48	-0.22	0.22	49.44	-0.03	0.03
VA00	38.0406	-78.5431	256.24	223.25	-0.13	0.13	246.83	-0.04	0.04

Table 5.1: Calculated errors for the "annual" and "monthly" wet deposition models

Site ID	Latitude (°N)	Longitude (°W)	Measured Wet Cl Deposition ($mg/m^2/yr$))	"Annual" Model Predicted Deposition ($mg/m^2/yr$)	"Annual" Model Error	"Annual" Absolute Error	"Monthly" Model Predicted Deposition ($mg/m^2/yr$)	"Monthly" Model Error	"Monthly" Absolute Error
VA13	37.3314	-80.5575	118.50	108.24	-0.09	0.09	112.14	-0.05	0.05
VA28	38.5225	-78.4358	243.55	213.35	-0.12	0.12	222.89	-0.08	0.08
VT01	42.8761	-73.1633	136.67	122.03	-0.11	0.11	128.31	-0.06	0.06
VT99	44.5283	-72.8689	82.01	77.94	-0.05	0.05	87.20	0.06	0.06
WA14	47.8600	-123.9319	2591.84	3196.42	0.23	0.23	3077.40	0.19	0.19
WA19	48.5406	-121.4453	418.47	333.86	-0.20	0.20	346.74	-0.17	0.17
WA21	46.8353	-122.2867	336.51	443.59	0.32	0.32	448.00	0.33	0.33
WA24	46.7606	-117.1847	37.53	35.67	-0.05	0.05	36.61	-0.02	0.02
WI09	45.7964	-88.3994	52.75	51.99	-0.01	0.01	55.91	0.06	0.06
WI25	45.0533	-88.3728	69.22	64.84	-0.06	0.06	68.21	-0.01	0.01
WI28	44.6644	-89.6525	67.82	69.41	0.02	0.02	77.45	0.14	0.14
WI36	46.0528	-89.6531	54.44	52.04	-0.04	0.04	52.90	-0.03	0.03
WI37	45.8228	-91.8744	55.57	52.00	-0.06	0.06	52.79	-0.05	0.05
WI98	43.7022	-90.5686	68.02	59.91	-0.12	0.12	64.14	-0.06	0.06
WI99	42.5792	-88.5006	98.47	93.80	-0.05	0.05	98.49	0.00	0.00
WV04	37.9800	-80.9500	131.59	125.09	-0.05	0.05	124.88	-0.05	0.05
WV18	39.0897	-79.6622	150.18	141.04	-0.06	0.06	143.29	-0.05	0.05
WY02	42.7339	-108.8500	29.38	28.97	-0.01	0.01	29.78	0.01	0.01
WY06	42.9289	-109.7867	33.89	43.39	0.28	0.28	39.34	0.16	0.16
WY08	44.9172	-110.4203	37.27	39.18	0.05	0.05	37.94	0.02	0.02
WY99	43.8733	-104.1922	31.47	25.89	-0.18	0.18	26.99	-0.14	0.14
				Average Error	**-0.09**			**-0.05**	
				Average Absolute Error		**0.13**			**0.10**

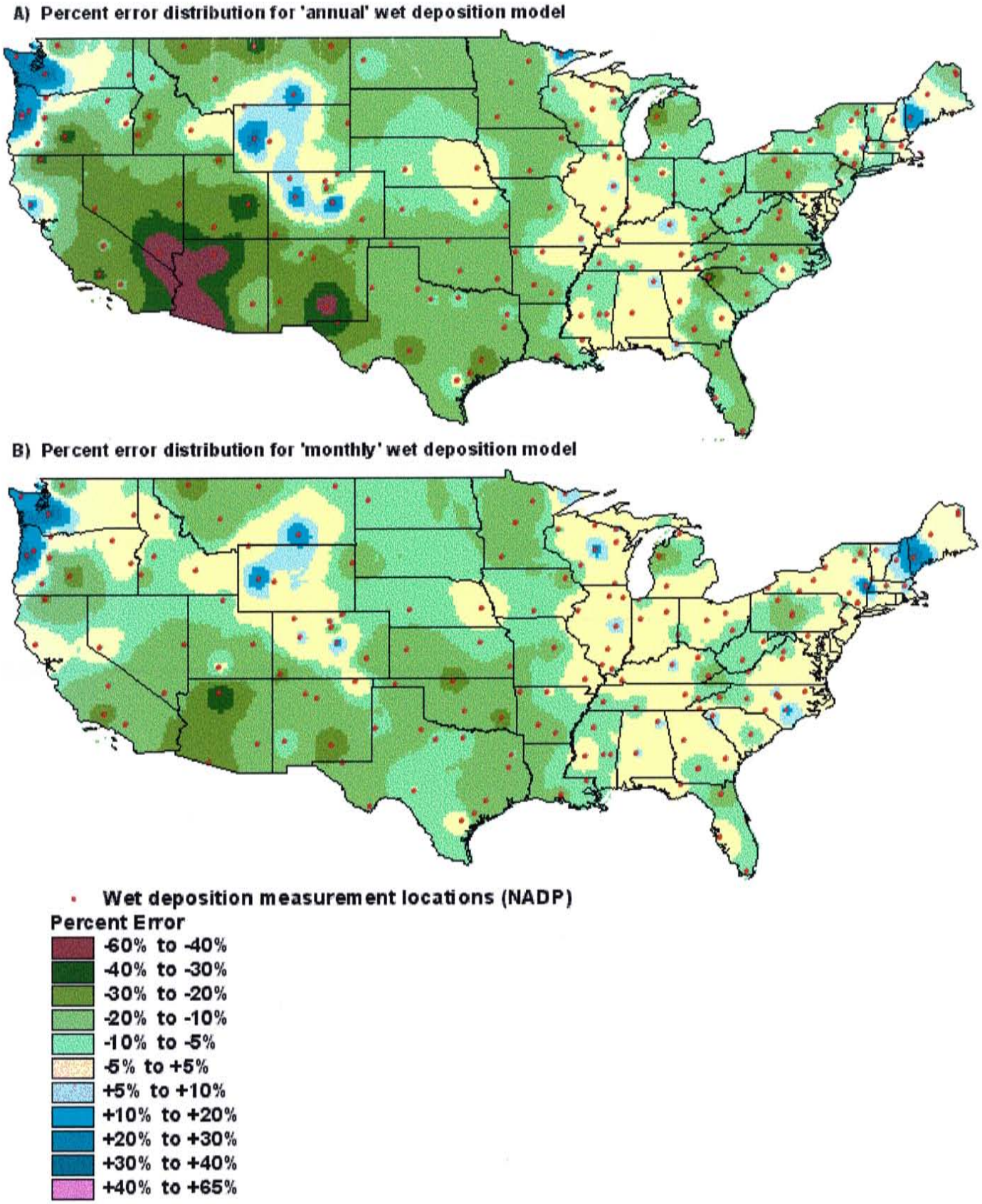

Figure 5.1: Wet deposition model error distributions for the "annual" (a) and "monthly" wet deposition models. Points represent stations with measured values (Table 5.1) to which the modeled values were compared.

country, and within ±10% over a significant portion. The average absolute error of the "monthly" wet deposition model was 10 percent, versus 13 percent for the "annual" model (Table 5.1). Figure 5.1 illustrates that both wet deposition models are biased toward underprediction across most of the country. This may be a result of the ceiling value in chloride collection at high precipitation values. The linear regressions may be overly influenced by these ceiling values, which would act to reduce the regression slope slightly.

The chloride collection / precipitation slopes were evaluated at each NADP/NTN station, and had to be remapped to the same resolution as the PRISM precipitation data. This was done using an interpolation with an inverse distance weighting scheme. The interpolation process introduces another source of potential error. To assess this potential interpolation error, a cross-validation technique was incorporated whereby individual stations were removed from the map followed by reinterpolation without the presence of that station. The predicted values from the interpolation performed with and without the station's presence could then be compared. To simplify the interpolation error analysis, the "annual" wet deposition model was used. With the "annual" model, a single regression slope was used over the entire year at each station such that a single interpolation of these slopes across the country was required after each station removal. Using the "monthly" model to assess the interpolation error would require twelve interpolations each time a station was removed. As previously shown, the "monthly" model offered superior fit to the measured data in many areas of the country, particularly in the Southwest. In order to avoid compounding errors arising from use of the poorer fitting "annual" model, the percent difference between the two model predictions was calculated to delineate those

regions where the two models were in good agreement. The percent difference between the two models was calculated using

$$\text{Percent difference} = \frac{[Monthly]-[Annual]}{[Monthly]} * 100 \qquad \text{Eqn 5.2}$$

The distribution of this percent difference across the country is shown in Figure 5.2. While areas of significant difference exist in the Southwest, the two models are within ±5% over much of the country. Only those stations within regions of ±10% "annual" versus "monthly" percent differences were used for the interpolation error assessment. Further, because the interpolation error was also quantified for the dry deposition component (discussed later), only stations where both wet and dry deposition measurements were available were used for the interpolation error assessment. Sixty-two NADP/NTN stations met both the percent difference (within 10%) and measurement (wet and dry) stipulations and are highlighted in Figure 5.3, which illustrates the total number of stations available for both the wet and dry interpolations. Each of these 62 stations was individually removed with a reinterpolation of the chloride collection / precipitation slope field (using all available points in Figure 5.3) performed after each removal, and recalculation of the wet deposition distribution. The deposition value interpolated at the location of the missing station was compared with the measured value at that station and summarized in Table 5.2. The interpolation error was calculated as the percent change in deposition value with and without a station's presence. The average absolute interpolation error for the wet deposition model was 20 percent (Table 5.2). The distribution of the wet deposition model interpolation error is shown in Figure 5.4. The interpolation error is within ±10% over

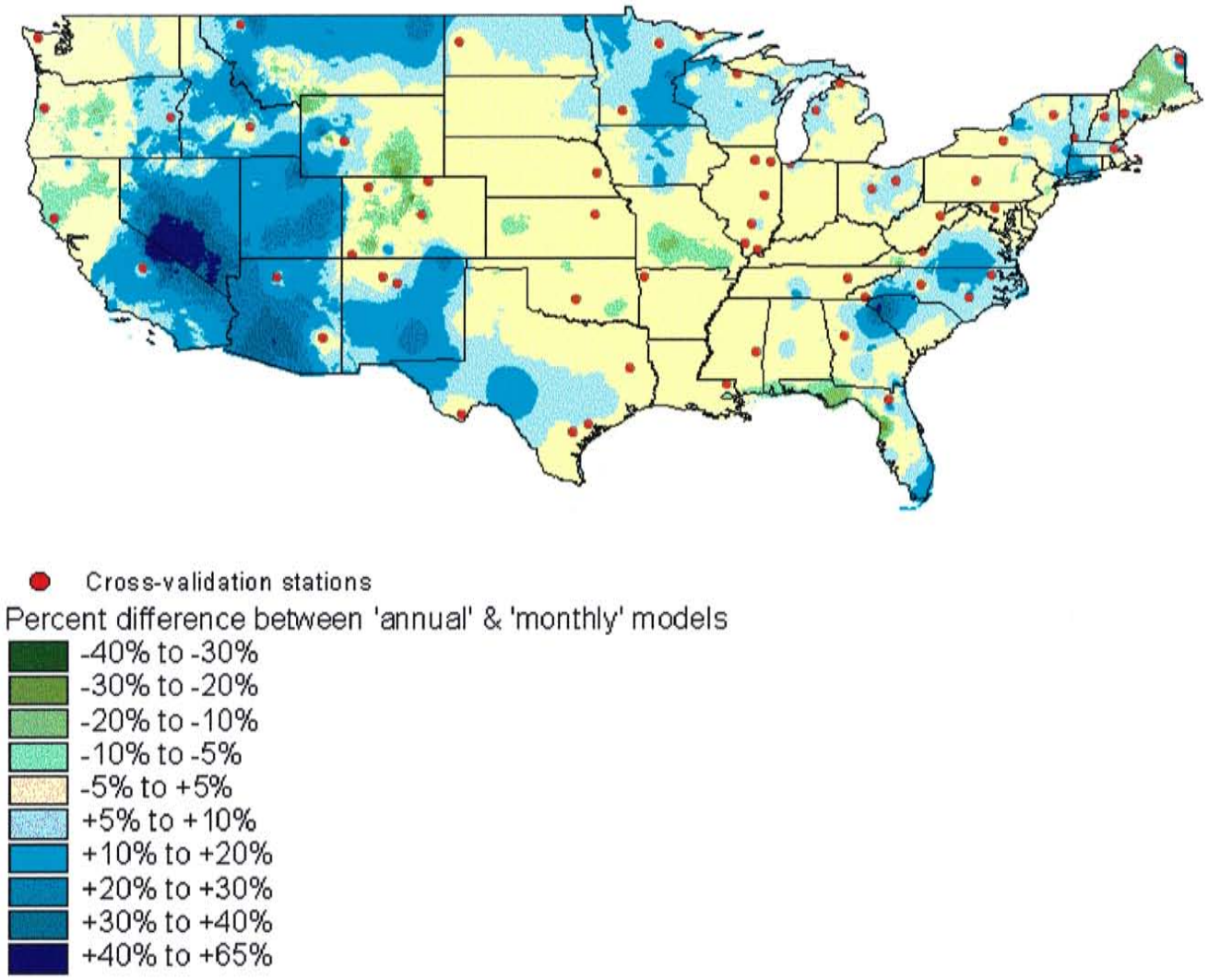

Figure 5.2: Calculated agreement between "annual" and "monthly" wet deposition models (calculated as the percent difference between the two model predictions). Points indicate stations where the model agreement is within 10 percent and both wet and dry deposition measurements are available (62 points).

Table 5.2: Wet interpolation errors from cross-validation analysis

Site ID	Latitude (°N)	Longitude (°W)	"Annual" Model Wet Deposition ($mg/m^2/yr$)	Value from Interpolation Without Station ($mg/m^2/yr$)	Interpolation Error *	Absolute Error
AR27	36.1006	-94.1733	164.83	131.53	-0.20	0.20
AZ03	36.0717	-112.1550	28.75	28.75	0.00	0.00
AZ99	33.0714	-109.8647	39.04	32.51	-0.17	0.17
CA45	39.0047	-123.0847	570	886.97	0.56	0.56
CA75	36.5669	-118.7772	87.14	71.31	-0.18	0.18
CO15	40.5075	-107.7019	39.46	51.81	0.31	0.31
CO21	39.1011	-105.0919	44.29	49.52	0.12	0.12
CO22	40.8064	-104.7547	29.02	31.73	0.09	0.09
CO99	37.1981	-108.4903	33.26	33.08	-0.01	0.01
FL03	29.9747	-82.1981	500.04	435.33	-0.13	0.13
GA41	33.1778	-84.4061	298.48	294.08	-0.01	0.01
ID03	43.4614	-113.5547	44.89	34.66	-0.23	0.23
IL11	40.0533	-88.3719	136.55	134.71	-0.01	0.01
IL18	41.8414	-88.8511	100.62	82.72	-0.18	0.18
IL19	41.7011	-87.9953	147.75	183.68	0.24	0.24
IL35	37.7100	-89.2689	181.93	178.33	-0.02	0.02
IL47	38.6433	-88.9669	150.35	174.52	0.16	0.16
IL63	37.4356	-88.6719	218.42	248.38	0.14	0.14
IN34	41.6325	-87.0878	129.97	133.25	0.03	0.03
KS31	39.1022	-96.6092	93.44	76.54	-0.18	0.18
LA30	30.8114	-90.1808	742.4	983.86	0.33	0.33
MA01	41.9758	-70.0247	2563.19	4545.73	0.77	0.77
MA13	42.3839	-71.2147	684.56	539.56	-0.21	0.21
MD03	39.4089	-76.9953	294.57	300.59	0.02	0.02
ME00	46.8689	-68.0131	95.4	79.18	-0.17	0.17
ME02	44.1075	-70.7289	349.14	237.12	-0.32	0.32
ME97	46.6547	-68.0089	94.3	82.35	-0.13	0.13
MI09	45.5608	-84.6783	65.99	70.33	0.07	0.07
MI53	44.2242	-85.8186	78.57	81.12	0.03	0.03
MN16	47.5311	-93.4686	44.6	51.63	0.16	0.16
MN18	47.9464	-91.4961	47.41	55.52	0.17	0.17
MN27	44.2372	-95.3006	52.74	60.21	0.14	0.14
MS14	32.3344	-88.7450	399.82	473.23	0.18	0.18
MT05	48.5103	-113.9958	33.11	35.94	0.09	0.09
NC03	36.1325	-77.1714	469.52	603.75	0.29	0.29
NC25	35.0606	-83.4306	341.85	443.58	0.30	0.30
NC34	35.6969	-80.6225	273.61	367.06	0.34	0.34
NC35	35.0258	-78.2783	552.74	770.91	0.39	0.39
ND07	47.6014	-103.2642	24.37	23.89	-0.02	0.02
NE15	41.1531	-96.4928	87.3	103.39	0.18	0.18
NH02	43.9431	-71.7033	196.91	93.35	-0.53	0.53
NM07	35.7817	-106.2675	28.91	26.83	-0.07	0.07
NM09	36.0408	-106.9714	30.14	35.37	0.17	0.17
NY08	42.7339	-76.6597	108.44	106.43	-0.02	0.02
NY20	43.9731	-74.2231	94	101.93	0.08	0.08
OH17	40.3553	-83.0661	136.47	146.34	0.07	0.07
OH71	40.7822	-81.9200	122.65	111.56	-0.09	0.09
OK17	34.9800	-97.5214	141.97	108.64	-0.23	0.23
OR02	44.3856	-123.6153	3271.32	5258.06	0.61	0.61
OR11	43.8994	-117.4269	20.55	23.57	0.15	0.15
PA15	40.7883	-77.9458	126.1	108.67	-0.14	0.14
TN00	35.9614	-84.2872	258.25	346.81	0.34	0.34
TX03	28.4667	-97.7069	548.68	625.74	0.14	0.14
TX04	29.3022	-103.1772	36.62	18.58	-0.49	0.49

Table 5.2: Wet interpolation errors from cross-validation analysis

Site ID	Latitude (°N)	Longitude (°W)	"Annual" Model Wet Deposition ($mg/m^2/yr$)	Value from Interpolation Without Station ($mg/m^2/yr$)	Interpolation Error *	Absolute Error
TX38	31.5606	-94.8608	361.01	389.67	0.08	0.08
TX53	28.8453	-96.9203	635.64	752.95	0.18	0.18
VA13	37.3314	-80.5575	108.24	95.41	-0.12	0.12
VT01	42.8761	-73.1633	122.03	92.56	-0.24	0.24
WA14	47.8600	-123.9319	3196.42	4328.9	0.35	0.35
WI36	46.0528	-89.6531	52.04	45.07	-0.13	0.13
WV18	39.0897	-79.6622	141.04	85.96	-0.39	0.39
WY02	42.7339	-108.8500	28.97	14.5	-0.50	0.50
				Average Error	**0.03**	
				Average Absolute Error		**0.20**

* The interpolation error is calculated using {([interpolated] - [measured]) / [measured]}

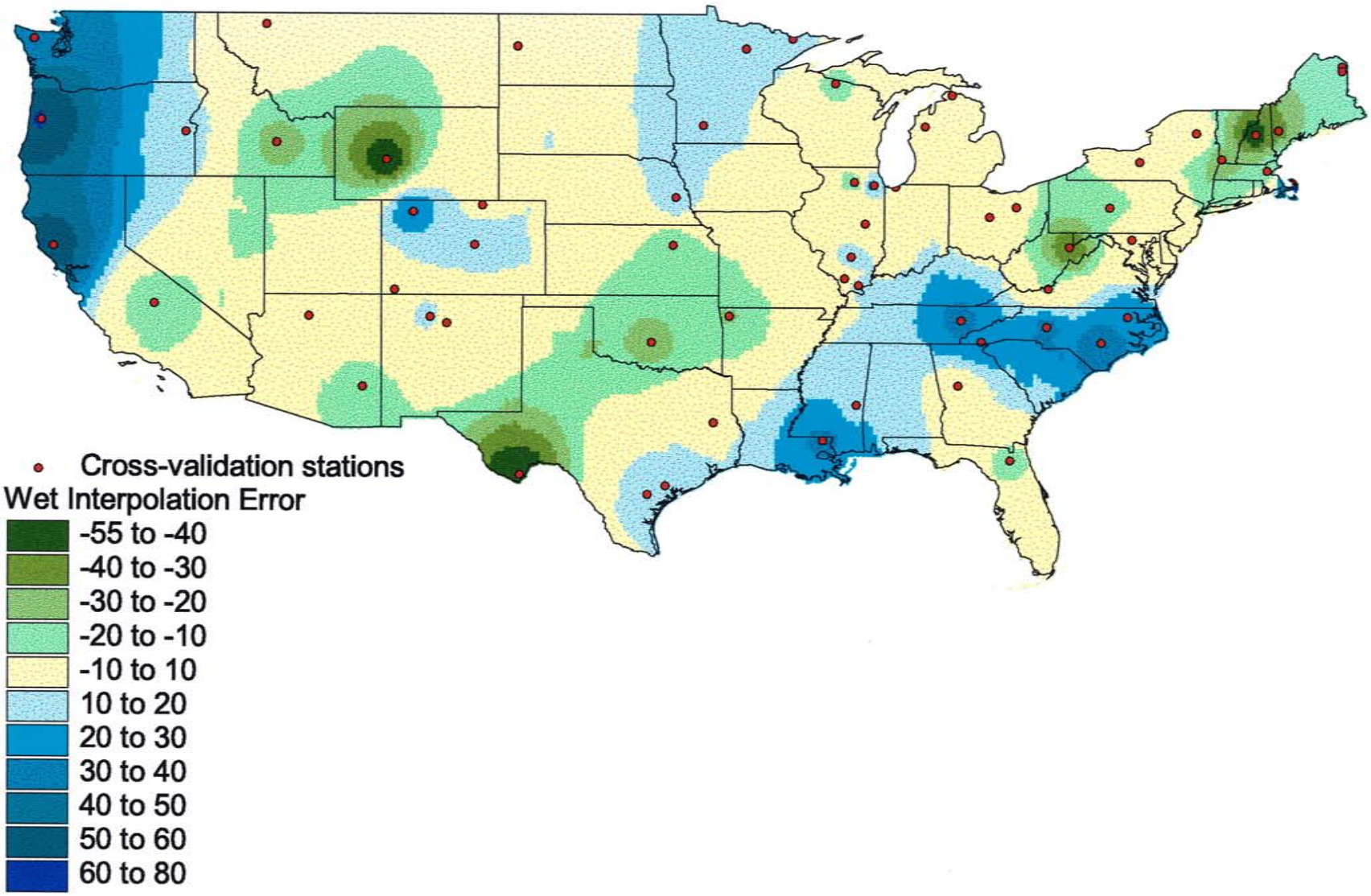

Figure 5.4: Distribution of the wet deposition model interpolation error.
Points represent stations from the cross validation (Table 5.2) where comparisons were made.

large regions of the country. Significant interpolation errors are generally concentrated near the coasts. This error is greatest near coastal stations because, when a coastal station is removed, inland stations are used by the interpolator and coastal conditions are not maintained. The interpolator is not constrained to uphold known relations near the coasts, such as increased chloride / precipitation regression slopes.

5.3 Errors in Dry Deposition

The dry deposition data collected by NADP/NTN stations could be questionable due to the unknown ability of a surrogate surface (such as a collector funnel) to emulate the ground surface chloride capture characteristics. However, as virtually no other data exists with the number of stations in the NADP network, the NADP/NTN dry deposition data provided the best current source for analysis. The dry deposition component used in the $^{36}Cl/Cl$ ratio model is simply an interpolation of measured values. It was not modeled like the wet deposition component, so comparison between modeled and measured dry deposition was not appropriate (it would show a perfect match). Since the dry deposition component was an interpolated field of values, however, the interpolation error could be assessed in the same way as the wet interpolation error. In the same manner as with the wet deposition model, each of 62 stations was removed from the map and the dry deposition reinterpolated. The interpolated value at a station both with and without the station's presence was compared, and is summarized in Table 5.3. The average absolute interpolation error for the dry deposition component is 109 percent. A map of the dry interpolation errors is shown in Figure 5.5. The dry interpolation error greatly exceeds the wet interpolation error due in large part to the far fewer data points on which the dry

Table 5.3: Dry interpolations errors from cross-validation analysis

Site ID	Latitude (°N)	Longitude (°W)	Measured Dry Deposition ($mg/m^2/yr$)	Value from Interpolation without station ($mg/m^2/yr$)	Interpolation Error *	Absolute Error
AR27	36.1006	-94.1733	83.52	52.82	-0.37	0.37
AZ03	36.0717	-112.1550	50.41	30.97	-0.39	0.39
AZ99	33.0714	-109.8647	15.58	39.63	1.54	1.54
CA45	39.0047	-123.0847	104.15	64.83	-0.38	0.38
CA75	36.5669	-118.7772	34.3	42.09	0.23	0.23
CO15	40.5075	-107.7019	15.91	16.36	0.03	0.03
CO99	37.1981	-108.4903	15.76	19.44	0.23	0.23
CO21	39.1011	-105.0919	9.3	18.57	1.00	1.00
CO22	40.8064	-104.7547	13.42	14.65	0.09	0.09
FL03	29.9747	-82.1981	223.24	219.25	-0.02	0.02
GA41	33.1778	-84.4061	43.96	56.27	0.28	0.28
ID03	43.4614	-113.5547	61.86	82.75	0.34	0.34
IL11	40.0533	-88.3719	51.83	120.13	1.32	1.32
IL18	41.8414	-88.8511	56.85	197.29	2.47	2.47
IL19	41.7011	-87.9953	253.41	113.02	-0.55	0.55
IL35	37.7100	-89.2689	37.4	68.03	0.82	0.82
IL47	38.6433	-88.9669	52.28	63.85	0.22	0.22
IL63	37.4356	-88.6719	68.92	47.46	-0.31	0.31
IN34	41.6325	-87.0878	208.39	170.9	-0.18	0.18
KS31	39.1022	-96.6092	17.56	47.16	1.69	1.69
LA30	30.8114	-90.1808	109.59	62.79	-0.43	0.43
MA01	41.9758	-70.0247	706.32	97.63	-0.86	0.86
MA13	42.3839	-71.2147	137.35	280.8	1.04	1.04
MD03	39.4089	-76.9953	74.14	69.8	-0.06	0.06
ME00	46.8689	-68.0131	68.01	30.99	-0.54	0.54
ME02	44.1075	-70.7289	63.59	114.64	0.80	0.80
ME97	46.6547	-68.0089	29.64	69.09	1.33	1.33
MI09	45.5608	-84.6783	16.11	57.69	2.58	2.58
MI53	44.2242	-85.8186	14.95	86.55	4.79	4.79
MN16	47.5311	-93.4686	11.44	27.58	1.41	1.41
MN18	47.9464	-91.4961	12.58	31.49	1.50	1.50
MN27	44.2372	-95.3006	74.53	23.19	-0.69	0.69
MS14	32.3344	-88.7450	57.12	78.47	0.37	0.37
MT05	48.5103	-113.9958	15.02	9.93	-0.34	0.34
NC03	36.1325	-77.1714	60.69	77.61	0.28	0.28
NC25	35.06	-83.43	14.83	29.39	0.98	0.98
NC34	35.6969	-80.6225	149.28	43.65	-0.71	0.71
NC35	35.0258	-78.2783	110.4	62.86	-0.43	0.43
ND07	47.6014	-103.2642	10.9	14.13	0.30	0.30
NE15	41.1531	-96.4928	38.44	34.62	-0.10	0.10
NH02	43.94	-71.70	18.85	113.96	5.05	5.05
NM07	35.7817	-106.2675	20.28	18	-0.11	0.11
NM09	36.0408	-106.9714	16.2	20.22	0.25	0.25
NY08	42.7339	-76.6597	54.18	74.87	0.38	0.38
NY20	43.9731	-74.2231	8.99	56.78	5.32	5.32
OH17	40.3553	-83.0661	56.03	69.52	0.24	0.24
OH71	40.7822	-81.9200	76.4	47.42	-0.38	0.38
OK17	34.9800	-97.5214	51.4	159.03	2.09	2.09
OR02	44.3856	-123.6153	91.71	76.79	-0.16	0.16
OR11	43.8994	-117.4269	21.65	42.84	0.98	0.98
PA15	40.7883	-77.9458	40.15	72.98	0.82	0.82
TN00	35.9614	-84.2872	19.74	29.08	0.47	0.47
TX03	28.47	-97.71	498.53	568.07	0.14	0.14

Table 5.3: Dry interpolations errors from cross-validation analysis

Site ID	Latitude (°N)	Longitude (°W)	Measured Dry Deposition ($mg/m^2/yr$)	Value from Interpolation without station ($mg/m^2/yr$)	Interpolation Error *	Absolute Error
TX04	29.3022	-103.1772	36.89	243.69	5.61	5.61
TX38	31.5606	-94.8608	100.9	301.72	1.99	1.99
TX53	28.8453	-96.9203	621.56	449.73	-0.28	0.28
VA13	37.3314	-80.5575	10.42	80.47	6.72	6.72
VT01	42.8761	-73.1633	27.84	65.27	1.34	1.34
WA14	47.8600	-123.9319	121.52	64.75	-0.47	0.47
WI36	46.0528	-89.6531	23.57	46.97	0.99	0.99
WV18	39.0897	-79.6622	19.91	45.71	1.30	1.30
WY02	42.7339	-108.8500	30.66	12.3	-0.60	0.60
				Average Error	**0.82**	
				Average Absolute Error		**1.09**

* The interpolation error is calculated using {([interpolated] - [measured]) / [measured]}

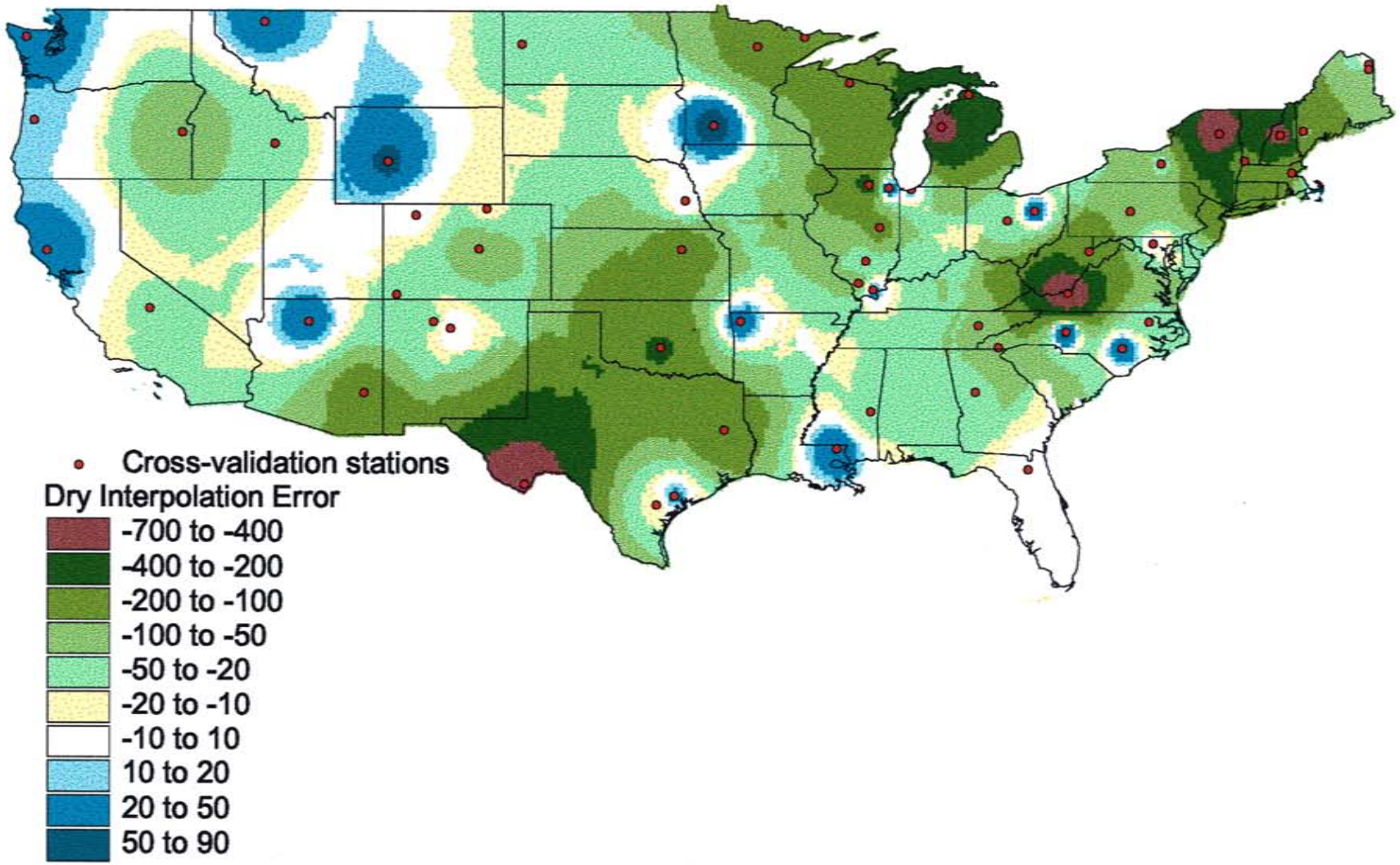

Figure 5.5: Distribution of dry deposition interpolation error.
Points represent stations from the cross validation (Table 5.3) where comparisons were made.

interpolation is based. Removing a single dry deposition value from the interpolation significantly alters the local station density, resulting in a poor match to the measurements after reinterpolation of the data.

5.4 Errors with the ^{36}Cl Deposition Model

A limited number of meteoric ^{36}Cl deposition measurements exist with which to compare to the new ^{36}Cl model developed by Phillips (1999). The ^{36}Cl deposition model was compared to the measured values in Table 3.1, and to some additional measurements by Hainsworth (1994), with the exception of the Black Hills, South Dakota sample which presented problems in Hainsworth's study. Table 5.4 and Figure 5.6 illustrate the performance of the model. The model fits the measured data moderately well, with an average absolute error of 27 percent. The model does not seem to preferentially over- or underestimate the ^{36}Cl deposition across the United States, as indicated by Figure 5.6. The value of the $S_p(\lambda_o)/D_{36}(\lambda_o)$ ratio in Equation 4.6 is not well constrained and Phillips (1999) proposed a value of 1.11 x 10^{-3} yr mm^{-1}, but has indicated that this value could be modified as a fitting parameter (Phillips, personal communication, 2000). A simple analysis was performed to determine whether modification of the $S_p(\lambda_o)/D_{36}(\lambda_o)$ term improved the performance of the ^{36}Cl model. The stations from Table 3.1 considered the most reliable by Phillips (1999) were Hanford, Lafayette, Elms, and Socorro. Using these four stations, the value of the $S_p(\lambda_o)/D_{36}(\lambda_o)$ ratio was varied from 5 x 10^{-4} to 1.5 x 10^{-3} yr mm^{-1}, and the resulting ^{36}Cl deposition at each station calculated. Minimization of the sum of squared residuals using these four stations yielded a value of 9.6 x 10^{-4} yr mm^{-1} as providing the best fit to the measured data. This indicates that a slight decrease in the

Table 5.4: Calculated errors for the ^{36}Cl deposition model

Site ID	Latitude (°N)	Longitude (°W)	Measured ^{36}Cl Deposition (atoms/m^2/s)	Model-Predicted ^{36}Cl Deposition (atoms/m^2/s)	^{36}Cl Deposition Model Error	Absolute Error
Elms, MD	38.42	-76.37	59	63.13	0.07	0.07
Lewes, DE	38.75	-75.13	47	64.11	0.36	0.36
Harpers Ferry, WV	39.33	-77.92	42	55.81	0.33	0.33
State College, PA	40.68	-77.92	82	56.99	-0.31	0.31
Victor, NY	42.97	-77.47	64	45.68	-0.29	0.29
Laingsburg, MI	42.92	-84.25	63	43.86	-0.30	0.30
Lafayette, IN	40.45	-87.01	68	53.08	-0.22	0.22
Socorro, NM	34.29	-106.92	18	20	0.11	0.11
Hanford, WA	46.58	-119.38	19	11	-0.42	0.42
				Average Error	**-0.07**	
				Average Absolute Error		**0.27**

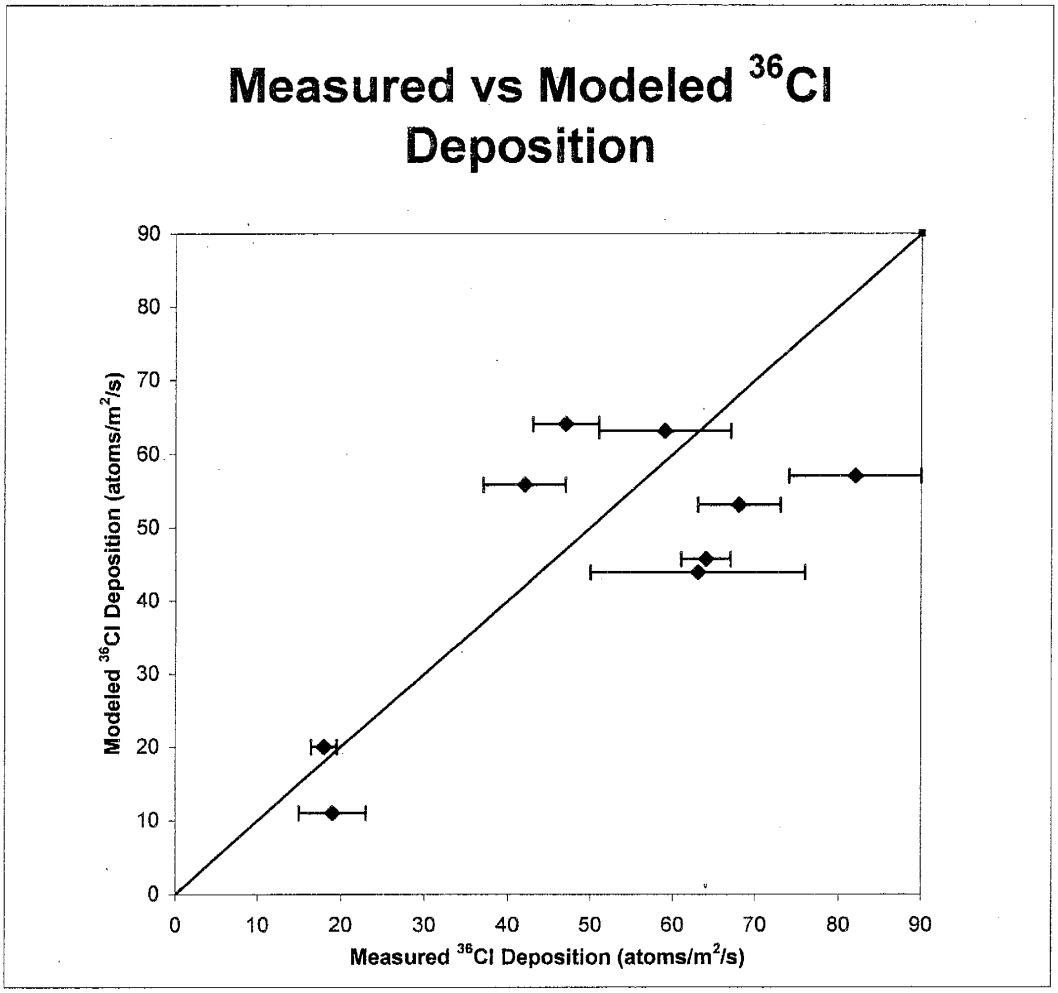

Figure 5.6: Modeled versus measured atmospheric ^{36}Cl deposition. Measured values are from Table 5.4.

$S_p(\lambda_o)/D_{36}(\lambda_o)$ ratio is warranted. Decreasing the $S_p(\lambda_o)/D_{36}(\lambda_o)$ ratio will have the effect of lowering the ^{36}Cl deposition in areas of high precipitation while increasing the ^{36}Cl deposition in arid regions.

5.5 Errors in the ^{36}Cl/Cl Ratio Distribution

The ^{36}Cl/Cl ratio distribution map presented in Figure 4.23 includes measured values of the ratio across the country from numerous sources, summarized in Table 5.5. The model's performance was evaluated by calculating the percent difference between the model-predicted values and the measured values using Equation 5.1, as presented in Table 5.5. Positive values of this difference indicate model overprediction while negative values indicate underprediction. The distribution of error in the ^{36}Cl/Cl ratio model is presented in Figure 5.7. Since the "monthly" wet deposition model provided better fit to the measured wet deposition data, only the ^{36}Cl/Cl ratio model based on the "monthly" wet deposition model was evaluated. The new ^{36}Cl/Cl ratio model significantly overestimates the ratio over most of the eastern United States, and significantly underestimates the ratio in the northwest. The new model performs well in the northern midwest states, and moderately well in the south-central U.S. The average absolute error for the ^{36}Cl/Cl ratio model was 89 percent. The "monthly" wet deposition model provided excellent fit to the measured data over most of the eastern United States and the ^{36}Cl deposition model fit the measured data moderately well, so this magnitude of error in the ^{36}Cl/Cl model was not anticipated.

Overprediction of the ^{36}Cl/Cl ratio is caused either by an overestimation of the ^{36}Cl deposition, or an underestimation of the stable chloride flux. An analysis of the ^{36}Cl

Table 5.5: Previous measurements of $^{36}Cl/Cl$ ratios and modeling errors

Location	Reference	Map ID	Latitude (°N)	Longitude (°W)	Measured $^{36}Cl/Cl$ Ratio ($\times 10^{-15}$)	Modeled $^{36}Cl/Cl$ Ratio ($\times 10^{-15}$) *	Model Error	Absolute Model Error	Hainsworth Approach Ratio ($\times 10^{-15}$) **	Hainsworth Approach Error	Hainsworth Approach Absolute Error	Bentley Approach Ratio ($\times 10^{-15}$) ***	Bentley Approach Error	Bentley Approach Absolute Error
W. Georgia	Moysey (1999)	1	32.4667	-83.7333	156	291	0.87	0.87	366	1.35	1.35	282	0.80	0.80
E. Georgia	Moysey (1999)	2	33.1833	-82.5167	97	295	2.04	2.04	381	2.93	2.93	293	2.02	2.02
Florida	Moysey (1999)	4	27.4667	-81.4667	45	78	0.73	0.73	118	1.61	1.61	90	1.01	1.01
Arkansas	Moysey (1999)	6	35.2500	-90.5500	139	439	2.16	2.16	611	3.40	3.40	470	2.38	2.38
Mississippi	Moysey (1999)	7	31.2833	-89.4000	50	237	3.74	3.74	377	6.54	6.54	290	4.80	4.80
Oklahoma	Moysey (1999)	8	35.6500	-97.5000	277	480	0.73	0.73	491	0.77	0.77	377	0.36	0.36
N. Dakota	Moysey (1999)	9	45.9833	-97.8333	900	738	-0.18	0.18	800	-0.11	0.11	615	-0.32	0.32
S. Dakota	Moysey (1999)	10	44.5833	-103.8500	1215	1104	-0.09	0.09	1163	-0.04	0.04	895	-0.26	0.26
Nebraska	Moysey (1999)	11	41.0833	-100.7500	493	1103	1.24	1.24	934	0.89	0.89	718	0.46	0.46
W. Virginia	Moysey (1999)	12	39.6167	-78.2167	386	478	0.24	0.24	530	0.37	0.37	408	0.06	0.06
Arizona	Moysey (1999)	14	31.8833	-110.2000	364	481	0.32	0.32	806	1.21	1.21	620	0.70	0.70
S. Utah	Moysey (1999)	15	37.2167	-113.7667	403	356	-0.12	0.12	530	0.31	0.31	407	0.01	0.01
E. Oregon	Moysey (1999)	18	44.4833	-121.2833	499	187	-0.63	0.63	36	-0.93	0.93	28	-0.94	0.94
W. Oregon	Moysey (1999)	19	44.7500	-122.9167	219	141	-0.36	0.36	141	-0.36	0.36	108	-0.50	0.50
W. Colorado	Moysey (1999)	21	38.5167	-104.7500	952	999	0.05	0.05	1225	0.29	0.29	942	-0.01	0.01
Kansas	Moysey (1999)	22	38.0000	-97.5167	500	652	0.30	0.30	687	0.37	0.37	528	0.06	0.06
Tahoe, CA	Moysey (1999)	24	38.9000	-119.9833	952	512	-0.46	0.46	190	-0.80	0.80	146	-0.85	0.85
Fresno, CA	Moysey (1999)	25	36.7000	-119.6167	219	506	1.31	1.31	246	0.12	0.12	189	-0.14	0.14
N. Wyoming	Moysey (1999)	27	43.8333	-104.1833	930	1013	0.09	0.09	910	-0.02	0.02	700	-0.25	0.25
S. Wyoming	Moysey (1999)	28	41.1667	-104.7833	1210	973	-0.20	0.20	1315	0.09	0.09	1011	-0.16	0.16
Indiana	Moysey (1999)	29	40.9500	-85.2333	275	405	0.47	0.47	739	1.69	1.69	568	1.07	1.07
Kentucky	Moysey (1999)	31	37.4833	-83.1333	218	724	2.32	2.32	614	1.82	1.82	472	1.17	1.17
E. Alabama	Moysey (1999)	32	32.0667	-85.5333	110	288	1.62	1.62	412	2.75	2.75	317	1.88	1.88
W. Alabama	Moysey (1999)	33	32.5333	-87.8333	129	320	1.48	1.48	358	1.78	1.78	276	1.14	1.14
Montana	Moysey (1999)	34	48.2500	-114.4833	1087	1171	0.08	0.08	785	-0.28	0.28	604	-0.44	0.44
Iowa	Moysey (1999)	35	42.1167	-93.5333	492	716	0.46	0.46	951	0.93	0.93	732	0.49	0.49
Minnesota	Moysey (1999)	37	45.0667	-93.2000	657	814	0.24	0.24	1178	0.79	0.79	906	0.38	0.38
Tucson, AZ	Bentley et al. (1986a)	AZ	32.1600	-110.9300	380	409	0.08	0.08	535	0.41	0.41	412	0.08	0.08
California	Phillips et al. (1995)	CA	37.7800	-118.7000	732	593	-0.19	0.19	451	-0.38	0.38	347	-0.53	0.53
Lewes, DE	Hainsworth (1994)	DE	38.7500	-75.1333	23	217	8.43	8.43	366	14.91	14.91	281	11.24	11.24
Idaho	Beasley et al. (1993)	ID	44.2000	-113.0600	580	454	-0.22	0.22	1173	1.02	1.02	902	0.56	0.56
Lafayette, IN	Knies (1994)	IN	40.4478	-87.0133	545	356	-0.35	0.35	728	0.34	0.34	560	0.03	0.03
Elms, MD	Hainsworth (1994)	MD	38.4167	-76.3667	61	244	3.00	3.00	379	5.21	5.21	292	3.78	3.78
Laingsburg, MI	Hainsworth (1994)	MI	42.9167	-84.2500	453	497	0.10	0.10	700	0.54	0.54	538	0.19	0.19
Socorro, NM	Phillips et al. (1988)	NM1	34.2952	-106.9241	718	901	0.25	0.25	828	0.15	0.15	637	-0.11	0.11
Las Cruces, NM	Phillips et al. (1988)	NM2	32.3400	-106.7800	465	799	0.72	0.72	755	0.62	0.62	581	0.25	0.25
New Mexico	Plummer (1996)	NM3	35.9500	-107.7700	765	937	0.22	0.22	889	0.16	0.16	684	-0.11	0.11
Nevada	Plummer et al. (1997)	NV1	36.9600	-116.0500	600	301	-0.50	0.50	234	-0.61	0.61	180	-0.70	0.70
Nevada	Plummer et al. (1997)	NV2	37.6700	-115.0700	600	307	-0.49	0.49	337	-0.44	0.44	259	-0.57	0.57
Nevada	Fabryka-Martin et al. (1997)	NV3	35.9400	-115.6200	450	261	-0.42	0.42	267	-0.41	0.41	205	-0.54	0.54
Victor, NY	Hainsworth (1994)	NY	42.9667	-77.4667	337	561	0.66	0.66	614	0.82	0.82	472	0.40	0.40
Texas	Scanlon (1992)	TX1	30.7400	-104.3400	450	670	0.49	0.49	546	0.21	0.21	420	-0.07	0.07
Texas	Bentley et al. (1986a)	TX2	28.6700	-98.8600	80	73	-0.09	0.09	110	0.37	0.37	85	0.06	0.06
Hanford, WA	Murphy et al. (1996)	WA	46.5833	-119.3912	896	349	-0.61	0.61	32	-0.96	0.96	24	-0.97	0.97
						Average Error	**0.67**			**1.12**			**0.63**	
						Average Absolute Error		**0.89**			**1.37**			**0.97**

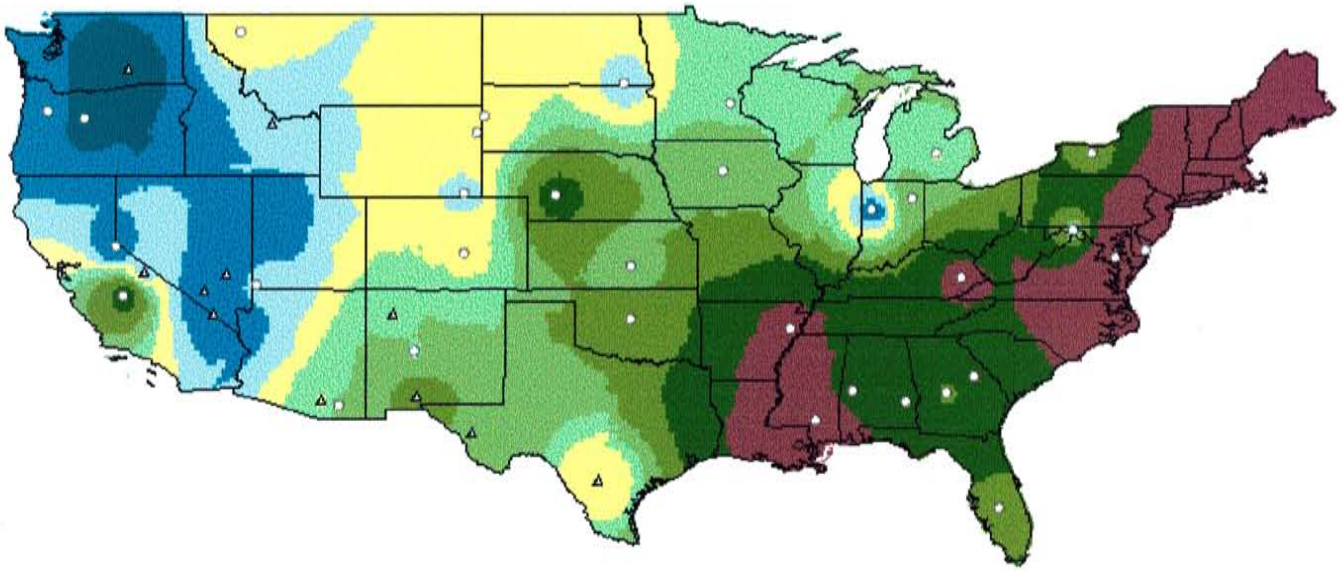

Measured Chlorine-36 Ratios

- △ Location estimated
- ○ Location known

Percent Error

- -100 to -50
- -50 to -25
- -25 to -10
- -10 to 10
- 10 to 25
- 25 to 50
- 50 to 100
- 100 to 200
- > 200

Figure 5.7: Distribution of errors in the 36Cl/Cl ratio model.
Error is interpolated between measurement stations from Table 5.5. The high error interpolated for the northeast U.S. is based on very few measurement points, as discussed in the text.

deposition model error indicated that a decrease in the $S_p(\lambda_o)/D_{36}(\lambda_o)$ ratio was justified. This would lower the effective ^{36}Cl deposition over the eastern U.S. where the precipitation is generally high, and improve the ^{36}Cl/Cl ratio prediction. While the "monthly" wet deposition model fit the measured data rather well throughout most of the eastern United States, the bias of the model was toward underprediction of the wet deposition. This underprediction of wet deposition would cause overprediction of the ^{36}Cl/Cl ratio. The dry deposition component is likely a major source of the current error in the ^{36}Cl/Cl ratio model. The dry deposition was interpolated over the United States, using approximately 90 measurement stations. The dry interpolation error discussed previously shows that this interpolation can present large errors when even a single station is removed from the dataset. A method to allow smoother interpolation of the dry deposition data is needed, and is discussed later in Chapter 6. This new interpolation method should incorporate some form of dry deposition / distance from the coast relationship, as the map of dry deposition shown in Figure 4.19 suggests that such a relationship may exist. Constraining the interpolation to honor known relationships would help to smooth the interpolation and would allow better estimation of values even if a station is removed from the dataset.

In an effort to compare the new ^{36}Cl/Cl ratio model more directly with those of previous investigators, an approach more similar to these previous models was analyzed. The Hainsworth (1994) model did not incorporate dry deposition, and used a theoretical model of ^{36}Cl deposition in combination with the measured stable chloride deposition from the NADP. The Bentley et al. (1986a) model used the same approach, but the wet deposition was calculated using only a single year of measurements, and was multiplied by

130 percent to account for dry deposition. To compare the new $^{36}Cl/Cl$ ratio model to the Hainsworth (1994) model, the ^{36}Cl deposition model was divided by the annual average wet chloride deposition measured at all NADP/NTN stations. The dry deposition was not incorporated. To compare the new $^{36}Cl/Cl$ ratio model to the Bentley et al. (1986a) model, the NADP/NTN wet deposition measurements were multiplied by 130 percent prior to division into the ^{36}Cl deposition model. The distribution of the $^{36}Cl/Cl$ ratio using these two approaches is shown in Figure 5.8. The output using the Hainsworth and Bentley et al. approaches (Figure 5.8) is generally similar to that using the new $^{36}Cl/Cl$ model (Figure 4.23), with the notable exception along the west coast. The percent difference between the Hainsworth approach and the Bentley et al. approach models and measured $^{36}Cl/Cl$ ratios across the country was calculated using Equation 5.1; a map of the percent difference is shown in Figure 5.9. These two modeling approaches have similar error distributions, with significant overprediction in the eastern United States, and significant underprediction in the west. Table 5.5 compares the calculated errors using all three models of the $^{36}Cl/Cl$ ratio distribution. The new $^{36}Cl/Cl$ ratio model developed in this study seems to provide the best overall fit to the measured data, particularly along the west coast.

5.6 Additional Error Assessment Comments

There are numerous factors that influence the various errors that have been discussed in the preceding sections. These factors include the reliability of the measurements used for comparison, the number of available measurements, and the method used to map these errors.

A) Chlorine-36 Ratio distribution using the Hainsworth approach (no dry deposition)

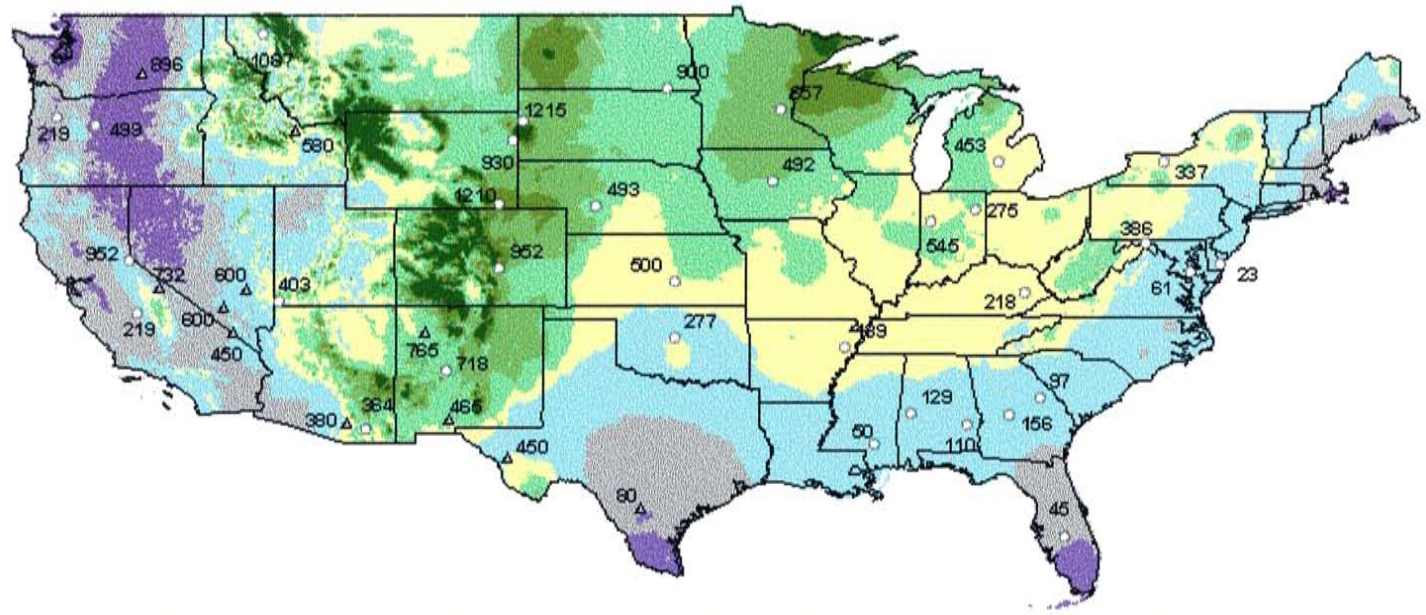

) Chlorine-36 Ratio distribution using the Bentley approach (total stable deposition equals 130 percent of wet deposition)

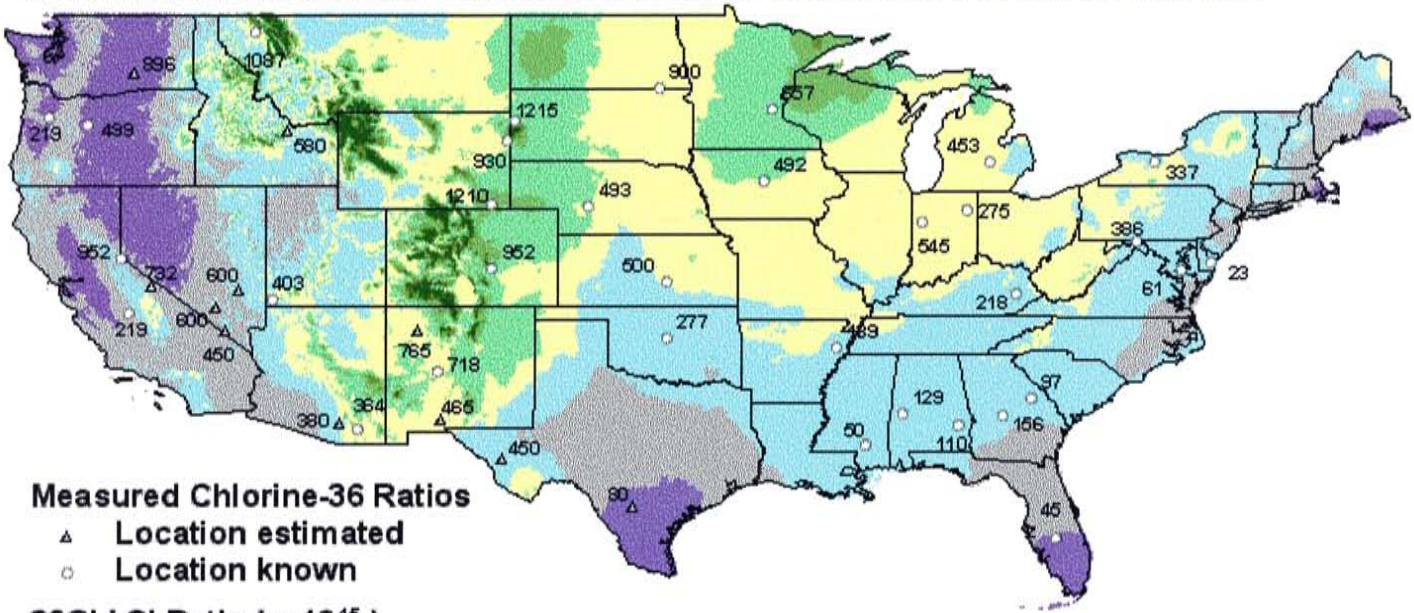

Measured Chlorine-36 Ratios

△ **Location estimated**

○ **Location known**

36Cl / Cl Ratio (x 10^{15})

- **0 - 100**
- **100 - 250**
- **250 - 500**
- **500 - 750**
- **750 - 1000**
- **1000 - 1250**
- **1250 - 1500**
- **> 1500**

Figure 5.8: Distribution of 36Cl/Cl ratios using the Hainsworth and Bentley modeling approaches. Measured 36Cl/Cl ratios are provided in Table 5.5.

A) Error distribution using the Hainsworth approach

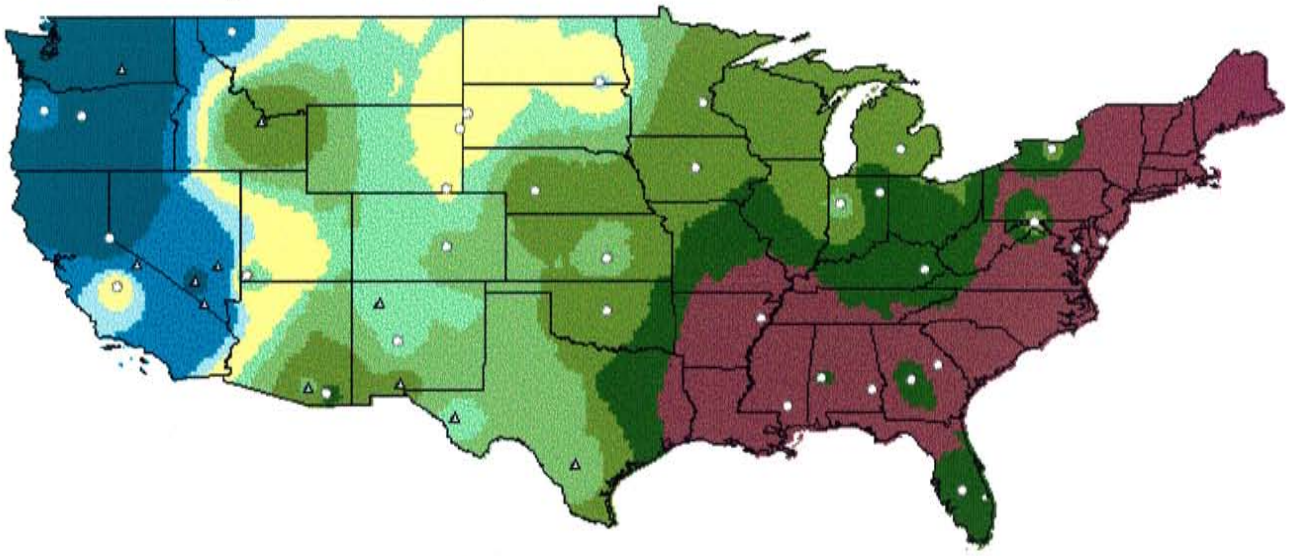

B) Error distribution using the Bentley approach

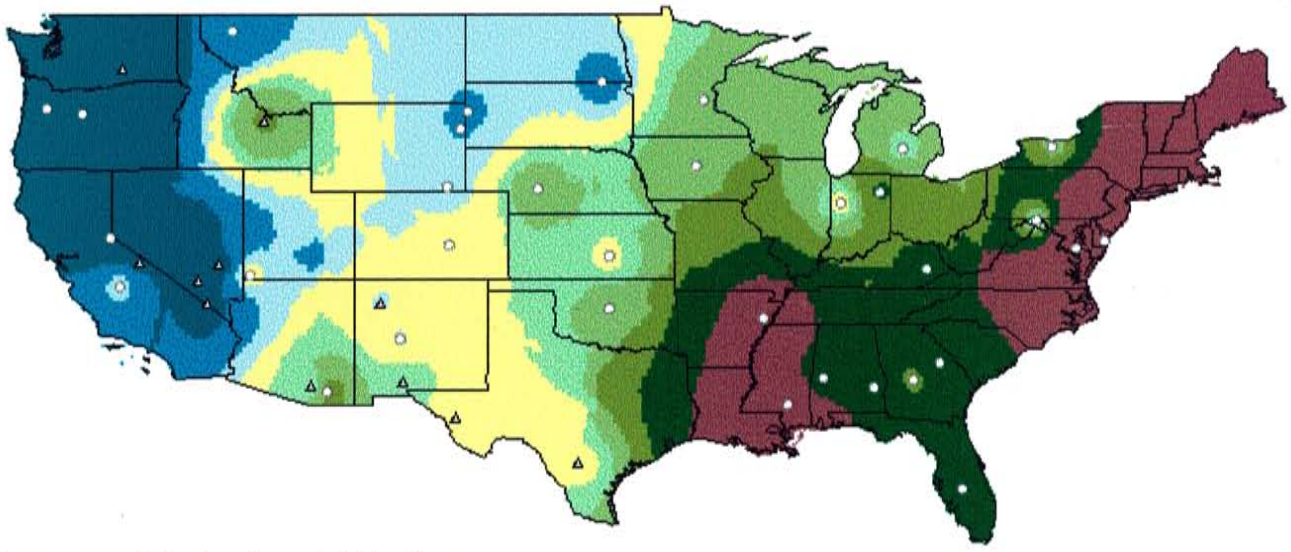

Measured Chlorine-36 Ratios

- Location estimated
- Location known

Interpolated Error

- -100 to -50
- -50 to -25
- -25 to -10
- -10 to 10
- 10 to 25
- 25 to 50
- 50 to 100
- 100 to 200
- > 200

Figure 5.9: Distribution of error for the Hainsworth approach (a) and Bentley approach (b) 36Cl/Cl ratio models (compare with Figure 5.7).

5.6.1 Reliability of measured values

The error assessments for the new $^{36}Cl/Cl$ ratio model, and its components, were performed by comparing the model outputs with measured data at points throughout the country. The amount of error is thus dependant upon the quality of the measured data used for comparison. In the case of the wet deposition model error assessment, the measured values were average wet deposition at each NADP/NTN station, and were based on numerous years of available data. The use of average values over many years should have reduced the effect of temporal anomalies, and provided reliable measurements for comparison. The "monthly" wet deposition model provided good fit to the measured NADP/NTN data (Figure 5.1). It is possible that the regions of very localized high errors are due to the presence of less reliable measured data at those stations.

Many of the ^{36}Cl deposition measurements used for comparison with the new ^{36}Cl deposition model proposed by Phillips (1999) were based on a single year of measurement, or on an individual sampling event (Hainsworth and Knies results from Table 3.1). The reliability of these measured data to represent the long-term average ^{36}Cl deposition calculated by the model is questionable due to the short duration of measurements. Had a measurement been taken during a year of anomalous ^{36}Cl deposition, the model error could be compounded over the true error. The ^{36}Cl deposition model fit the measured data presented in Figure 5.6 only moderately well but, if comparison could be made with more long-term measurements (such as at Hanford and Socorro), could possibly be performing better than Figure 5.6 would suggest.

Similar to the ^{36}Cl deposition measurements, the measurements of the $^{36}Cl/Cl$ ratio (Table 5.5) across the United States have varying reliability. Some of the measurements

(such as those by Hainsworth (1994)) are based on a single year of data. Most of the measurements used for comparison are from Moysey (1999), who measured the ratio in shallow groundwater. This method of measurement should provide somewhat of an average meteoric ratio, over many years of recharge. The method is subject to error when stable chloride or ^{36}Cl is introduced to groundwater from non-meteoric sources. Only the data deemed the most reliable by Moysey (1999) were included in Table 5.5, but some of those data contain substantial uncertainty. The suitability of each of these measurements for comparison with the $^{36}Cl/Cl$ ratio model needs to be further assessed, and lower model error may exist after the removal of less reliable measurements.

5.6.2 Number of available measurements

The number of measurements available for comparison with the modeling results is important, and more confidence can be placed on the results of an error assessment that incorporates a larger number of measurements. Relatively few data exist on meteoric ^{36}Cl deposition with which to compare the new ^{36}Cl deposition model presented in this study. More data on meteoric ^{36}Cl deposition, particularly over several year intervals, is needed to more adequately assess the performance of the ^{36}Cl deposition model. While more data are available on the $^{36}Cl/Cl$ ratio throughout the country, additional measurements would provide greater confidence in the modeling results, or reveal additional shortcomings of the model. The model can best be improved by the collection of additional data.

5.6.3 Error mapping discussion

An important consideration when evaluating the errors presented in the preceding sections is the method used to display the errors. The error assessments compared the model components to measured data at particular points across the country. The amount of error was only known at these points but, in order to determine trends in the error distribution, the error values were interpolated across the United States. The interpolation process allows the visualization of regions with under- or overprediction, but can exaggerate the extent of these regions. For example, Figures 5.7 and 5.9 illustrate the distribution of model errors for different versions of the $^{36}Cl/Cl$ model. In each case, large errors exist over the entire eastern United States, particularly near the coast. However, the large error (> 200%) shown along the entire east coast is based only on two points where an actual comparison was made. There is no data to support whether the error in the far northeastern states is actually this large. Similarly, the interpolation of errors in the northwest (Oregon and Washington) is based on only three comparison points, and there are no data to support whether the high errors extending into northern Nevada and eastern Utah are actually as high as the map suggests. A similar situation exists in Figures 5.4 and 5.5, where there are relatively few points in certain areas of the country on which to base the interpolation. The distribution of errors shown for the wet deposition model (Figure 5.1) is interpolated from a much larger number of comparison points than the other error maps, giving a more reliable estimate of the error distribution. The error values calculated at each comparison point are provided in tables in the preceding sections, and represent the true measure of error in the $^{36}Cl/Cl$ model and its components. The error distribution maps

only provide a general idea of the spatial variability of errors across the country, and the limitations of the interpolation process should be kept in mind when viewing them.

5.6.4 Summary of error analyses

The $^{36}Cl/Cl$ ratio model presented in this study is composed of three basic components, the wet deposition model, the dry deposition distribution, and the ^{36}Cl deposition model. Each of these components has associated error, leading to error in the $^{36}Cl/Cl$ ratio model. The calculated error for each component, and for the full model, were presented in tables earlier in this chapter.

Two types of error were measured to assess the performance of the model and its components. The first type of error calculation involved the simple comparison of the model-predicted values with the actual measured values at numerous points across the country. The second type of measured error was an interpolation error, which was calculated using a cross-validation technique. The interpolation error was a measure of the dependence of the model on individual measurement points. The importance of individual measurements was assessed by removing points from the interpolation field prior to interpolation. The interpolated value at the location of the missing station was compared with the actual measurement at the station. Large errors following individual station removal indicate that the model is heavily dependent upon individual measurement points, while low errors indicate little dependence. The wet deposition model had a low interpolation error of 20 percent, indicating that it remains robust even when data are removed from consideration. In contrast, the dry deposition component had large interpolation error (109 percent) when individual stations were removed, indicating a

strong dependence on individual measurements. In this case, the dry deposition component benefits from the inclusion of as many stations as possible in the analysis.

The average absolute error of the wet deposition model was 10 percent, indicating the ability to accurately predict wet deposition using a linear relationship between chloride deposition and rainfall. The average absolute error of the ^{36}Cl deposition model, proposed by Phillips (1999) was 27 percent. The average absolute error in the $^{36}Cl/Cl$ ratio model was 89 percent. This amount of error was unexpected given the excellent predictions from the wet deposition model and the moderately good predictions from the ^{36}Cl deposition model. The dry deposition may be one source of the current high amount of error. Another problem is that several of the measured $^{36}Cl/Cl$ ratio values used for comparison (Table 5.5) may be unreliable, and should be further assessed regarding the appropriateness of their use. Despite the large average error in the $^{36}Cl/Cl$ ratios, the model performs quite well within much of the Midwest, particularly to the north. The high average error is due in large part to the systematic overprediction of values over the eastern United States, and systematic underprediction in the Pacific Northwest. The geographic distribution of errors indicates that the distance from the coasts may be an important consideration to include in the model. The model exhibits the poorest performance near the coasts, and good performance further inland. The incorporation of certain coastal relationships may improve the performance of the model, and are discussed in Chapter 6.

CHAPTER 6 - MODEL DISCUSSION AND FUTURE IMPROVEMENTS

After assessing the errors involved with each component of the $^{36}Cl/Cl$ ratio model, some components were found to work quite well and some did not match measured values as well as anticipated. The new wet chloride deposition model (particularly the "monthly" version) was found to match the measured data quite well across the majority of the country, although it was slightly biased toward underprediction. The ^{36}Cl deposition model fit the measured data moderately well, but there was justification for a decrease in the $S_p(\lambda_o)/D_{36}(\lambda_o)$ ratio. The overall $^{36}Cl/Cl$ ratio distribution was overpredicted in the eastern United States, and underpredicted in the west. Methods to improve each of the $^{36}Cl/Cl$ model components are discussed below.

6.1 Future Improvements to the Wet Chloride Deposition Model

In general, the wet chloride deposition model constructed as part of this study provided good fit to the measured data from the NADP/NTN stations. The model was based on a linear regression between chloride deposition and precipitation, identified using the NADP/NTN data. The slope of this linear regression was found to change across the country, with high slopes found near the coasts and shallow slopes in the continental interior. A mathematical relationship between the chloride deposition / precipitation regression slope and the distance from the coast was not incorporated, and the change in slopes across the country was simply interpolated from the measured values. This represents an area of potential model improvement. One of the original goals of this study was to construct a mathematical model that was parameter based. The model in its current form is not technically a fully mathematical model, since it incorporates two major

interpolations. These interpolations are of the chloride deposition / precipitation regression slopes across the United States and the dry deposition distribution across the country. To construct a complete mathematical model requires that these two interpolations be replaced with functional relationships.

The wet chloride deposition model can be converted to a fully mathematical model by replacing the interpolation of the chloride deposition / precipitation regression slopes with a functional relationship between the two. Analysis of Figures 4.8, 4.9, and 4.10 indicates that a simple relationship may exist, as the regression slope seems to change smoothly from high values along the coasts to low values in the continental interior. To identify whether a simple relationship existed between the regression slope and the distance from the coast, the value of the regression slope at each NADP/NTN station in Figure 4.8 (from the "annual" model) was plotted against the shortest straight-line distance of that station from the coast, as presented in Figure 6.1. The regression slope decreases rapidly up to approximately 300 kilometers inland, and then decreases very slowly with increasing distance. The data in Figure 6.1 are fit using a power-law relationship, although other relationships, such as a log-normal distribution, should be explored. Figure 6.1 provides strong evidence that a simple relationship between the regression slope and inland distance exists, and could be incorporated into the wet chloride deposition model. Thus, a complete mathematical model describing wet chloride deposition could be constructed. A major difficulty in incorporating the wet deposition / distance relationship arises from the fact that the regression slope changes throughout the year, as determined using the "monthly" wet deposition approach (Figures 4.9 and 4.10). The change in regression slopes is likely a function of large-scale weather patterns over the course of a year. A

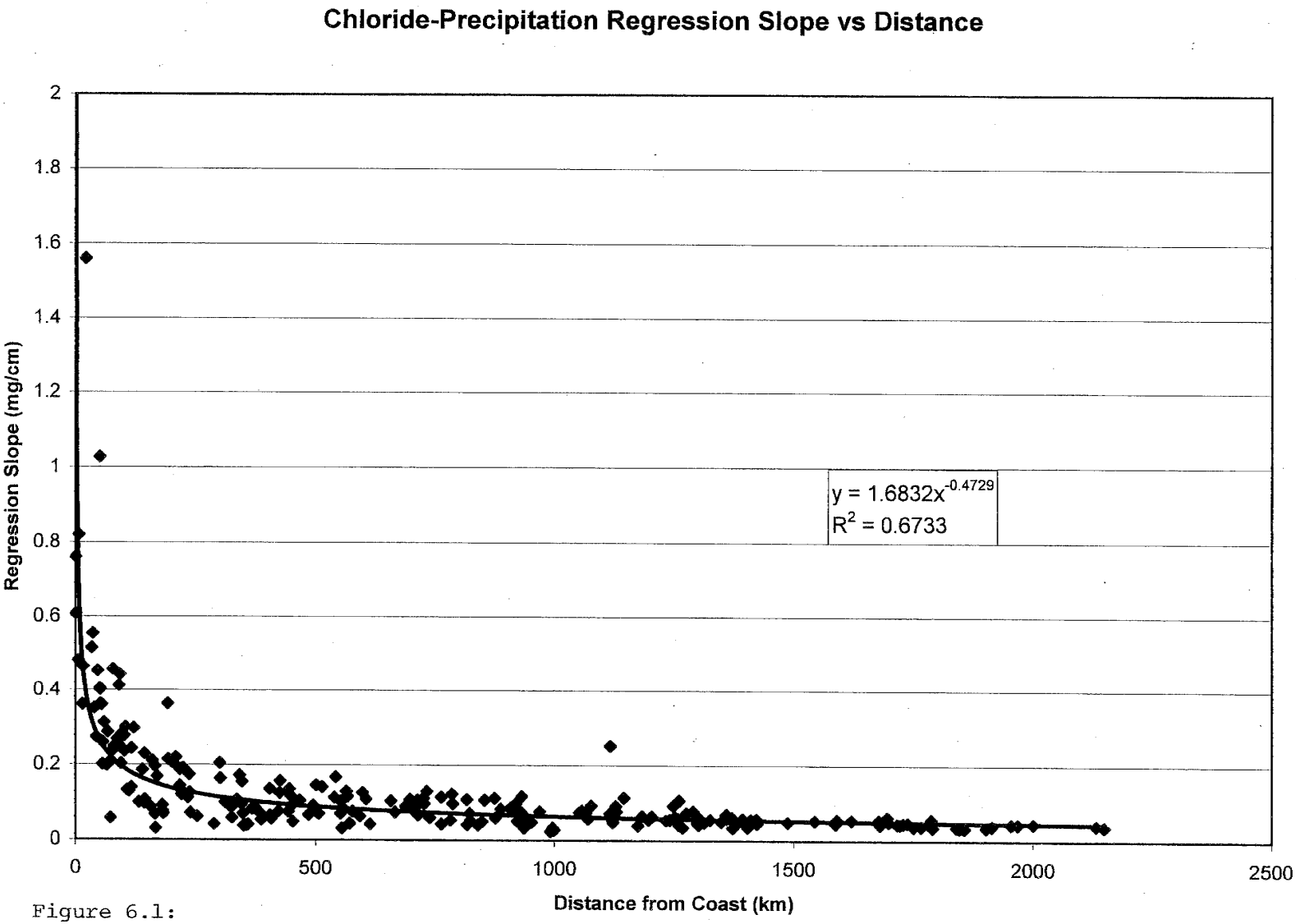

Figure 6.1:
Relationship between chloride collection / precipitation regression slopes and distance from the coast. The data are fit with a power-law regression, although other functional forms could be used.

separate regression slope / distance from the coast relationship could be calculated for each individual month. However, an approach more in keeping with a parameter-based model would require a functional relationship describing the cyclic change in regression slopes throughout the year to be developed. Such a relationship has not yet been pursued.

Both the "annual" and "monthly" wet deposition models were biased toward underprediction of the wet chloride deposition. One possible explanation for this underprediction arises from ceiling values in chloride deposition at very high precipitation, discussed in section 4.2.2. A linear regression fit through data that includes relatively constant chloride deposition at high precipitation amounts will have a slightly lower slope than a linear regression fit through data without such ceiling values. Over most of the country, average monthly precipitation does not approach amounts that lead to ceiling values in chloride deposition. Since the PRISM model output is a long-term average of precipitation, the PRISM precipitation used in the model will not produce a ceiling value in chloride deposition over most of the country. In order to reduce the overall underprediction of the wet chloride deposition model, the ceiling data represented by the highest precipitation values (greatest one to five percent) could be removed for most stations prior to fitting a linear regression through the data. This would tend to slightly increase the chloride deposition / precipitation regression slopes over most of the country, which would lead to greater chloride deposition and improve the fit with the measured deposition.

The wet chloride deposition model overpredicts the chloride flux in the Pacific Northwest. In this case, the ceiling value in chloride deposition at high precipitation amounts is more important. Within the Pacific Northwest, even average monthly

precipitation may be sufficient to remove nearly all available chloride from the local atmosphere, and attain a ceiling value in chloride deposition. Applying a linear regression to the data from stations in the Pacific Northwest can lead to chloride deposition values greater than the ceiling value by extending the linear relationship farther than warranted. This may lead to overprediction of the wet chloride deposition. In order to improve the model in the Pacific Northwest region, a separate regression should be explored that places a ceiling value on chloride deposition. A regression with the form of the spherical variogram would be one possibility. The spherical variogram increases linearly until reaching a sill value, after which it remains constant.

6.2 Future Improvements to the Dry Deposition Component

The $^{36}Cl/Cl$ ratio model constructed in this study is the first to incorporate measured dry deposition from across the country. Dry deposition was measured at all stations within the NADP/NTN prior to 1984, and continued at several stations until 1998. Although there is controversy over the collection technique used at the NADP/NTN stations, these data represent the only dry deposition measurements available from a large number of stations across the entire country. The current $^{36}Cl/Cl$ ratio model uses an interpolation of the NADP/NTN dry deposition measurements across the country. This interpolation is combined with the wet deposition model to calculate the total stable chloride deposition, which is then divided into the ^{36}Cl deposition model output to produce the $^{36}Cl/Cl$ ratio distribution across the United States. As mentioned in the previous section, a true mathematical model requires that the dry deposition interpolation be replaced by a functional description of the dry deposition distribution. Examination of

Figure 4.19 suggests that, like wet deposition, dry deposition is related to the distance from the coast. The region surrounding the Great Salt Lake, Utah is a local exception. The dry deposition values from each station in Figure 4.19 were plotted against the shortest straight-line distance of the station from the coast to determine whether a simple relationship existed, as presented in Figure 6.2. As with the chloride deposition / precipitation regression slopes, dry deposition decreases rapidly with increasing distance from the coast. Dry deposition reaches an approximately constant value beyond about 300 kilometers from the coast. Three stations are distinct outliers, one in Illinois, one in Indiana, and one near the Great Salt Lake, Utah. The Utah outlier was expected, and is likely due to local atmospheric entrainment of evaporite deposits. The Illinois and Indiana stations are near the Great Lakes region, and may be affected by significant use of road salt during the winter months. Figure 6.3 presents the same data without three outlier stations. The data in Figures 6.2 and 6.3 were fit with a power-law relationship although other functional forms should be explored, such as a log-normal distribution. This analysis supports the use of a functional relationship between dry deposition and the distance from the coast. Local anomalies, such as near the Great Salt Lake, Utah, would not be represented by such a relationship.

6.3 Future Improvements to the ^{36}Cl Deposition Model

The ^{36}Cl/Cl ratio model incorporated the recently proposed ^{36}Cl model by Phillips (1999). This model is already in a purely mathematical form, and is dependent on both precipitation and latitude. The ^{36}Cl deposition model output matched the measured data moderately well, although there were relatively few measurements with which to compare.

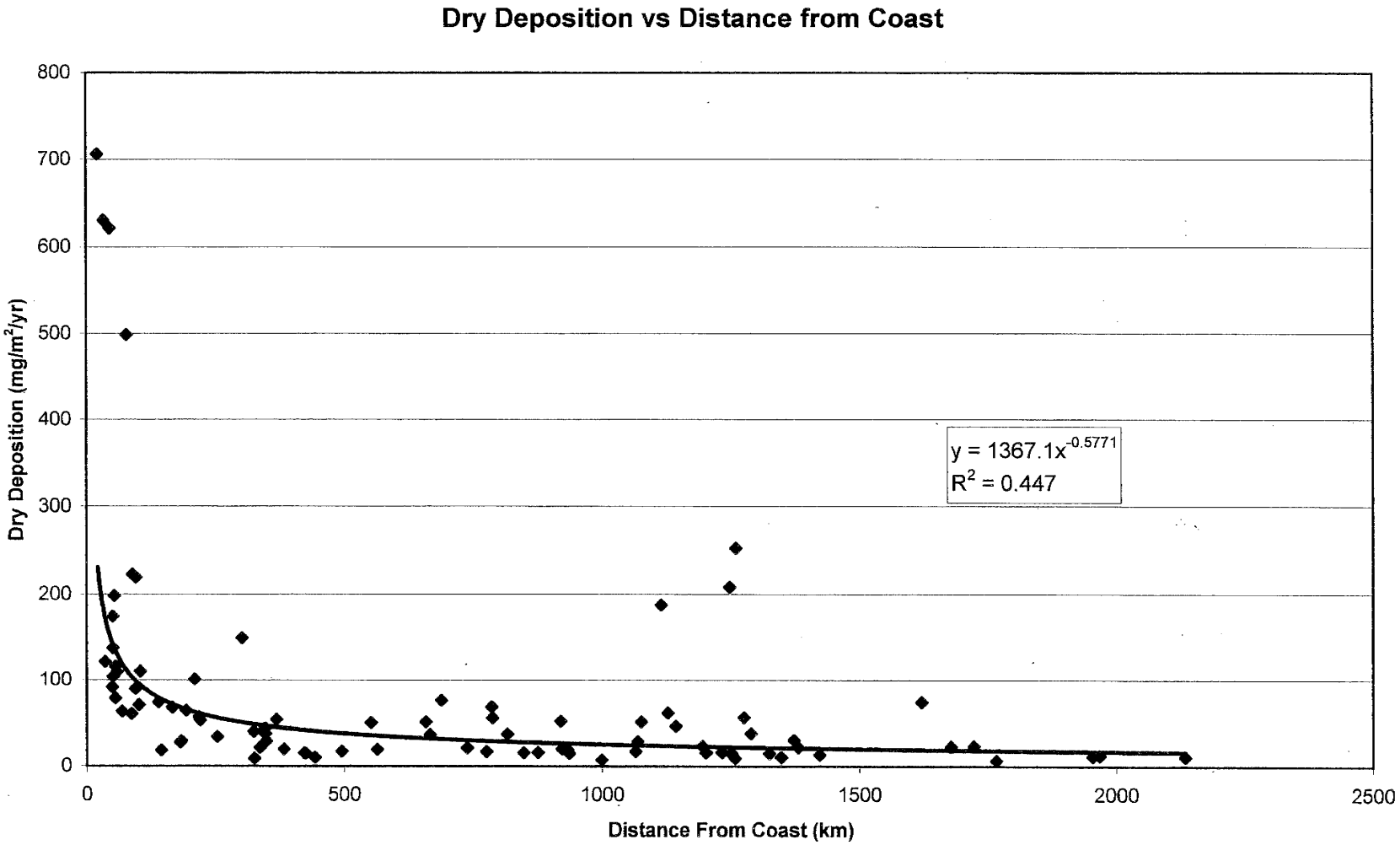

Figure 6.2: Relationship between dry deposition and distance from the coast. The The three apparent outliers are the station nearest the Great Salt Lake,UT, and two stations near the Great Lakes region, where additional natural and anthropogenic sources of salt, respectively, may be present.

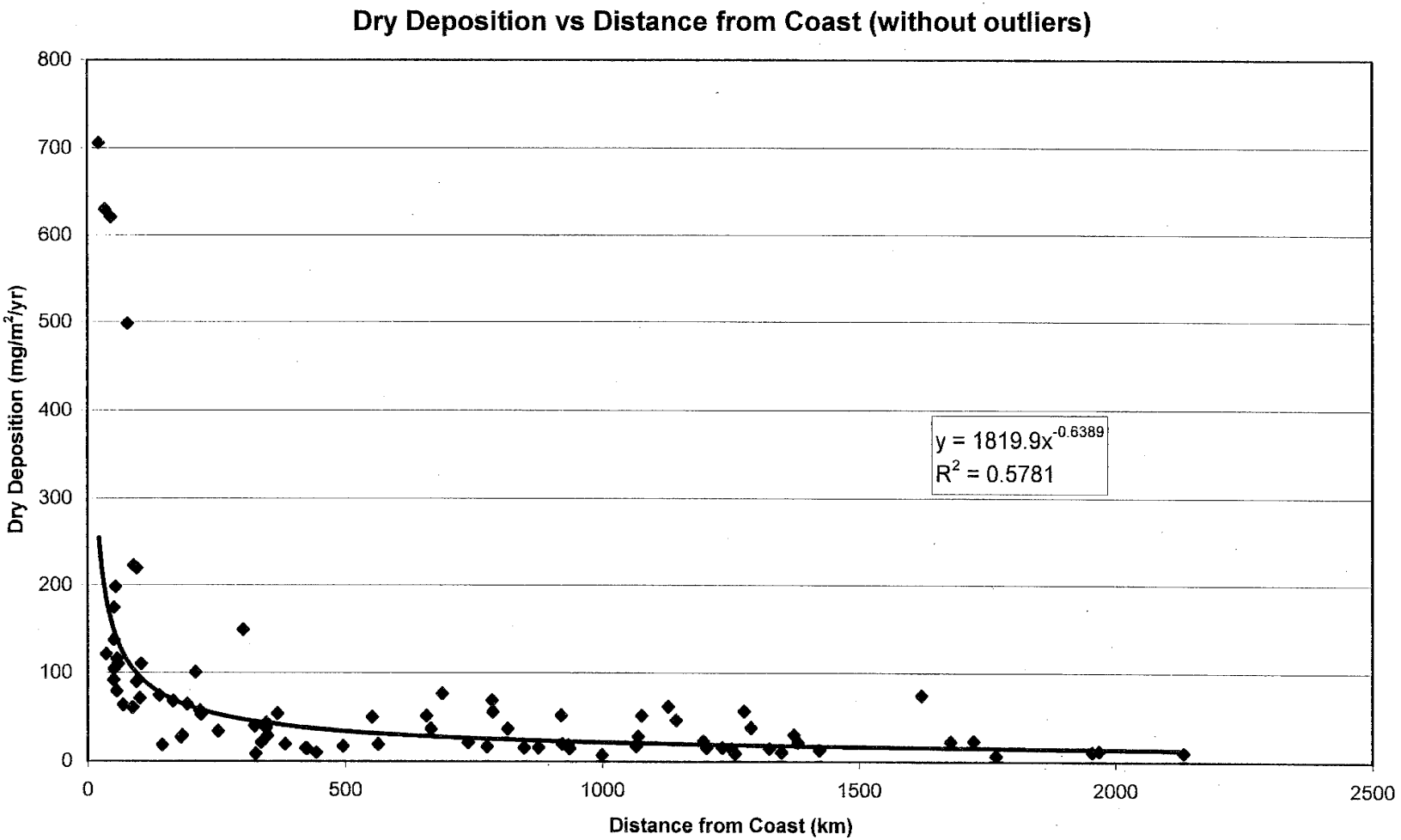

Figure 6.3: Relationship between dry deposition and distance from the coast without outliers.

The main variable which can be adjusted in the ^{36}Cl deposition model, to improve the fit with measured data, is the value of the $S_p(\lambda_o)/D_{36}(\lambda_o)$ ratio. This ratio is determined in part using the linear relationship between ^{36}Cl deposition and precipitation, illustrated in Figure 3.9. The slope of this relationship is not well constrained. An analysis was performed to determine the value of the $S_p(\lambda_o)/D_{36}(\lambda_o)$ ratio that provided the best fit to the ^{36}Cl deposition values at four of the most reliable measurement stations. This analysis supported a slight decrease in this ratio, from 1.11 x 10^{-3} (suggested by Phillips (1999)) to 9.6 x 10^{-4} yr mm^{-1}. Decreasing the $S_p(\lambda_o)/D_{36}(\lambda_o)$ ratio will decrease the ^{36}Cl deposition in regions of high precipitation, such as the eastern United States, and increase the ^{36}Cl deposition in arid regions. This would improve the $^{36}Cl/Cl$ ratio model by creating better fit to the measured ratios in the eastern United States. Further changes in the $S_p(\lambda_o)/D_{36}(\lambda_o)$ ratio could be justified if additional measurements of meteoric ^{36}Cl deposition are incorporated.

6.4 Future Improvements to the Overall Modeling Approach

The $^{36}Cl/Cl$ ratio model was constructed from three main components, the wet deposition model, the dry deposition distribution, and the ^{36}Cl deposition model. Improvements to the $^{36}Cl/Cl$ ratio model can be made by incorporating the suggested changes from the preceding sections. The $^{36}Cl/Cl$ ratio model is currently based on both mathematical relationships and on interpolations of values. A major goal of this study was to produce a mathematical model of the spatial distribution of $^{36}Cl/Cl$ ratios across the country that was based on simple climatic and geographic parameters. The current model is not a fully mathematical model because it relies on two interpolations, one of the

chloride deposition / precipitation regression slopes and one of the dry deposition distribution across the country. A complete mathematical model of the spatial $^{36}Cl/Cl$ ratio variability can be completed by incorporating the distance from the coast relationships discussed in the preceding sections. These relationships will remove the interpolations from the model, and allow the $^{36}Cl/Cl$ ratio model to be purely parameter based. The parameters required for calculation of the $^{36}Cl/Cl$ ratio anywhere in the United States would be the distance from the coast (or simple a station's location), the amount of precipitation, and the latitude. The distance from the coast and the precipitation would be used to calculate the wet chloride deposition, while the dry deposition would be calculated knowing only the distance to the coast. The ^{36}Cl deposition would be calculated knowing the amount of precipitation and the latitude. The advantage of a model that does not rely on interpolations arises from the ability to modify the functional relationships between the various parameters to arrive at the best possible fit to the measured data. The model would also not suffer from interpolation errors, introduced as a consequence of limited data points. There are some current difficulties involved with incorporating the distance from the coast relationships, such as determining the cause and functional form of the chloride deposition / precipitation regression slope changes during the year. Additional work needs to be done to describe these changes. The dry deposition / distance from the coast relationship could be added to the model more easily, but additional work to accurately describe the relationship should be performed, and the data should again be carefully screened.

Once each component has been modified as discussed, the $^{36}Cl/Cl$ ratio model could be recalculated by allowing each functional relationship to be modified until the best

fit with the measured data is found. For instance, the functional relationship between the chloride deposition / precipitation regression slope and the distance from the coast could be varied to provide the best fit to the measured wet deposition values at each NADP/NTN station. Simultaneously, the dry deposition / distance from the coast relationship and the value of the $S_p(\lambda_o)/D_{36}(\lambda_o)$ ratio from the ^{36}Cl deposition model could be varied to produce the best fit to the measured $^{36}Cl/Cl$ ratios across the country. The functional relationships could be modified as new data becomes available, and the model easily recalculated. Additionally, new parameters could later be incorporated into the model, as new relationships are discovered.

CHAPTER 7 - CONCLUSIONS

Chlorine-36 applications in the hydrogeologic sciences have grown rapidly since the application of accelerator mass spectrometry (AMS) to ^{36}Cl measurement. Most of these applications listed by Fabryka-Martin (1987) require that the initial $^{36}Cl/Cl$ ratio is known but, to date, there have been few studies to determine both the temporal and spatial atmospheric input function for ^{36}Cl. The main purpose of this study was to construct a mathematical model describing the spatial distribution of atmospheric $^{36}Cl/Cl$ ratios across the United States. This study incorporated a new approach to the modeling of the spatial distribution of $^{36}Cl/Cl$ ratios, involving the use of a parameter-based model such that the $^{36}Cl/Cl$ ratio could be calculated at any point in the country using simple climatic and geographic parameters. The $^{36}Cl/Cl$ ratio model incorporated three major components, a wet chloride deposition model, the dry deposition distribution, and a ^{36}Cl deposition model proposed by Phillips (1999).

The stable chloride distribution was determined using a new model of the wet deposition component, and using measurements of dry deposition at numerous stations across the country. The wet deposition model incorporated a linear regression between chloride deposition and precipitation, where the slope of the regression changed with varying distance from the coast. The regression slope was highest near the coasts and decreased with increasing distance from the coast, due to the reduction in atmospheric chloride concentrations further from the coast. An analysis of the long-term average chloride / precipitation relationship revealed a strong linear relationship at low to moderately high precipitation amounts, and that a ceiling value for chloride deposition was reached at extreme values of precipitation. The presence of ceiling values in chloride

deposition was most important in the Pacific Northwest, where a modification to the simple linear regression may be necessary. The model constructed in this study used an interpolation of the chloride deposition / precipitation regression slopes, rather than incorporating a functional relationship to describe the change in these slopes across the country. The dry deposition distribution was interpolated from numerous NADP/NTN measurement stations. The ^{36}Cl deposition was calculated using a model proposed by Phillips (1999) where ^{36}Cl deposition was dependent on both the latitude and on precipitation.

The $^{36}Cl/Cl$ ratio model overpredicted the ratio throughout the eastern United States and underpredicted the value in the Pacific Northwest. An assessment of the errors in each of the model components was undertaken to determine where the model could be improved. The new wet chloride deposition model was in good agreement (10 percent) with measured values from the NADP/NTN over most of the country, but was biased toward slight underprediction. This underprediction was attributed to the presence of the ceiling values in chloride deposition at extreme precipitation values. A linear regression fit through such data has a reduced slope compared with a linear regression through data without such ceiling values. Removing the data representing the ceiling values may improve the model fit over much of the country by slightly increasing the chloride deposition / precipitation regression slopes and increasing the wet deposition component. The wet deposition model could also be improved by incorporating a functional relationship with the distance from the coast, rather than using the current interpolation. The chloride deposition / precipitation regression slopes were found to exhibit a power-law decline in value with increasing distance from the coast. A similar power-law decline in

dry deposition was found with increasing inland distance, and the incorporation of such a relationship was suggested as a method to improve the dry deposition distribution. The ^{36}Cl deposition model fit the limited measurements moderately well, but an analysis of the $S_p(\lambda_o)/D_{36}(\lambda_o)$ ratio indicated that it should be decreased from the suggested 1.11 x 10^{-3} to 9.6 x 10^{-4} yr mm^{-1}.

While the current form of the $^{36}Cl/Cl$ ratio model has met most of the original goals of this study, it has not been fully developed into a complete mathematical model. The current model is dependant upon two major interpolations, one of the chloride deposition / precipitation regression slopes and one of the dry deposition distribution across the country. In order to construct a complete mathematical model of $^{36}Cl/Cl$ ratios, these interpolations should be replaced with functional relationships. Both the chloride deposition / precipitation regression slopes and the dry deposition are related to the distance from the coast, and a power-law relationship (or similar) was suggested to describe their distributions across the country. Incorporation of these distance from the coast relationships will produce a completely mathematical model of $^{36}Cl/Cl$ ratios over the United States. The functional relationships can then be modified, independently or simultaneously, to provide the best fit to the measured data.

The pursuit of models to describe the spatial and temporal variability of $^{36}Cl/Cl$ ratios over the United States (and the world) can only be continually enhanced by the collection of more data. This study has provided evidence of particular relationships between climatic variables (such as precipitation) and chloride and ^{36}Cl deposition based on a large number of measurements by the NADP/NTN. New data regarding the relationship between ^{36}Cl deposition and precipitation allowed for an improved model of

^{36}Cl deposition to be developed. There are still a number of relationships that are presently unclear, and warrant additional study. Among these are the cause and functional form of the variability in chloride deposition / precipitation regression slopes at different times of the year, the most suitable relationship between ^{36}Cl deposition and precipitation, and additional climatic or geographic controls on stable chloride deposition. An updated, nationwide study of the dry deposition component using currently accepted techniques could provide more reliable measurements than the NADP/NTN measurements incorporated in this study, and would greatly advance the study of atmospheric chloride deposition. Finally, additional measurements of meteoric ^{36}Cl deposition and meteoric $^{36}Cl/Cl$ ratios throughout the country are needed to improve the understanding of the spatial distribution of ^{36}Cl over the United States. Of particular use would be new studies on the change in $^{36}Cl/Cl$ ratios (or ^{36}Cl deposition) with increasing distance from coastal areas, and additional studies on the relationship between ^{36}Cl deposition and precipitation at several locations across the country.

REFERENCES

Barnes-Svarney P.L. (1995) *The New York Public Library Science Desk Reference*. New York, Macmillan, 668 p.

Barry R.G. and Chorley R.J. (1992) *Atmosphere, Weather, and Climate*. New York, Routledge, 392 p.

Baumgartner A. and Reichel E. (1975) *The World Water Balance: Mean Annual Global Continental and Maritime Precipitation*. Elsevier, Amsterdam.

Baumgartner S., Beer J., Masarik J., Wagner G., Meynadier L., and Synal H.-A. (1998) Geomagnetic modulation of the ^{36}Cl flux in the GRIP ice core, Greenland. *Science* **279**, 1330-1332.

Bentley H.W., Phillips F.M., Davis S.N., Gifford S., Elmore E., Tubbs L.E., and Gove H.E. (1982) Thermonuclear ^{36}Cl pulse in natural water. *Nature* **300**, 737-740.

Bentley H.W., Phillips F.M., and Davis S.N. (1986a) Chlorine-36 in the terrestrial environment. In *Handbook of Environmental Isotope Geochemistry*, Vol. 2, eds. P. Fritz and J.-C. Fontes, pp. 427-480. Elsevier, Amsterdam.

Bentley H.W., Phillips F.M., Davis S.N., Airey P.L., Calf G.E., Elmore D., Habermehl M.A., and Torgersen T. (1986b) Chlorine-36 dating of very old ground water: 1. The Great Artesian Basin, Australia. *Water Resources Research* **22**, 1991-2002.

Blanchard D.C. and Woodcock A.H. (1957) Bubble formation and modification in the sea and its meteorological significance. *Tellus* **9**, 145-158.

Boyce S.G. (1951) Source of atmospheric salts. *Science* **113**, 620-621.

Ciceron R.J. (1981) Halogens in the atmosphere. *Review of Geophysics and Space Physics* **19**, 123-139.

Daly C., Neilson R.P., and Phillips D.L. (1994) A statistical-topographic model for mapping climatological precipitation over mountainous terrain. *Journal of Applied Meteorology* **33**, 140-158.

Daly C., Taylor G.H., and Gibson W.P. (1997) The PRISM approach to mapping precipitation and temperature. In *Proc., 10th AMS Conference on Applied Climatology*, Amer. Meteorological Soc., Reno, NV, Oct. 20-23, pp. 10-12.

Daly C. and Johnson G. (1999) PRISM Guide Book. Electronic document (http://www.ocs.orst.edu/prism/prisguid.doc), 49 p.

Davidson C.I. (1989) Mechanisms of wet and dry deposition of atmospheric contaminants to snow surfaces. In *The Environmental Record in Glaciers and Ice Sheets,* eds. H. Oeschger and Jr., C.C.L., pp. 29-51. John Wiley & Sons, Toronto.

Davis R.J. and Schaeffer O.A. (1955) Chlorine-36 in nature. *Ann. N.Y. Acad. Sci.* **62**, 105-122.

Davis S.N., Cecil D., Zreda M., and Sharma P. (1998) Chlorine-36 and the initial value problem. *Hydrogeology Journal* **6**, 104-114.

Dolske D.A. and Gatz D.F. (1984) Field intercomparison of sulfate dry deposition monitoring and measurement methods: Preliminary results. In *Deposition Both Wet and Dry*, ed. B.B. Hicks, pp. 121-131. Butterworth Publishers, Boston.

Elmore D., Fulton B.R., Clover M.R., Marsden J.R., Gove H.E., Naylor H., Purser K.H., Kilius L.R., Beukens R.P., and Litherland A.E. (1979) Analysis of ^{36}Cl in environmental water samples using an electrostatic accelerator. *Nature* **277**, 22-25.

Elsasser W., Ney E.P., and Winckler J.R. (1956) Cosmic-ray intensity and geomagnetism. *Nature* **178**, 1226-1227.

Eriksson E. (1960) The yearly circulation of chloride and sulfur in nature: Meteorological, geochemical and pedological implications, Part II. *Tellus* **12**, 63-109.

Erisman J.W., Hogenkamp J.E.M., Van Putten E.M., Uiterwijk J.W., Kemkers E., Wiese C.J., and Mennen M.G. (1999) Long-term continuous measurements of SO_2 dry deposition over the Speulder forest. *Water, Air, and Soil Pollution* **109**, 237-262.

Fabryka-Martin J.T., Davis S.N., and Elmore D. (1987) Applications of ^{129}I and ^{36}Cl in hydrology. *Nuclear Instruments and Methods in Physics Research* **B29**, 361-371.

Feth J.H. (1981) Chloride in natural continental water, U.S. Geological Survey Water Supply Paper 2176, 36 pp.

Fuquay J.J. (1970) Scavenging in perspective. In *Precipitation Scavenging, Proc. of a symposium held at Richland, WA June 2-4, 1970*, Coords. Engelmann R.J. and Slinn W.G.N., U.S. Atomic Energy Commission, pp.1-5.

Hainsworth L.J. (1994) Spatial and temporal variations in chlorine-36 deposition in the northern United States. Unpublished PhD thesis, University of Maryland, College Park.

Hicks B.B., Baldocchi D.D., Meyers T.P., Hosker Jr. R.P., and Matt D.R. (1987) A preliminary multiple resistance routine for deriving dry deposition velocities from measured quantities. *Water, Air, and Soil Pollution* **36**, 311-330.

Holton J.R., Haynes P.H., McIntyre M.E., Douglas A.R., Rood R.B., and Pfister L. (1995) Stratosphere-troposphere exchange. *Rev. Geophysics* **33**, 403-439.

Junge C.E. (1972) Our knowledge of the physico-chemistry of aerosols in the undisturbed marine environment. *Journal of Geophysical Research* **77**, 5183-5200.

Junge C.E. and Werby R.T. (1958) The concentration of chloride, sodium, potassium, calcium and sulfate in rain water over the United States. *Journal of Meteorology* **15**, 417-425.

Knies D.L. (1994) Cosmogenic radionuclides in precipitation. Unpublished PhD thesis, Purdue University, West Lafayette, Indiana.

Lal D. and Peters B. (1967) Cosmic ray produced radioactivity on the earth. In *Handbuch der Physik.* Vol. 46, ed. K. Sitte, pp. 551-612. Springer-Verlag, Berlin.

Li Y.,-H. (1992) Seasalt and pollution inputs over the continental United States. *Water, Air, and Soil Pollution* **64**, 561-573.

Moore D. (1998) Precipitation chemistry data on the Sevilleta National Wildlife Refuge (1989-1998). Sevilleta LTER, University of New Mexico, Department of Biology, Albuquerque, NM 87131-1091. (http://sevilleta.unm.edu).

Moysey S. (1999) Meteoric ^{36}Cl in the contiguous United States. Unpublished MS thesis, University of Arizona, Tucson.

National Atmospheric Deposition Program / National Trends Network (NADP/NTN) (1998) NADP Program Office, Illinois State Water Survey, 2204 Griffith Dr., Champaign, IL 61820; NADP Coordination Office, Natural Resource Ecology Laboratory, Colorado State University, Fort Collins, CO 80523; (http://nadp.sws.uiuc.edu).

Parrat Y., Hajdas W., Baltensperger U., Synal H.-A., Kubik P.W., Gäggeler H.W., and Suter M. (1996) Atmospheric production rate of ^{36}Cl. In *Paul Scherrer Institut, Annual Report 1996, Annex IIIA*, eds. U. Baltensperger and R. Lorenzen. p. 87. Villigen, Switzerland.

Phillips F.M. (1999) Chapter 10: Chlorine-36. In *Environmental Tracers in Subsurface Hydrology*, eds. P.G. Cook and A.L. Herczeg. pp. 299-348. Kluwer Academic, Dordrecht.

Plummer M.A., Phillips F.M., Fabryka-Martin J., Turin H.J., Wigand P.E., and Sharma P. (1997) Chlorine-36 in fossil rat urine: an archive of cosmogenic nuclide deposition over the past 40,000 years. *Science* **277**, 538-541.

PRISM (1998) Gridded precipitation data. Oregon Climate Service, Oregon State University, 326 Strand Ag. Hall, Corvallis, OR 97331; (http://www.ocs.orst.edu/prism).

Prodi F. (1980) Wet and dry removal of aerosol particles from the planetary boundary layer. In *Atmospheric Planetary Boundary Layer Physics,* ed. A. Longhetto, pp. 267-272. Elsevier, Torino.

Reiter E. (1975) Stratospheric-tropospheric exchange processes. *Review of Geophysics and Space Physics* **13**, 459-474.

Schaeffer O.A., Thompson S.O., and Lark N.L. (1960) Chlorine-36 radioactivity in rain. *Journal of Geophysical Research* **65**, 4013-4016.

Scott B.C. (1981) Modeling of atmospheric wet deposition. In *Atmospheric Pollutants in Natural Waters,* ed. S.J. Eisenreich, pp. 3-21. Ann Arbor Science.

Seinfeld J.H. and Pandis S.N. (1998) *Atmospheric Chemistry and Physics*. Wiley & Sons, Toronto.

Sevilleta National Wildlife Refuge (SNWR). Sevilleta LTER, University of New Mexico, Department of Biology, Albuquerque, NM 87131-1091. (http://sevilleta.unm.edu).

Simpson H.J. and Herczeg A.L. (1994) Delivery of marine chloride in precipitation and removal by rivers in the Murray-Darling Basin, Australia. *Journal of Hydrology* **154**, 323-350.

Slinn W.G.N. and Hales J.M. (1970) Phoretic processes in scavenging. In *Precipitation Scavenging, Proc. of a symposium held at Richland, WA June 2-4, 1970*, Coords. Engelmann R.J. and Slinn W.G.N., U.S. Atomic Energy Commission, pp. 411-423.

Sumner G. (1988) *Precipitation: Process and Analysis*. John Wiley & Sons, Chichester.

Whitehead H.C. and Feth J.H. (1964) Chemical composition of rain, dry fallout, and bulk precipitation at Menlo Park, California, 1957-1959. *Journal of Geophysical Research* **69**, 3319-3333.